Downloaded from orbit.dtu.dk on: May 05, 2023

DTU Library

Detection and processing of phase modulated optical signals at 40 Gbit/s and beyond

Geng, Yan

Publication date:
2007

Document Version
Publisher's PDF, also known as Version of record

Link back to DTU Orbit

Citation (APA):
Geng, Y. (2007). *Detection and processing of phase modulated optical signals at 40 Gbit/s and beyond*. Technical University of Denmark.

General rights
Copyright and moral rights for the publications made accessible in the public portal are retained by the authors and/or other copyright owners and it is a condition of accessing publications that users recognise and abide by the legal requirements associated with these rights.

- Users may download and print one copy of any publication from the public portal for the purpose of private study or research.
- You may not further distribute the material or use it for any profit-making activity or commercial gain
- You may freely distribute the URL identifying the publication in the public portal

If you believe that this document breaches copyright please contact us providing details, and we will remove access to the work immediately and investigate your claim.

Detection and Processing of Phase Modulated Optical Signals at 40 Gbit/s and Beyond

Yan Geng

March 2007

COM•DTU
Department of Communications, Optics & Materials
Technical University of Denmark
Building 345V
2800 Kgs. Lyngby
DENMARK

Abstract

This thesis addresses demodulation in direct detection systems and signal processing of high speed phase modulated signals in future all-optical wavelength division multiplexing (WDM) communication systems where differential phase shift keying (DPSK) or differential quadrature phase shift keying (DQPSK) are used to transport information. All-optical network functionalities—such as optical labeling, wavelength conversion and signal regeneration—are experimentally investigated.

Direct detection of phase modulated signals requires phase-to-intensity modulation conversion in a demodulator at the receiver side. This is typically implemented in a one bit delay Mach-Zehnder interferometer (MZI). Two alternative ways of performing phase-to-intensity modulation conversion are presented. Successful demodulation of DPSK signals up to 40 Gbit/s is demonstrated using the proposed two devices.

Optical labeling has been proposed as an efficient way to implement packet routing and forwarding functionalities in future IP-over-WDM networks. An in-band subcarrier multiplexing (SCM) labeled signal using 40 Gbit/s DSPK payload and 25 Mbit/s nonreturn-to-zero (NRZ) SCM label, is successfully transmitted over 80 km post-compensated non-zero dispersion shifted fiber (NZDSF) span. Using orthogonal labeling, an amplitude shift keying (ASK)/DPSK labeled signal using 40 Gbit/s return-to-zero (RZ) payload and 2.5 Gbit/s DPSK label, is generated. WDM transmission and label swapping are demonstrated for such a signal.

In future all-optical WDM networks, wavelength conversion is an essential functionality to provide wavelength flexibility and avoid wavelength blocking. Using a 50 m long highly nonlinear photonic crystal fiber (HNL-PCF), with a simple four-wave mixing (FWM) scheme, wave-

length conversion of single channel and multi-channel high-speed DPSK signals is presented. Wavelength conversion of an 80 Gbit/s RZ-DPSK-ASK signal generated by combining different modulation formats, is also reported.

Amplitude distortion accumulated over transmission spans will eventually be converted into nonlinear phase noise, and consequently degrade the performance of systems making use of RZ-DPSK format. All-optical signal regeneration avoiding O-E-O conversion is desired to improve signal quality in ultra long-haul transmission systems. Proof-of-principle numerical simulation results are provided, that suggest the amplitude regeneration capability based on FWM in a highly nonlinear fiber (HNLF). The first reported experimental demonstration of amplitude equalization of 40 Gbit/s RZ-DPSK signals using a 500 m long HNLF is presented.

Using four possible phase levels to carry the information, DQPSK allows generation of high-speed optical signals at bit rate that is twice the operating speed of the electronics involved. Generation of an 80 Gbit/s DQPSK signal is demonstrated using 40 Gbit/s equipment. The first demonstration of wavelength conversion of such a high-speed signal is implemented using FWM in a 1 km long HNLF. No indication of error floor is observed. Using polarization multiplexing and combination of DQPSK with ASK and RZ pulse carving at a symbol rate of 40 Gbaud, a 240 Gbit/s RZ-DQPSK-ASK signal is generated and transmitted over 50 km fiber span with no power penalty.

In summary, we show that direct detection and all-optical signal processing—including optical labeling, wavelength conversion and signal regeneration—that already have been studied intensively for signals using conventional on-off keying (OOK) format, can also be successfully implemented for high-speed phase modulated signals. The results obtained in this work are believed to enhance the feasibility of phase modulation in future ultra-high speed spectrally efficient optical communication systems.

Resumé

Denne afhandling omhandler demodulation i direkte detekterede systemer samt signal behandling af højhastigheds fasemodulerede signaler som vil blive benyttet i fremtidens hel-optiske wavelength division multiplexed (WDM) systemer hvor differential phase shift keying (DPSK) eller differential quadrature phase shift keying (DQPSK) bliver benyttet til at sende information. Hel-optiske netværks funktionaliteter såsom optisk mærkning, bølgelængde konvertering og signal regenerering vil blive undersøgt eksperimentelt.

Direkte detektering af fasemodulerede signaler kræver konvertering af fasen til intensitet vha. demodulatoren i modtager enden. Dette bliver typisk implementeret vha. af et eet bit forsinkelses Mach-Zehnder interferometer (MZI). To forskellige teknikker til at konverterer fasen til intensitet vil blive præsenteret. Succesfuld demodulation af DPSK signaler op til 40 Gbit/s bliver demonstreret ved at benytte de to foreslåede komponenter.

Optisk mærkning er blevet foreslået som en effektiv måde til at implementere pakke dirigering samt fremad rettede funktionaliteter i fremtidens IP-over-WDM netværk. Et in-band subcarrier multiplexing (SCM) mærket signal baseret på 40 Gbit/s nyttelast og 25 Mbit/s nonreturn-to-zero (NRZ) SCM mærke, er succesfuldt blevet transmitteret over et 80 km post-kompenseret non-zero dispersion skiftet fiber (NZDSF) spand. Ved at benytte ortogonal mærkning blev et amplitude shift keying (ASK)/DPSK mærket signal genereret baseret på 40 Gbit/s return-to-zero (RZ) nyttelast og 2.5 Gbit/s DPSK mærke. WDM transmission samt mærke skift er blevet demonstreret for dette signal.

I fremtidens hel-optiske WDM netværk er bølgelængde konvertering en essentiel funktionalitet for at sikre bølgelængde fleksibilitet og

dermed undgå bølgelængde blokering. Bølgelængde konvertering vha. firebølge blanding (FWM) i 50 m stærkt ulineær fotonisk krystal fiber (HNL-PCF) af DPSK signaler både af en enkelt højhastigheds kanal samt multiple kanaler bliver præsenteret. Bølgelængde konvertering af et 80 Gbit/s RZ-DPSK-ASK signal som er dannet ved at kombinere forskellige modulations formater vil også blive beskrevet.

Akkumuleret amplitude forvrængning hen over transmissions spand vil uvægerligt blive konverteret til ikke lineær fasestøj og vil derfor degradere ydelsen af systemer baseret på RZ-DPSK formatet. Hel-optisk signal regenerering som undgår O-E-O konvertering er ønskværdig til at forbedre signal kvaliteten i systemer som inkludere ekstreme transmissions distancer. Amplitude regenerering vha. FWM i stærkt ulineære fibre (HNLF) bliver princip demonstreret vha. numeriske simuleringer. Den første eksperimentelle demonstration af amplitude udligning i 500 m HNLF af 40 Gbit/s RZ-DPSK signaler bliver præsenteret.

Ved at benytte fire mulige faseniveauer til at bære data information, DQPSK, medfører muligheden for at danne et højhastigheds optisk signal som har en bit hastighed der er lig den dobbelte af den hastighed som den benyttede elektronik opererer ved. Generering af et 80 Gbit/s DQPSK signal vha. 40 Gbit/s udstyr bliver demonstreret. Den første demonstration af bølgelængde konvertering af et sådanne højhastigheds signal er blevet implementeret vha. FWM i en 1 km lang HNLF. Ingen antydning af fejl gulv er observeret. Ved at benytte polarisations multiplexing og kombinere DQPSK, ASK samt RZ puls formning ved en symbol hastighed på 40 Gbaud blev et 240 Gbit/s RZ-DQPSK-ASK signal genereret og transmitteret over 50 km fiber spand uden nogen power penalty.

I konklusion, bliver det vist at direkte detektering og hel-optisk signal behandling—dette inkluderer optisk mærkning, bølgelængde konvertering og signal regenerering—som tidligere er blevet undersøgt grundigt for signaler baseret på konventionel on-off keying (OOK) format, også succesfuldt kan blive implementeret i højhastigheds fasemodulerede signaler. Resultaterne som opnået i dette arbejde forventes at øge mulighederne for fasemodulation i fremtidens spektral-effektive ekstreme højhastigheds optiske kommunikations systemer.

Acknowledgements

First of all, I would like to thank my supervisors Palle Jeppesen and Christophe Peucheret, for their kind guidance, support, and helpful advices over the years. I would also like to thank Jianfeng Zhang, who was my supervisor during the first year of my Ph.D. study, for his fruitful discussions during his stay at COM•DTU.

The Systems Competence Area at COM•DTU has been a perfect place to perform this Ph.D. study, with a high level of scientific research. Special thanks go to Christophe, for all his suggestions and help during my study, and company in the laboratory, as well as the wonderful time we spent together during conference trips. I am grateful for Torger for always being there when I need help with my computer, simulations, or other things. I would like to thank Michael, Rasmus, Torger and Jesper for reading the thesis and for their valuable comments. And also thanks to Anders for helping me in writing the Danish resumé.

Many thanks go to my past and present colleagues, Nan, Jianfeng, Peter, Emir, Pablo, Darko, Jorge, Leif, Hans Christian and Idelfonso. I really enjoy your company and your cooperative work, and benefit a lot from the inspiring environment we create. Thanks to my office mate, Beata, for sharing good stories and wonderful girl talk.

Last but not least, I would like to thank my family, for the endless support and encouragement you gave me. Kun, thanks for your love, and for being patient.

Yan Geng
March 30, 2007

Ph.D. Publications

The following publications have resulted from this Ph.D. project.

[A] Y. Geng, C. Peucheret, and P. Jeppesen. "Amplitude equalization of 40 Gb/s RZ-DPSK signals using saturation of four-wave mixing in a highly non-linear fiber", in *Technical Digest IEEE Lasers and Electro-Optics Society Annual Meeting, LEOS'06,* Montreal, Quebec, Canada, pp. 158–159, Paper MP5, October 2006

[B] J. B. Jensen, T. Tokle, Y. Geng, P. Jeppesen, M. Serbay, and W. Rosenkranz. "Dispersion tolerance of 40 Gbaud multilevel modulation formats with up to 3 bits per symbol", in *Technical Digest IEEE Lasers and Electro-Optics Society Annual Meeting, LEOS'06,* Montreal, Quebec, Canada, pp. 494–495, Paper WH4, October 2006

[C] T. Tokle, M. Serbay, J. B. Jensen, Y. Geng, W. Rosenkranz, and P. Jeppesen. "Investigation of multilevel phase and amplitude modulation formats in combination with polarisation multiplexing up to 240 Gbit/s", *IEEE Photonics Technology Letters*, vol. 18, no. 20, pp. 2090–2092, October 2006

[D] C. Peucheret, Y. Geng, B. Zsigri, T. T. Alkeskjold, T. P. Hansen, and P. Jeppesen. "Demodulation of DPSK signals up to 40 Gb/s using a highly birefringent photonic bandgap fiber", *IEEE Photonics Technology Letters*, vol. 18, no. 12, pp. 1392–1394, June 2006

[E] Y. Geng, C. Peucheret, T. Tokle, P. A. Andersen, and P. Jeppesen. "Wavelength conversion of high speed DPSK signals", in *T-System,*

HHI, Kiel University, Munich University of Technology, and COM annual workshop 2006 on Optical Communication Systems, Munich, Germany, February 2006, Presentation

[F] T. Tokle, M. Serbay, Y. Geng, J. B. Jensen, W. Rosenkranz, and P. Jeppesen. "Penalty-free transmission of multilevel 240 Gbit/s RZ-DQPSK-ASK using 40 Gbit/s equipment", in *Proceedings European Conference on Optical Communication, ECOC'05,* Glasgow, Scotland, vol. 6, pp. 11–12, Paper Th4.1.6, September 2005, Post-deadline paper

[G] Y. Geng, P. A. Andersen, T. Tokle, C. Peucheret, and P. Jeppesen. "Wavelength conversion of a 6 × 40 Gb/s DPSK WDM signal using FWM in a highly non-linear photonic crystal fiber", in *Proceedings European Conference on Optical Communication, ECOC'05,* Glasgow, Scotland, vol. 2, pp. 205–206, Paper Tu3.3.4, September 2005

[H] Y. Geng, P. A. Andersen, T. Tokle, C. Peucheret, and P. Jeppesen. "Broadband wavelength conversion of a 40 Gbit/s RZ-DPSK signal using dispersion flattened highly nonlinear photonic crystal fiber", in *Proceedings OptoElectronics and Communications Conference, OECC'05,* Seoul, Korea, pp. 796–797, Paper 8B3-4, July 2005

[I] C. Peucheret, Y. Geng, B. Zsigri, T. T. Alkeskjold, T. P. Hansen, and P. Jeppesen. "Demodulation of DPSK signals up to 40 Gb/s using a highly birefringent photonic bandgap fibre", in *Proceedings OptoElectronics and Communications Conference, OECC'05,* Seoul, Korea, pp. 50–51, Paper 5D1-2, July 2005

[J] P. A. Andersen, T. Tokle, Y. Geng, C. Peucheret, and P. Jeppesen. "Wavelength conversion of a 40 Gbit/s RZ-DPSK signal using Four-Wave Mixing in a dispersion flattened highly nonlinear photonic crystal fiber", *IEEE Photonics Technology Letters*, vol. 17, no. 9, pp. 1908–1910, September 2005

[K] T. Tokle, Y. Geng, C. Peucheret, and P. Jeppesen. "Wavelength conversion of 80 Gbit/s optical DQPSK using FWM in a highly non-

linear fibre", in *Technical Digest Conference on Lasers and Electro-Optics, CLEO'05,* Baltimore, Maryland, U.S.A., vol. 3, pp. 1708–1710, Paper JThE50, May 2005

[L] T. Tokle, P. A. Andersen, Y. Geng, B. Zsigri, C. Peucheret, and P. Jeppesen. "Generation, transmission and wavelength conversion of an 80 Gbit/s RZ-DBPSK-ASK signal", in *Technical Digest Conference on Lasers and Electro-Optics, CLEO'05,* Baltimore, Maryland, U.S.A., vol. 1, pp. 294–296, Paper CMQ4, May 2005

[M] C. Peucheret, Y. Geng, M. Svalgaard, B. Zsigri, H. R. Sørensen, N. Chi, H.-J. Deyerl, M. Kristensen, and P. Jeppesen. "Direct UV written Michelson interferometer for RZ signal generation using phase-to-intensity modulation conversion", *IEEE Photonics Technology Letters*, vol. 17, no. 8, pp. 1674–1676, August 2005

[N] N. Chi, L. Xu, J. Zhang, P. V. Holm-Nielsen, C. Peucheret, Y. Geng, and P. Jeppesen. "Transmission and optical label swapping for 4 × 40 Gb/s WDM signals deploying orthogonal ASK/DPSK labeling", *IEEE Photonics Technology Letters*, vol. 17, no. 6, pp. 1325–1327, June 2005

[O] T. Flarup, C. Peucheret, J. J. Vegas Olmos, Y. Geng, J. Zhang, I. Tafur Monroy, and P. Jeppesen. "Labeling of 40 Gbit/s DPSK payload using in-band subcarrier multiplexing", in *Technical Digest Optical Fiber Communication Conference, OFC'05,* Anaheim, California, U.S.A., Paper OWB7, March 2005

[P] Y. Geng, C. Peucheret, J. Zhang, and P. Jeppesen. "Numerical and experimental investigation of differential phase-shift keying transmission systems at 40 Gb/s", in *Summer school "New Concepts in Photonics and Optical Communication",* Dijon, France, June 2004, Poster

List of Figures

Contents

Chapter 1

Introduction

During the past three decades, optical communication systems have been developed and deployed tremendously all over the world. Since the installation of first undersea fiber-optic systems across the Atlantic and Pacific oceans in 1988–1989, the state-of-the-art of fiber-optic communication systems has advanced dramatically [1]. Today, the vast majority of long-haul, high capacity communications are carried by optical transmission systems [2, 3].

The current generation of lightwave systems benefit from increased transmission distance by using optical amplification and increased capacity by using wavelength division multiplexing (WDM) technology [4, 5]. The fiber links are typically operating at 1550 nm where the fiber loss is minimum, at a per channel bit rate of 10 Gbit/s with erbium doped fiber amplifiers (EDFAs) spaced 60–80 km apart.

The next generation of fiber-optic communication systems is concerned with extending the wavelength range over which a WDM system can operate simultaneously [1] and increasing the bit rate of each channel within the WDM signal. The realization relies on, among other things, Raman amplification to extend the conventional wavelength window to both shorter and longer wavelength sides, the development of forward error correction (FEC) technique, and advanced modulation formats suitable for high-speed transmission [6].

Although on-off keying (OOK) modulation format is used exclusively in current long-haul optical communication systems operating at 10 Gbit/s, differential phase shift keying (DPSK) performs better at

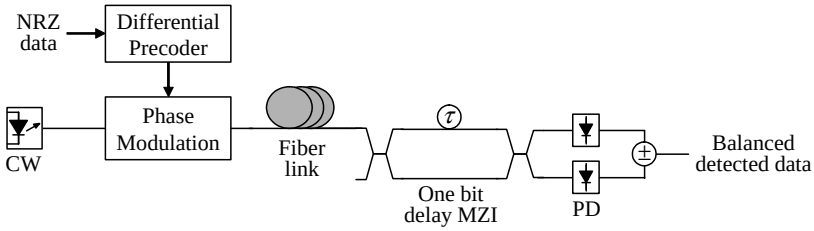

Figure 1.1: Schematic illustration of a DPSK transmission system. CW: continuous wave; NRZ: nonreturn-to-zero; MZI: Mach-Zehnder interferometer; PD: photodiode.

40 Gbit/s [7]. Instead of using the absolute phase of the optical signal to carry the information as in phase shift keying (PSK) format, DPSK signal uses the previous bit as its own phase reference. The use of DPSK in optical coherent systems operating at moderate bit rates and using heterodyne detection was investigated in the early 1990s [8–11]. Ten years later, DPSK gained a renewed interest, as direct detection of DPSK with a one bit delay Mach-Zehnder interferometer (MZI) is much more practical to implement at high signal bit rate [12]. This is mainly because the strict requirements on the laser source linewidth is relaxed for an increased bit rate, as the phase stability only need to be maintained over a duration of two bit slots (i.e. 50 ps for a 40 Gbit/s DPSK system). Since then, DPSK including its variants—such as return-to-zero DPSK (RZ-DPSK) and carrier suppressed return-to-zero DPSK (CSRZ-DPSK)—has been intensively studied and demonstrated as a promising modulation format for long-haul, high capacity optical communication systems [13–19].

Figure 1.1 shows a schematic illustration of a DPSK transmission system. Light from a continuous wave (CW) laser is phase modulated by differentially precoded electrical data. The differential precoding can be realized in an exclusive OR (XOR) gate with one bit delay feedback [20] or using an AND gate and a T-flip-flop [21]. If a pseudo random bit sequence (PRBS) is transmitted, precoding is not necessary, since the differentially precoded bit stream is identical to a time delayed version of the original PRBS [22]. Phase modulation can be performed by driving a phase modulator with V_π peak-to-peak voltage to add a π phase shift. This can also be achieved by using a Mach-Zehnder modulator (MZM)

driven with $2V_\pi$ voltage swing in single-drive mode or V_π voltage swing to each of the two arms in dual-drive mode. For direct detection, a one bit delay MZ interferometer lets two adjacent bits interfere and performs phase-to-intensity modulation conversion at its two output ports. Each output can be detected in a single-ended receiver, or both outputs can be differentially detected in a balanced receiver as shown in Figure 1.1. In a similar configuration, RZ-DPSK and CSRZ-DPSK signals can be generated and detected, provided an additional MZM is used for pulse carving.

Advantages of DPSK compared to conventional OOK format include [7]: when balanced detection is used, about 3 dB lower optical signal-to-noise ratio (OSNR) is required for a given bit error rate (BER), because only half the average optical power is needed for DPSK as compared to OOK to achieve the same symbol distance; higher resilience to fiber nonlinear effects attributes to more evenly distributed optical power; larger tolerance towards signal power fluctuations in the receiver decision circuit due to the fact that a fixed detection threshold value is realized in balanced receiver. On the other hand, the implementation of DPSK format requires additional precoder and decoder, and fine-tuning of the demodulator to match the laser center frequency is necessary to achieve good interference quality [13]. Moreover, the overall opto-electronic conversion obtained at the two interferometer outputs should be equal in order to fully benefit from the balanced detection [15].

By year 2005, a number of record breaking (in terms of capacity and distance) transmission experiments making use of DPSK signals had been reported. A 96×10 Gbit/s RZ-DPSK field trial was successfully conducted over a 13,100 km optical undersea path [23]. Error-free dense wavelength division multiplexing (DWDM) transmission of 40×40 Gbit/s CSRZ-DPSK channels over trans-Pacific distance of 10,000 km was demonstrated [21]. Spectral efficiency of 0.8 bit/s/Hz was achieved in an experiment of transmitting 50 GHz spaced 64×42.7 Gbit/s CSRZ-DPSK signals over 8200 km [24]. Total capacity of 6 Tbit/s was obtained by WDM transmission of 42.7 Gbit/s DPSK signals [25]. Another WDM experiment reported a total capacity of 6.4 Tbit/s by transmitting 160×40 Gbit/s signals using CSRZ-DPSK format [26]. These results demonstrated the potential of DPSK in next generation fiber-optic communication systems.

The above mentioned records achieved using DPSK format were not improved in year 2006, since research interests have gradually moved to a more advanced modulation format, known as differential quadrature phase shift keying (DQPSK). By using four-level phase values, for a DQPSK signal, two bits are transmitted for each symbol, and the information is carried by the phase change between two consecutive symbols, resulting in a symbol rate that is half of the bit rate. The DQPSK format has been shown to have a doubled spectral efficiency, larger dispersion tolerance and increased polarization-mode dispersion (PMD) limited transmission range, but the transmitter and receiver structures are relatively complex [27].

Conventional OOK modulation format has been developed into a mature technology for optical communication systems. DPSK and DQPSK have been shown to have high potential in future long-haul transmission systems. If DPSK or DQPSK are to be used in the next generation of lightwave systems evolving towards higher bit rates, demodulation techniques combined with direct detection along with network functionalities that have already been studied intensively for OOK systems, need to be investigated also for phase modulated systems. The purpose of this thesis is to study the demodulation in direct detection system and processing of high-speed phase modulated signals in context of future all-optical networks where DPSK or DQPSK formats are used to carry the information. The work is focused on experimental investigations of above mentioned issues in system experiments. Network functionalities focused on include optical labeling, wavelength conversion and signal regeneration in DPSK optical communication systems. Generation, transmission and wavelength conversion of high speed DQPSK signals are also addressed.

The structure of the thesis is as follows.

In Chapter 2, two alternative ways of demodulation that allow DPSK to be detected by direct detection are investigated. By direct ultraviolet (UV) writing, a Michelson interferometer making use of waveguide gratings as reflective elements is presented. Demodulation of DPSK signals up to 40 Gbit/s is studied using this device. Utilizing the large birefringence of air-guiding photonic bandgap (PBG) fiber, a polarization delay interferometer capable of 10 and 40 Gbit/s DPSK demodulation is also presented.

In Chapter 3, optical labeling using DPSK signal as either payload or label in high speed core network is explored. First a brief introduction to optical labeling concept and schemes is given. Then the feasibility of in-band subcarrier multiplexing (SCM) labeling using 40 Gbit/s DPSK payload and 25 Mbit/s nonreturn-to-zero (NRZ) SCM label, is investigated. Using orthogonal labeling, generation, WDM transmission and label swapping of an amplitude shift keying (ASK)/DPSK signal are discussed.

In Chapter 4, wavelength conversion of high speed DPSK signals using four-wave mixing (FWM) in a highly nonlinear medium is addressed. First a brief introduction is given to the FWM process and the properties of the highly nonlinear photonic crystal fiber (HNL-PCF) used in all experiments presented in the chapter. Afterwards, several experimental investigations are presented. Using a 50 m long HNL-PCF, wavelength conversion of a 40 Gbit/s RZ-DPSK signal, 6×40 Gbit/s DPSK WDM signal, and an 80 Gbit/s RZ-DPSK-ASK signal generated using combination of different modulation formats, are demonstrated.

In Chapter 5, amplitude equalization of RZ-DPSK signals is studied. The principle of the RZ-DPSK signal amplitude regeneration process is presented. Simulation results suggesting the capability of amplitude equalization using FWM in a highly nonlinear fiber (HNLF) are provided. The first reported experimental demonstration of amplitude equalization of 40 Gbit/s RZ-DPSK signals utilizing saturation of FWM in a 500 m long HNLF is presented and discussed.

In Chapter 6, wavelength conversion and transmission of DQPSK signals at a per channel bit rate of 80 Gbit/s and above are reported. A brief introduction is given to the DQPSK transmitter and receiver structures and to the precoding procedure. The first demonstration of wavelength conversion of an 80 Gbit/s DQPSK signal using FWM in a 1 km long HNLF is presented. Generation of ultra high-speed RZ-DQPSK-ASK signals at 240 Gbit/s using only 40 Gbit/s equipment is presented. Transmission feasibility of such a multilevel modulated signal is demonstrated.

The thesis is concluded in Chapter 7.

References to Chapter 1

[1] G. P. Agrawal. *Fiber-Optic Communciation Systems.* Wiley, Third edition, 2002. ISBN 0-471-21571-6.

[2] P. R. Trischitta and W. C. Marra. "Global undersea communication networks", *IEEE Communication Magazine*, vol. 34, no. 2, pp. 20–21, February 1996.

[3] N. S. Bergano. *Undersea Communications Systems*, In I. Kaminow and T. Li, editors, *Optical Fiber Telecommunications IVB Components,* Chapter 4, Academic Press, March 2002. ISBN 0-12-395173-9.

[4] P. R. Trischitta and W. C. Marra. "Applying WDM technology to undersea cable networks", *IEEE Communication Magazine*, vol. 36, no. 2, pp. 62–66, February 1998.

[5] N. S. Bergano. "Wavelength division multiplexing in long-haul transoceanic transmission systems", *Journal of Lightwave Technology*, vol. 23, no. 12, pp. 4125–4139, December 2005.

[6] G. Charlet. "Challenges for introducing 40 Gb/s submarine systems", in *Proceedings of Optical Transmission, Switching, and Subsystems IV,* Gwangju, South Korea, September 2006, Invited paper.

[7] A. Gnauck. "40-Gb/s RZ-Differential Phase Shift Keyed transmisslon", in *Technical Digest Optical Fiber Communication Conference, OFC'03,* Atlanta, Georgia, U.S.A., Paper ThE1, March 2003.

[8] J.-M. P. Delavaux, L. D. Tzeng, and M. Dixon. "1.4 Gbit/s optical DPSK heterodyne transmission system experiment", *Electronics Letters*, vol. 24, no. 15, pp. 941–942, July 1988.

[9] M. J. Creaner, R. C. Steele, I. Marshall, G. R. Walker, N. G. Walker, J. Mellis, S. Al Chalabi, I. Sturgess, M. Rutherford, J. Davidson, and M. Brain. "Field demonstration of 565 Mbit/s DPSK coherent transmission system over 176 km of installed fibre", *Electronics Letters*, vol. 24, no. 22, pp. 1354–1356, October 1988.

[10] Y. H. Cheng and T. Okoshi. "Multichannel DPSK coherent optical communication systems", *Electronics Letters*, vol. 26, no. 17, pp. 1378–1380, August 1990.

[11] E. Iannone, F. S. Locati, F. Matera, M. Romagnoli, and M. Settembre. "High-speed DPSK coherent systems in the presence of chromatic dispersion and Kerr effect", *Journal of Lightwave Technology*, vol. 11, no. 9, pp. 1478–1485, September 1993.

[12] C. Xu, X. Liu, and X. Wei. "Differential phase-shift keying for high spectral efficiency optical transmissions", *IEEE Journal of Selected Topics in Quantum Electronics*, vol. 10, no. 2, pp. 281–293, March/April 2004.

[13] M. Rohde, C. Caspar, N. Heimes, M. Konitzer, E.-J. Bachus, and N. Hanik. "Robustness of DPSK direct detection transmission format in standard fibre WDM systems", *Electronics Letters*, vol. 36, no. 17, pp. 1483–1484, August 2000.

[14] N. S. Bergano. "Current and future technologies for submarine transmission", in *Technical Digest IEEE Lasers and Electro-Optics Society Annual Meeting, LEOS'04,* Rio Grande, Puerto Rico, vol. 2, pp. 465–466, Paper WB1, November 2004, Invited paper.

[15] A. H. Gnauck and P. J. Winzer. "Optical phase-shift-keyed transmission", *Journal of Lightwave Technology*, vol. 23, no. 1, pp. 115–130, January 2005.

[16] T. L. Huynh, L. N. Binh, and D. D. Tran. "Long-haul ASK and DPSK optical fibre transmission systems: Simulink modeling and experimental demonstration test-beds", in *Proceedings of the IEEE Region 10 Conference, TENCON 2005,* Melbourne, Australiz, November 2005.

[17] J.-X. Cai, C. R. Davidson, M. Nissov, H. Li, W. T. Anderson, Y. Cai, L. Liu, A. N. Pilipetskii, D. G. Foursa, W. W. Patterson, P. C. Corbett, A. J. Lucero, and N. S. Bergano. "Transmission of 40-Gb/s WDM signals over transoceanic distance using conventional NZ-DSF with receiver dispersion slope compensation", *Journal of Lightwave Technology*, vol. 24, no. 1, pp. 191–200, January 2006.

[18] J.-X. Cai, M. Nissov, W. Anderson, M. Vaa, C. R. Davidson, D. G. Foursa, L. Liu, Y. Cai, A. J. Lucero, W. W. Patterson, P. C. Corbett, A. N. Pilipetskii, and N. S. Bergano. "Long-haul 40 Gb/s RZ-DPSK transmission with long repeater spacing", in *Technical Digest Optical Fiber Communication Conference, OFC'06,* Anaheim, California, U.S.A., Paper OFD3, March 2006.

[19] Y. Cai, L. Liu, A. N. Pilipetskii, M. Nissov, and N. S. Bergano. "On performance of coherent phase-shift-keying modulation in 40 Gb/s long-haul optical fiber transmission systems", in *Technical Digest Optical Fiber Communication Conference, OFC'06,* Anaheim, California, U.S.A., Paper JThB11, March 2006.

[20] D. Penninckx, H. Bissessur, P. Brindel, E. Gohin, and F. Bakhti. "Optical differential phase shift keying (DPSK) direct dtection considered as a duobinary signal", in *Proceedings European Conference on Optical Communication, ECOC'01,* Amsterdam, The Netherlands, vol. 3, pp. 456–457, Paper We.P.40, September 2001.

[21] C. Rasmussen, T. Fjelde, J. Bennike, F. Liu, S. Dey, B. Mikkelsen, P. Mamyshev, P. Serbe, P. van der Wagt, Y. Akasaka, D. Harris, D. Gapontsev, V. Ivshin, and P. Reeves-Hall. "DWDM 40G transmission over trans-pacific distance (10000 km) using CSRZ-DPSK, enhanced FEC, and all-Raman-amplified 100 km UltraWave fiber spans", *Journal of Lightwave Technology*, vol. 22, no. 1, pp. 203–207, January 2004.

[22] P. V. Holm-Nielsen. *A Study on Optical Labelling Techniques for All-Optical Networks, Appendix A Differential XOR operation with PRBS.* Ph.D. thesis, COM•DTU, Department of Communications, Optics & Materials, Technical University of Denmark, Kgs. Lyngby, Denmark, April 2005.

[23] J.-X. Cai, D. G. Foursa, L. Liu, C. R. Davidson, Y. Cai, W. W. Patterson, A. J. Lucero, B. Bakhshi, G. Mohs, P. C. Corbett, V. Gupta, W. Anderson, M. Vaa, G. Domagala, M. Mazurczyk, H. Li, S. Jiang, M. Nissov, A. N. Pilipetskii, and N. S. Bergano. "RZ-DPSK field trial over 13 100 km of installed non-slope-matched submarine fibers", *Journal of Lightwave Technology*, vol. 23, no. 1, pp. 95–103, January 2005.

[24] I. Morita and N. Edagawa. "50GHz-spaced 64 × 42.7Gbit/s transmission over 8200km using pre-filtered CS-RZ DPSK signal and EDFA repeaters", in *Proceedings European Conference on Optical Communication, ECOC'03,* Rimini, Italy, vol. 6, pp. 60–61, Paper Th4.3.1, September 2003, Post-deadline paper.

[25] G. Charlet, E. Corbel, J. Lazaro, A. Klekamp, R. Dischler, P. Tran, W. Idler, H. Mardoyan, A. Konczykowska, F. Jorge, and S. Bigo. "WDM transmission at 6-Tbit/s capacity over transatlantic distance, using 42.7-Gb/s differential phase-shift keying without pulse carver", *Journal of Lightwave Technology*, vol. 23, no. 1, pp. 104–107, January 2005.

[26] B. Zhu, L. E. Nelson, S. Stulz, A. H. Gnauck, C. Doerr, J. Leuthold, L. Grüner-Nielsen, M. O. Pedersen, J. Kim, and J. Lingle, R. L. "High spectral density long-haul 40-Gb/s transmission using CSRZ-DPSK format", *Journal of Lightwave Technology*, vol. 22, no. 1, pp. 208–214, January 2004.

[27] R. A. Griffin and A. C. Carter. "Optical differential quadrature phase-shift key (oDQPSK) for high capacity optical transmission", in *Technical Digest Optical Fiber Communication Conference, OFC'02,* Anaheim, California, U.S.A., pp. 367–368, Paper WX6, March 2002.

Chapter 2

Demodulation of DPSK Signals

Direct detection of phase modulated signals relies on phase-to-intensity modulation conversion in a demodulator before the photodetection. This is typically realized in a one bit delay Mach-Zehnder interferometer (MZI), as presented in Chapter 1.

Other schemes have been proposed and demonstrated for phase-to-intensity modulation conversion. Demodulation of 2.5 Gbit/s differential phase shift keying (DPSK) signal has been achieved by proper injection locking of a semiconductor laser [1]. Furthermore, 10 Gbit/s DPSK demodulators based on an optical discriminator filter [2] and two fiber Bragg gratings together with an optically tunable phase shifter [3] have been reported, and recently 10 Gbit/s DPSK balanced detection utilizing a single uniform fiber Bragg grating has been demonstrated [4]. In another scheme [5], a 10 Gbit/s DPSK signal is first converted into a polarization shift keying (POLSK) signal through a birefringent element (e.g., a polarization maintaining fiber), and then the POLSK signal is converted into an intensity modulated signal by means of a polarization beam splitter (PBS). Demodulation of 10 Gbit/s DPSK signal has also been demonstrated using a birefringent fiber loop [6].

Phase-to-intensity modulation conversion at the transmitter side has also been suggested as a method to generate return-to-zero (RZ) alternate mark inversion (AMI) modulation formats with desired duty cycles [7–9]. This format has been suggested to exhibit improved optical

fiber nonlinearity tolerance over conventional on-off keying (OOK) at 40 Gbit/s [10].

In this chapter, we report two alternative ways of DPSK demodulation. In section 2.1, we present demodulation of DPSK signal up to 40 Gbit/s using a delay interferometer structure based on a directly ultra-violet (UV) written Michelson interferometer, where the reflective elements are realized by waveguide gratings. This work was done in cooperation with Christophe Peucheret and Mikael Svalgaard, both from COM•DTU. Mikael Svalgaard is acknowledged for his production, provision, and optimization of the device for the experiment. In section 2.2, we show a DPSK demodulator based on a short length special designed fiber, namely an air-guiding photonic bandgap (PBG) fiber, whose large birefringence is exploited to realize phase-to-intensity modulation conversion. Demodulation of 10 and 40 Gbit/s DPSK signals are successfully performed using this device. This scheme was developed by Christophe Peucheret, and the experiment was carried out in cooperation with Christophe Peucheret, Beáta Zsigri, and Thomas Tanggaard Alkeskjold, all from COM•DTU.

2.1 Demodulation using Direct UV Written Michelson Interferometer

In this section, we describe a DPSK demodulator based on a Michelson interferometer structure fabricated by direct UV writing with waveguide Bragg gratings as reflective elements.

2.1.1 Principle of Operation

Figure 2.1 shows the principle of phase-to-intensity modulation conversion that is essential for DPSK demodulation in direct detection systems. The electrical nonreturn-to-zero (NRZ) data b_k to be transmitted is first differentially encoded. This is done using a one bit delay feedback and an exclusive OR (XOR) gate. The encoded data e_k is then used to modulate the output from a continuous wave (CW) laser source through a phase modulator to obtain a DPSK signal. The following optical delay interferometer performs phase-to-intensity modulation conversion. The phases of the two interfering signals at the output of the interferometer

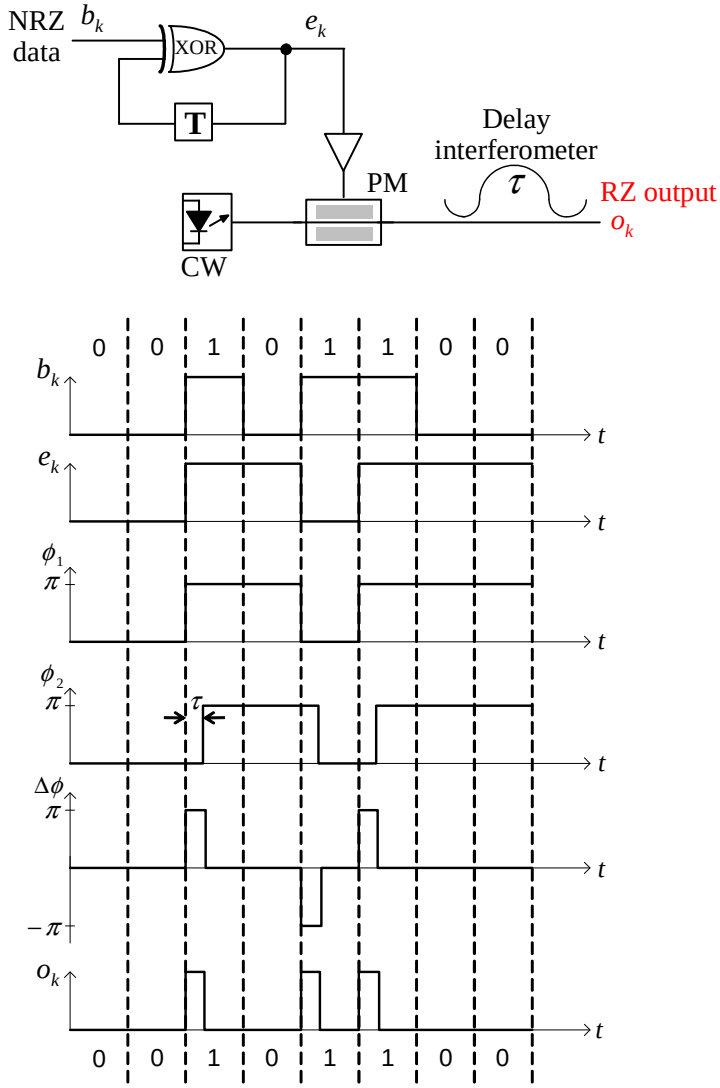

Figure 2.1: Principle of phase-to-intensity modulation conversion in DPSK demodulator. b_k is the electrical NRZ data to be transmitted, e_k is the differentially encoded data, ϕ_1 and ϕ_2 are the phases of the two interfering signals at the output of the interferometer, $\Delta\phi$ is the phase difference between the two arms of the interferometer, and o_k is the resulting optical signal in RZ format at the destructive output port of the interferometer. PM: phase modulator. τ: interferometer's delay.

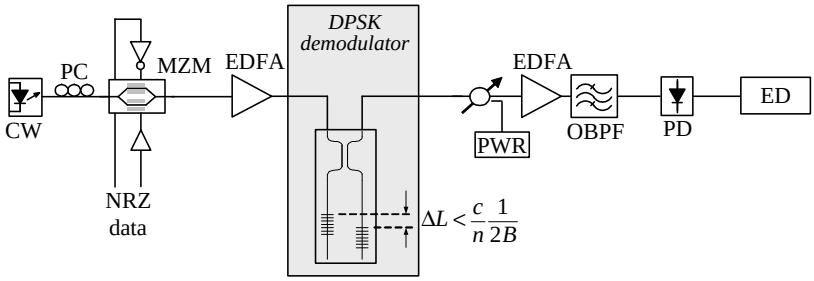

Figure 2.2: Experimental setup for Michelson interferometer based DPSK demodulator. CW: continuous wave; PC: polarization controller; NRZ: non return-to-zero; MZM: Mach-Zehnder modulator; EDFA: erbium doped fiber amplifier; PWR: optical power meter; OBPF: optical bandpass filter; PD: photodiode; ED: error detector [12].

ϕ_1 and ϕ_2 have a delay that is the same as the interferometer's delay τ. The phase difference between the two arms $\Delta\phi$ results in an intensity modulated signal o_k in RZ format at the outputs of the delay interferometer, provided the interferometer's delay τ is smaller than the electrical data bit slot duration $1/B$. Successful demodulation is achieved as the output signal o_k is identical with the transmitted data b_k. As discussed in [7], this way of demodulating DPSK signal converts the NRZ phase modulated signal into pulses in RZ-AMI modulation format at the destructive output port of the interferometer. And it has been shown that, the output pulse width depends on the speed of the NRZ modulation and the value of the delay [11].

2.1.2 Experimental Results

A schematic of the setup used for demonstration of Michelson interferometer based DPSK demodulator is shown in Figure 2.2 [12]. The output of a CW laser is phase modulated in a Mach-Zehnder modulator (MZM) driven with a 2^{31}-1 pseudo random bit sequence (PRBS), resulting in a DPSK signal. The modulator is biased at the null of the transfer function and operating in push-pull mode. The signal is then amplified and sent to the proposed DPSK demodulator. The demodulated signal is then detected in a receiver consisting of a erbium doped fiber amplifier (EDFA), an optical bandpass filter, a 50 GHz photodiode, and an error detector (ED).

The proposed DPSK demodulator consists of a Michelson interferometer made from a coupler and two waveguides, and the reflections are obtained by two Bragg gratings written in the waveguides. The Bragg grating in each arm of the coupler reflects light at certain wavelengths. By placing the gratings at different positions in the waveguides, certain delay is established between the two forward and backward (after reflection in the gratings) propagated signals in the two waveguides. This delay is the interferometer's delay. At the same coupler, the two fields interfere destructively which at the output results in an intensity modulated signal in RZ format.

The entire device is fabricated using direct UV writing technique. This technique has been suggested as a promising method for the fabrication of optical waveguide components due to its simplicity compared to conventional clean room processing and its potential for large-scale production at a reduced cost [13]. Low loss and low birefringence waveguides have been fabricated, and several functionalities have been demonstrated, for example, directional couplers and splitters [14, 15], and variable optical attenuators [16].

For the fabricated device, the component has a total length of 3 cm. Two waveguides, each with a length of 2 cm, are 250 μm apart. Two 4 mm long uniform Bragg gratings are written into each waveguide with a relative displacement ΔL of 2.406 mm, which corresponds to an interferometer delay of 23 ps. The coupling loss to standard single mode fiber (SMF) is about 0.2 dB per facet, and the total fiber-to-fiber loss is about 9 dB.

To verify the ability of demodulating DPSK signals in the device, 10, 20, 30, and 40 Gbit/s DPSK signals are generated and sent to the demodulator. Successful phase-to-intensity modulation conversion is obtained at the output of the delay interferometer, as shown in Figure 2.3. As expected, the output signal is in RZ format. Furthermore, the signal duty cycle increases as the input signal bit rate increases, which confirms the numerical simulation results presented in [17]. The spectra for different bit rate input DPSK signals measured at the output of the delay interferometer are shown in Figure 2.4. As indicated in the figure, for all operations, there is a notch in the spectra induced by destructive interference at the optical carrier frequency. The recorded spectra shown in Figure 2.4 have the typical features of the RZ-AMI format.

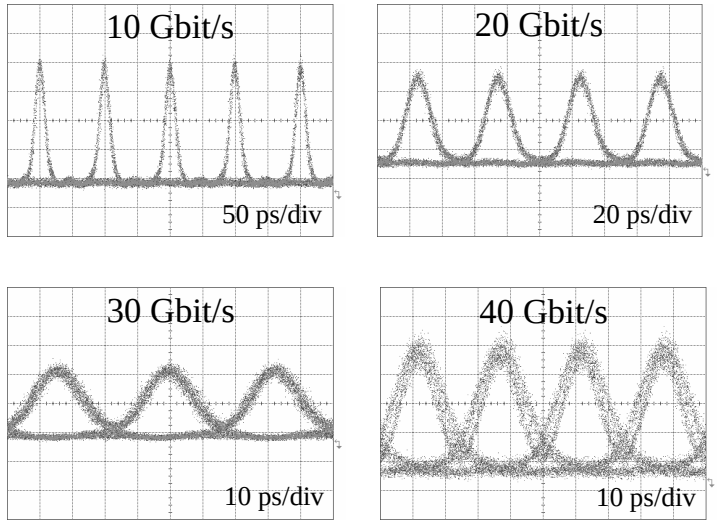

Figure 2.3: Eye diagrams of the demodulated signal in RZ format at the Michelson interferometer output for 10, 20, 30, and 40 Gbit/s DPSK input signal.

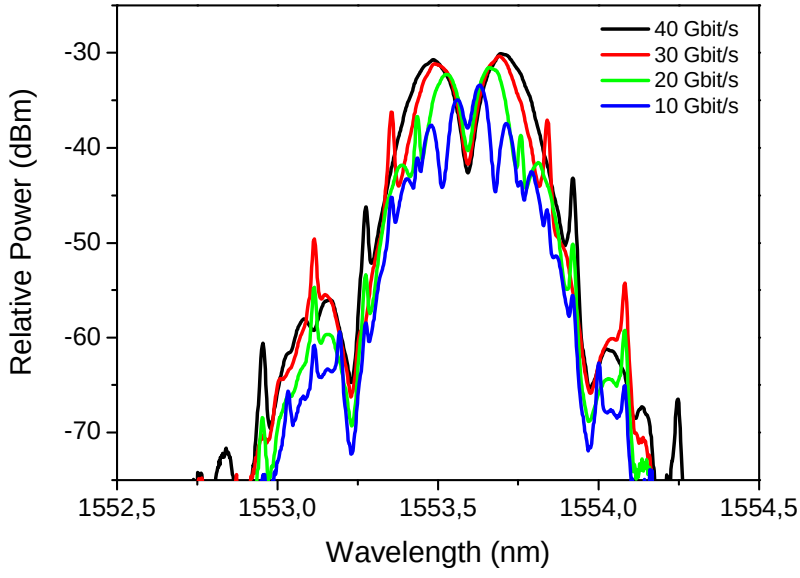

Figure 2.4: Spectra measured at the output of the Michelson interferometer for input DPSK signal at 10, 20, 30, and 40 Gbit/s. Resolution bandwidth: 0.01 nm.

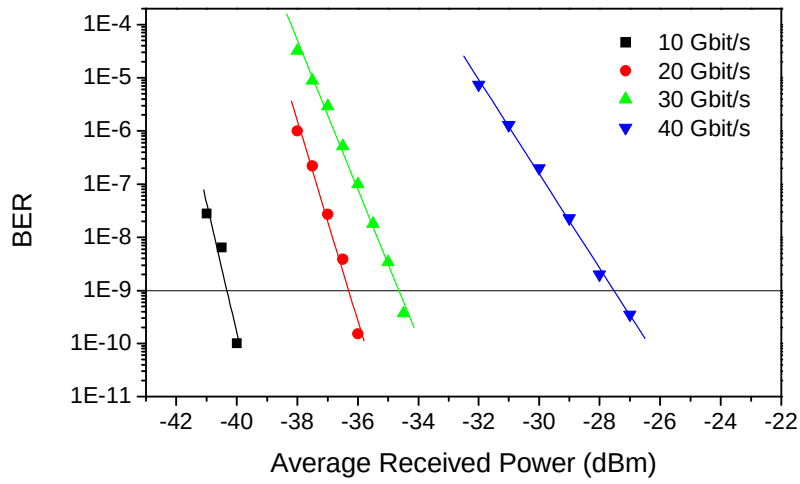

Figure 2.5: Measured BER curves for Michelson interferometer based DPSK demodulation at 10 to 40 Gbit/s operations.

Figure 2.5 shows the measured bit error rate (BER) curves for 10 to 40 Gbit/s operation. Error free demodulation of DPSK signal up to 40 Gbit/s is achieved. As presented in the figure, improved BER performance is obtained for lower bit rate input signals. This is believed to be due to the lower signal-to-noise ratio requirement and the reduced duty cycle at lower bit rate. These results demonstrate successful DPSK demodulation up to 40 Gbit/s using the proposed device. The device is compact and inherently stable compared to fiber-based solutions that would require active stabilization [17]. It should be noted that if the presented delay interferometer structure is used at the transmitter side, successful RZ-AMI signal generation can be realized up to 40 Gbit/s.

2.2 Demodulation using a Highly Birefringent Photonic Bandgap Fiber

In this section, we describe a DPSK demodulator based on a short length of air-guiding PBG fiber. The large birefringence of the fiber is exploited to realize phase-to-intensity modulation conversion.

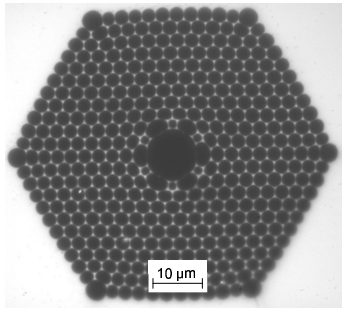

Figure 2.6: Microstructure of the air-guiding PBG fiber used in PBG fiber based DPSK demodulator. This figure is kindly provided by Crystal Fibre A/S.

2.2.1 Air-guiding Photonic Bandgap Fiber

Air-guiding PBG fiber is a type of specially designed fiber. Conventional fiber guides light because of higher refractive index in the core. In air-guiding PBG fiber, light propagates in a low refractive index core surrounded by a high effective index microstructured cladding, and is guided by the photonic bandgap effect [18]. Air-guiding PBG fibers have been shown to be very bending insensitive [19], and their polarization properties have been intensively studied [20–24]. Moreover, 10 Gbit/s data transmission at 1550 nm over 150 m air-guiding PBG fiber has been demonstrated [25].

The sample used in this experiment is a 2.4 m long air-guiding PBG fiber kindly provided by Crystal Fibre A/S. The cross section of the fiber is shown in Figure 2.6. The fiber has a triangular cladding structure with a pitch (center-to-center hole distance) of 3 μm. The core is defined by replacing the 7 central airholes with one large hole, thus the fiber supports a single mode in the core at 1550 nm. The core diameter is 10 μm measured from corner to corner.

In this experiment, the high birefringence of the air-guiding PBG fiber is used to implement a polarization delay interferometer for DPSK signal demodulation.

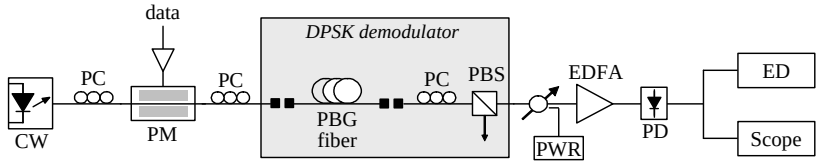

Figure 2.7: Experimental setup for PBG based DPSK demodulator. CW: continuous wave; PC: polarization controller; PM: phase modulator; PBG: photonic bandgap; PBS: polarization beam splitter; EDFA: erbium doped fiber amplifier; PWR: optical power meter; PD: photodiode; ED: error detector [26].

2.2.2 Experimental Results

Figure 2.7 [26] shows the experimental setup for PBG fiber based DPSK demodulator. The output from an CW laser is sent to a phase modulator that is capable for operation up to 40 Gbit/s. The phase modulator is driven with a 2^{31}-1 PRBS, resulting in a constant intensity DPSK signal. Phase-to-intensity modulation conversion is realized in a polarization delay interferometer, which is implemented by a 2.4 m long air-guiding PBG fiber followed by a polarization controller and a PBS. At the input of the demodulator, a polarization controller is used to rotate the state of polarization (SOP) of the DPSK signal, in order to couple it equally to the two eigen-axes of the PBG fiber. Due to fiber birefringence, certain delay between the two fields propagating in the two eigen-polarizations is accumulated. At the fiber output, another polarization controller is used to rotate the two orthogonal SOPs to 45° of the axes of the following PBS. As a result, at the outputs of the PBS, the two fields with certain delay between them interfere and two complementary demodulated DPSK signals appear. One of the outputs is then sent to a pre-amplified receiver consisting of an EDFA, a 50 GHz photodiode, and an ED.

To verify the delay accumulated in the PBG fiber based DPSK demodulator is suitable for 40 Gbit/s operation, the transfer function of the polarization delay interferometer is measured by using polarized white light as the input signal. The result is shown in Figure 2.8 [27]. The PBG fiber transmission is also measured and represented in the figure. It can be seen that the 3 dB bandwidth of the fiber bandgap extends up to 1600 nm. Wavelength dependence of the differential group delay is

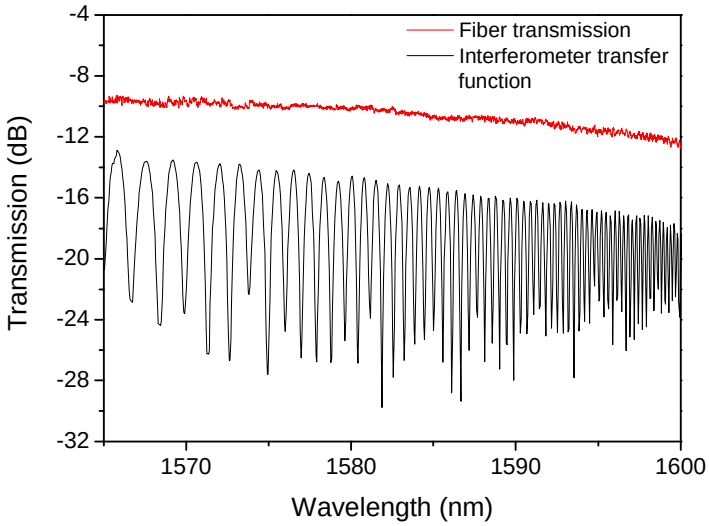

Figure 2.8: Transmission of the 2.4 m long PBG fiber and the measured transfer function of the polarization delay interferometer [27].

calculated from the periodicity of the interferometer transfer function, and is shown in Figure 2.9 [27]. The results obtained by Jones matrix eigenanalysis [28, 29] are also presented in the figure. Measurements obtained by two methods exhibit excellent agreement. As indicated in the figure, the delay increases significantly with wavelength at the edge of the fiber bandgap. At a wavelength of 1592 nm, a delay of 25 ps (corresponding to one bit duration of a 40 Gbit/s DPSK signal) can be obtained. This value corresponds to a birefringence of 3.1×10^{-3}. It should be noted that operating at this wavelength range requires a L-band optical amplifier at the receiver. Therefore, a L-band EDFA consisting of a C-band EDFA followed by a 120 m long erbium doped fiber is used [30].

A 39.8 Gbit/s DPSK signal is then generated and input to the demodulator. Several wavelengths are selected, and the corresponding demodulated eye diagrams are recorded and shown in Figure 2.10. Demodulation is also performed on a 9.95 Gbit/s DPSK signal at 1580 nm, and the result is also presented in Figure 2.10. As can be seen in the figure, when the input DPSK signal is at 39.8 Gbit/s, as the signal

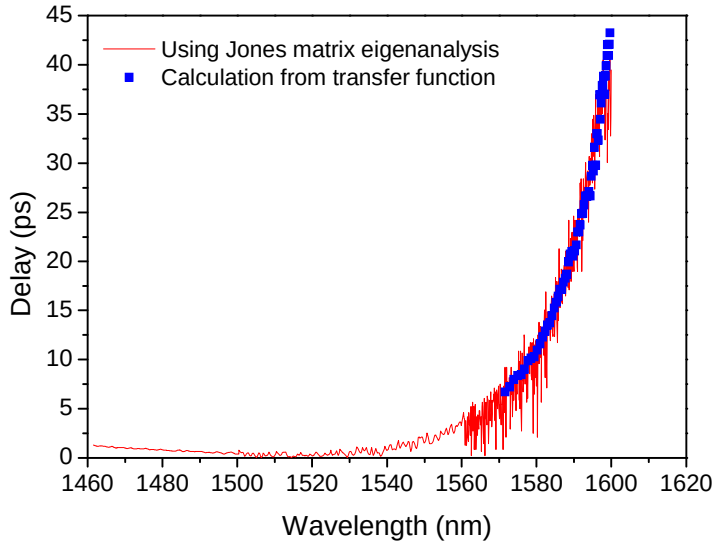

Figure 2.9: Delay of the PBG fiber based DPSK demodulator as a function of wavelength. The red curve is obtained by using Jones matrix eigenanalysis (measurement data provided by T. T. Alkeskjold), and the blue dots are calculations from the measured transfer function of the polarization delay interferometer [27].

wavelength increases, the delay of the polarization delay interferometer increases, thus the demodulated signal pulsewidth increases accordingly. In case of a 9.95 Gbit/s signal, very narrow pulse is obtained after demodulation. This is because at this wavelength, the interferometer delay is very small compared to the 100 ps bit duration.

Figure 2.11 shows the measured BER curves for the demodulation performed on a 39.8 Gbit/s DPSK signal at 1580, 1585, and 1591 nm and a 9.95 Gbit/s signal at 1580 nm. Receiver sensitivities (at a BER of 10^{-9}) of -23.3, -24.0, and -21.7 dBm are observed for 39.8 Gbit/s operation at 1580, 1585, and 1591 nm, respectively. In principle, better receiver sensitivities could be obtained for shorter wavelengths, due to the lower demodulated signal duty cycle associated with smaller interferometer delay at shorter wavelengths. The slightly improved sensitivity measured at 1585 nm is attributed to the local variations in the bandgap transmission and interferometer extinction ratio. For a 9.95 Gbit/s DPSK signal at 1580 nm, receiver sensitivity of -30.7 dBm is achieved. The

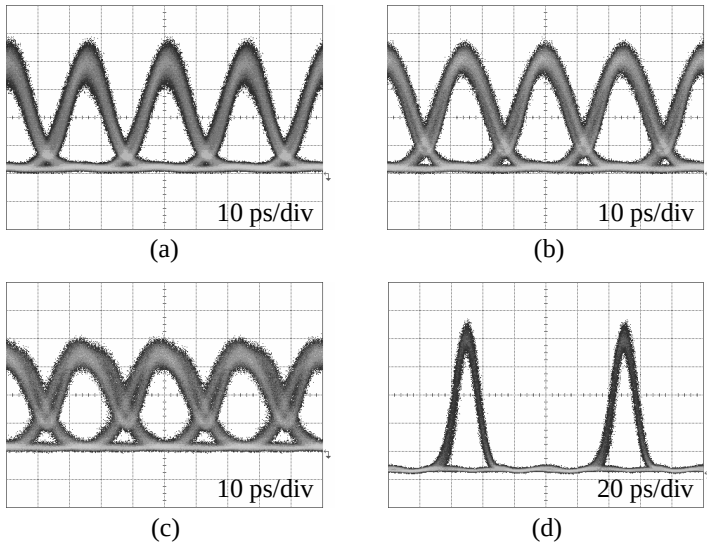

Figure 2.10: Eye diagrams for 39.8 Gbit/s DPSK demodulated signal at (a) 1580 nm, (b) 1585 nm, (c) 1591 nm, and (d) for 9.95 Gbit/s DPSK demodulated signal at 1580 nm, using the PBG fiber based DPSK demodulator.

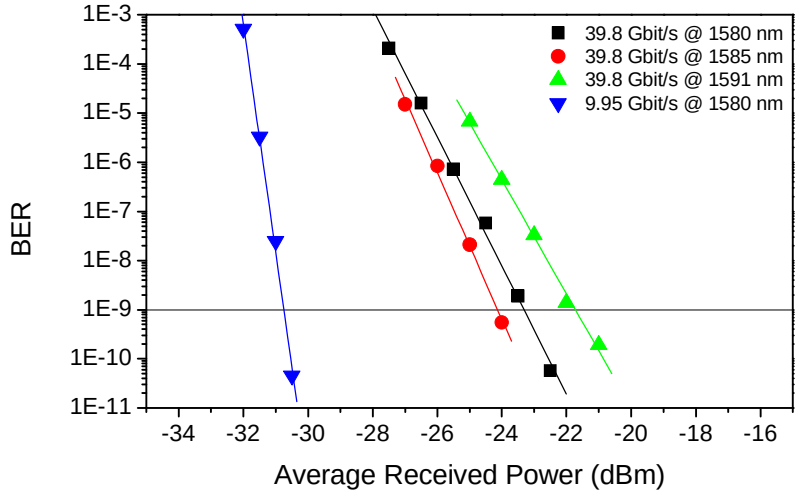

Figure 2.11: Measured BER curves for for 39.8 Gbit/s DPSK demodulated signal at 1580 nm, 1585 nm, and 1591 nm, and for 9.95 Gbit/s DPSK demodulated signal at 1580 nm, using the PBG fiber based DPSK demodulator.

improved sensitivity compared to the 39.8 Gbit/s operation is due to the reduced signal bit rate and much lower demodulated signal pulse duty cycle. These results demonstrate successful DPSK demodulation at 10 and 40 Gbit/s using a polarization delay interferometer implemented by a 2.4 m air-guiding PBG fiber. Very stable operation is observed during the measurements. Therefore, the short length of the fiber shows the potential for a compact and stable polarization delay interferometer, that is suitable for DPSK demodulation in direct detection systems.

2.3 Summary

In this chapter, we presented two alternative ways of performing phase-to-intensity modulation conversion in a demodulator that allows DPSK to be detected by direct detection.

Demodulation of DPSK signals up to 40 Gbit/s using a Michelson interferometer based demodulator was experimentally investigated. The proposed demodulator consisted of a Michelson interferometer made from a coupler and two waveguides, and the reflections were obtained by two Bragg gratings written in the waveguides. By placing the gratings at different positions in the waveguides, certain delay (between the two forward and backward propagating signals in the two waveguides) was accumulated, and phase-to-intensity modulation conversion was achieved at the output of the device. Error free demodulation of DPSK signals at 10, 20, 30, and 40 Gbit/s was successfully demonstrated. At the output of the demodulator, it was observed that, the duty cycle of the demodulated signal in RZ-AMI format increased as the input signal bit rate increased. Compared to the fiber based one bit delay MZI that requires active stabilization, the device only uses one coupler, therefore is compact and inherently stable. In Mach-Zehnder delay interferometers, the periodicity of their transfer functions allows easy adjustment to different signal wavelengths. However, the proposed structure needs to be customized for a given wavelength range due to the limited bandwidth of the Bragg gratings.

A polarization delay interferometer utilizing the large birefringence of air-guiding photonic bandgap fiber was also presented and experimentally investigated. Using only 2.4 m long PBG fiber, phase-to-intensity modulation conversion was successfully performed for DPSK signal at 10

and 40 Gbit/s. Fiber birefringence of 3.1×10^{-3} was observed and used to realize the $\sim$ 25 ps interferometer delay. Such a high birefringence value is an order of magnitude higher than for conventional polarization maintaining fibers. Therefore, to obtain the same interferometer delay, an order of magnitude shorter air-guiding PBG fiber can be used instead of the conventional polarization maintaining fiber. In the presented implementation, butt coupling of the PBG fiber to and from standard single mode fiber resulted in a large total device loss. Such coupling loss could be minimized by proper splicing, as shown in [19]. Moreover, utilizing the large birefringence of the PBG fiber at the bandgap edge limits the ability of the PBG fiber based demodulator to be easily tuned to different channel wavelengths. Operations at desired wavelengths would require scaling of the PBG structure that could shift the bandgap of the fiber.

Both structures can be used at the transmitter side to generate optical RZ-AMI signals with desired duty cycles. For the Michelson interferometer based structure, various signal pulse widths can be realized by tailoring the relative positions of the two waveguide Bragg gratings in each arm of the coupler. For the PBG fiber based structure, careful selection of the operating wavelength will lead to generated signals with desired duty cycles.

References to Chapter 2

[1] Y. Awaji, T. Kuri, and W. Chujo. "Differential-phase-to-intensity conversion based on injection locking of a semiconductor laser", *Optics Letters*, vol. 26, no. 20, pp. 1538–1540, October 2001.

[2] I. Lyubomirsky and C. C. Chien. "DPSK demodulator based on optical discriminator filter", *IEEE Photonics Technology Letters*, vol. 17, no. 2, pp. 492–494, February 2005.

[3] T.-Y. Kim, S. Hann, W.-T. Han, and C.-S. Park. "π-phase shifted fiber Bragg grating-based optical DPSK demodulator with optically tunable phase shifter", in *Technical Digest Optical Fiber Communication Conference, OFC'06,* Anaheim, California, U.S.A., Paper OWI49, March 2006.

[4] L. Christen, Y. K. Lizé, S. Nuccio, J.-Y. Yang, P. Saghari, and A. E. Willner. "Fiber Bragg grating balanced DPSK demodulation", in *Technical Digest IEEE Lasers and Electro-Optics Society Annual Meeting, LEOS'06,* Montreal, Quebec, Canada, pp. 563–564, Paper WP2, October 2006.

[5] E. Ciaramella, G. Contestabile, and A. D'Errico. "A novel scheme to detect optical DPSK signals", *IEEE Photonics Technology Letters*, vol. 16, no. 9, pp. 2138–2140, September 2004.

[6] C. W. Chow and H. K. Tsang. "Polarization-independent DPSK demodulation using a birefringent fiber loop", *IEEE Photonics Technology Letters*, vol. 17, no. 6, pp. 1313–1315, June 2005.

[7] P. J. Winzer and J. Leuthold. "Return-to-zero modulator using a single NRZ drive signal and an optical delay interferometer", *IEEE Photonics Technology Letters*, vol. 13, no. 12, pp. 1298–1300, December 2001.

[8] X. Wei, X. Liu, S. Chandrasekhar, A. H. Gnauck, G. Raybon, J. Leuthold, and P. J. Winzer. "40 Gb/s duobinary and modifiend duobianry transmitter based on an optical delay interferometer", in *Proceedings European Conference on Optical Communication, ECOC'02,* Copenhagen, Denmark, vol. 4, Paper 9.6.3, September 2002.

[9] Y. Miyamoto, A. Hirano, S. Kuwahara, M. Tomizawa, and Y. Tada. "Novel modulation and detection for bandwidth-reduced RZ formats using duobinary-mode splitting in wideband PSK/ASK conversion", *Journal of Lightwave Technology*, vol. 20, no. 12, pp. 2067–2078, December 2002.

[10] X. Wei, A. H. Gnauck, X. Liu, and J. Leuthold. "Nonlinearity tolerance of RZ-AMI format in 42.7 Gbit/s long-haul transmission over standard SMF spans", *Electronics Letters*, vol. 39, no. 20, pp. 1459–1460, October 2003.

[11] P. J. Winzer, A. H. Gnauck, G. Raybon, S. Chandrasekhar, Y. Su, and J. Leuthold. "40 Gb/s return-to-zero alternate-mark-inversion

(RZ-AMI) transmission over 2000 km", *IEEE Photonics Technology Letters*, vol. 15, no. 5, pp. 766–768, May 2003.

[12] C. Peucheret, Y. Geng, M. Svalgaard, B. Zsigri, H. R. Sørensen, N. Chi, H.-J. Deyerl, M. Kristensen, and P. Jeppesen. "Direct UV written Michelson interferometer for RZ signal generation using phase-to-intensity modulation conversion", *IEEE Photonics Technology Letters*, vol. 17, no. 8, pp. 1674–1676, August 2005.

[13] M. Svalgaard. "Direct UV-written integrated optical components", in *Technical Digest Optical Fiber Communication Conference, OFC'04,* Los Angeles, California, U.S.A., Paper FK2, February 2004.

[14] M. Svalgaard. "Direct writing of planar waveguide power splitters and directional couplers using a focused ultraviolet laser beam", *Electronics Letters*, vol. 33, no. 20, pp. 1694–1695, September 1997.

[15] G. D. Maxwell and B. J. Ainslie. "Demonstration of a directly written directional coupler using UV-induced photosensitivity in a planar silica waveguide", *Electronics Letters*, vol. 31, no. 2, pp. 95–96, January 1995.

[16] M. Svalgaard, K. Færch, and L.-U. Andersen. "Variable optical attenuator fabricated by direct UV writing", *Journal of Lightwave Technology*, vol. 21, no. 9, pp. 2097–2103, September 2003.

[17] C. Peucheret, B. Zsigri, H. R. Sørensen, M. Svalgaard, N. Chi, H.-J. Deyerl, M. Kristensen, and P. Jeppesen. "Direct UV written Michelson interferometer for RZ signal generation using phase-to-intensity modulation conversion", in *Proceedings European Conference on Optical Communication, ECOC'04,* Stockholm, Sweden, vol. 2, pp. 288–289, Paper Tu4.7.5, September 2004.

[18] J. C. Knight, J. Broeng, T. A. Birks, and P. S. J. Russell. "Photonic bandgap guidance in optical fibers", *Science*, vol. 282, no. 5393, pp. 1476–1478, November 1998.

[19] T. P. Hansen, J. Broeng, C. Jakobsen, G. Vienne, H. R. Simonsen, M. D. Nielsen, P. M. W. Skovgaard, J. R. Folkenberg,

and A. Bjarklev. "Air-guiding photonic bandgap fibers: Spectral properites, macrobending loss, and practical handling", *Journal of Lightwave Technology*, vol. 22, no. 1, pp. 11–15, January 2004.

[20] X. Chen, M.-J. Li, N. Venkataraman, M. T. Gallagher, W. A. Wood, A. M. Crowley, J. P. Carberry, L. A. Zenteno, and K. W. Koch. "Highly birefringent hollow-core photonic bandgap fiber", *Optics Express*, vol. 12, no. 16, pp. 3888–3893, August 2004.

[21] M. Wegmuller, N. Gisin, T. P. Hansen, C. Jakobsen, and J. Broeng. "Polarization properties of an air-guiding photonic bandgap fibre for 1550 nm transmission", in *Proceedings European Conference on Optical Communication, ECOC'04,* Stockholm, Sweden, vol. 1, pp. 78–79, Paper Mo4.3.7, September 2004.

[22] M. Wegmuller, M. Legré, N. Gisin, T. P. Hansen, C. Jakobsen, and J. Broeng. "Experimental investigation of the polarization properties of a hollow core photonic bandgap fiber for 1550 nm", *Optics Express*, vol. 13, no. 5, pp. 1457–1467, March 2005.

[23] M. Shah Alam, K. Saitoh, and M. Koshiba. "High group birefringence in air-core photonic bandgap fibers", *Optics Letters*, vol. 30, no. 8, pp. 824–826, April 2005.

[24] F. Poletti, N. G. R. Broderick, D. J. Richardson, and T. M. Monro. "The effect of core asymmetries on the polarization properties of hollow core photonic bandgap fibers", *Optics Express*, vol. 13, no. 22, pp. 9115–9124, October 2005.

[25] C. Peucheret, B. Zsigri, T. Hansen, and P. Jeppesen. "10 Gbit/s transmission over air-guiding photonic bandgap fibre at 1550 nm", *Electronics Letters*, vol. 41, no. 1, pp. 27–29, January 2005.

[26] C. Peucheret, Y. Geng, B. Zsigri, T. T. Alkeskjold, T. P. Hansen, and P. Jeppesen. "Demodulation of DPSK signals up to 40 Gb/s using a highly birefringent photonic bandgap fibre", in *Proceedings OptoElectronics and Communications Conference, OECC'05,* Seoul, Korea, pp. 50–51, Paper 5D1-2, July 2005.

[27] C. Peucheret, Y. Geng, B. Zsigri, T. T. Alkeskjold, T. P. Hansen, and P. Jeppesen. "Demodulation of DPSK signals up to 40 Gb/s using a highly birefringent photonic bandgap fiber", *IEEE Photonics Technology Letters*, vol. 18, no. 12, pp. 1392–1394, June 2006.

[28] B. L. Heffner. "Automated measurement of polarization mode dispersion using Jones matrix eigenanalysis", *IEEE Photonics Technology Letters*, vol. 4, no. 9, pp. 1066–1069, September 1992.

[29] B. L. Heffner. "Accurate, automated measurement of differential group delay dispersion and principal state variation using Jones matrix eigenanalysis", *IEEE Photonics Technology Letters*, vol. 5, no. 7, pp. 814–817, July 1993.

[30] A. Buxens, H. N. Poulsen, A. T. Clausen, and P. Jeppesen. "Gain flattened L-band EDFA based on upgraded C-band EDFA using forward ASE pumping in an EDF section", *Electronics Letters*, vol. 36, no. 9, pp. 821–823, October 2000.

Chapter 3

Optical Labeling using DPSK Signals

3.1 Introduction

With the introduction of wavelength division multiplexing (WDM) as a technology to make effective use of the fiber bandwidth and achieve high system capacity, the concept of carrying Internet protocol (IP) directly over WDM has attracted a lot of interest [1]. By avoiding the intermediate synchronous digital hierarchy (SDH) and/or asynchronous transfer mode (ATM) layers, IP-over-WDM would provide a significant improvement of the network throughput, thus yield a more efficient network [2]. The use of optical labels to implement packet routing and forwarding functionalities directly in the optical layer without touching the optical payload would overcome the electronic bottlenecks, by allowing low speed electronics in the core nodes for label processing [3].

Several techniques have been proposed for labeling optical packets [4], amongst them bit-serial method [5–8], label wavelength method [9–11], optical subcarrier multiplexing (SCM) method [12–14], and orthogonal modulation method [15–24].

The optical label signal contains the information needed to route and/or forward packets. The label is only of local importance. At each core node, the label is extracted and the information is used to forward the packets further. Meanwhile, a new label is added for the usage at next node. This process is called label swapping. In general,

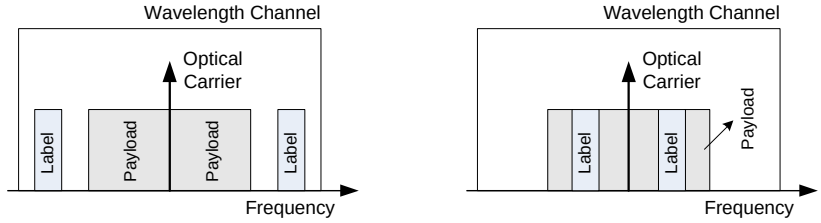

Figure 3.1: SCM label and payload in frequency domain. Conventional SCM (left) and in-band SCM (right) [25].

the label signal has a bit rate that is much lower than the payload bit rate, because of the small amount of control information. This lower bit rate feature allows us to process the label in the electronic domain and keep the payload in the optical domain, and therefore avoids the electronic bottleneck in the core network nodes. In the following we give a brief introduction to two ways of adding the optical label onto a data payload, namely, the optical SCM method and the orthogonal modulation method.

3.1.1 Optical Subcarrier Multiplexing Labeling

Optical SCM labeling has been suggested as a possible way to code the optical label onto the data payload, where the labeling information is carried on a subcarrier frequency along with the payload [13]. By accommodating both the label and payload on the same optical wavelength, two subcarrier sidebands appear centered around the payload spectrum. This is referred to as conventional SCM labeling, and illustrated in Figure 3.1 [25].

Using optical SCM labeling, the bookkeeping in the routing nodes becomes simpler, as the label and payload travel simultaneously through the network. Furthermore, the label data can be completely asynchronous to the payload data, resulting in simplified network control.

The main drawback is the radio-frequency (RF) fading due to the interaction between the subcarrier and the fiber dispersion [26]. Moreover, for high bit rate payload, the subcarrier needs to be placed at a very high frequency, which requires more advanced and expensive electronics as well as increased wavelength channel spacing.

In-band SCM labeling is proposed to provide better spectral efficiency and reduce the RF signal generation/detection complexity (due to the lower subcarrier frequency) [27]. This is also presented in Figure 3.1. The in-band SCM labeling using differential phase shift keying (DPSK) payload as proposed in [27] additionally takes advantages of the attractive properties of the DPSK format, and can be used for signaling, as presented in [28], by benefiting from e.g. the possibility of attaching additional labels or tones to the payload signal. Recently, in-band SCM has been suggested as a WDM monitoring technique by using the amplitude modulated (AM) subcarrier signal as the pilot tone to monitor DPSK WDM systems [29].

In section 3.2, we present an experimental investigation of in-band SCM labeling using 40 Gbit/s DPSK payload and 25 Mbit/s nonreturn-to-zero (NRZ) SCM label. We verify the transmission feasibility of such a labeling scheme by sending the labeled signal over an 80 km nonzero dispersion shifted fiber (NZDSF) span. The work was initiated by Thomas Flarup (former COM•DTU student), and done in cooperation with Thomas Flarup, Christophe Peucheret from COM•DTU, and Juan Jose Vegas Olmos who formerly worked at Eindhoven University of Technology, The Netherlands.

3.1.2 Orthogonal Labeling

Orthogonal labeling schemes encode the optical label information using the optical carrier itself, while using orthogonal modulation formats for the payload and label separately. In this thesis, the term 'orthogonal' is used to imply that the two modulation formats do not interact significantly. Therefore, if the payload is intensity modulated, the label can be added by either phase [18,23] or frequency [17,19] modulation of the optical carrier.

This technique allows all-optical label swapping and has a compact spectrum, as well as high scalability to high bit-rate [23]. Since the payload is coupled to the label in the same wavelength channel, the bookkeeping in the routing nodes becomes easier. Furthermore, the label and payload are decoupled regarding timing, thus only synchronization at packet level is needed, not at bit level.

The main drawback is related to crosstalk between the two mod-

ulation formats used for the payload and label. A limited extinction ratio (ER) of the payload is necessary to minimize the crosstalk [16]. Moreover, fiber dispersion and nonlinearities also affect this labeling scheme, through phase (or frequency) to intensity conversion due to dispersion and interferometric effects in the fiber links during propagation [4].

In section 3.3, we report a study of an orthogonal labeling scheme using a 40 Gbit/s return-to-zero (RZ) payload and a 2.5 Gbit/s DPSK label. By deploying a DC-balanced line encoding to the payload, the crosstalk between the two orthogonal modulation formats is significantly suppressed. The transmission and label swapping functionality is demonstrated for a 4×40 Gbit/s WDM labeled signal. The work was done in cooperation with Nan Chi and Lin Xu, who both worked formerly at COM•DTU.

3.2 In-band SCM Labeling with 40 Gbit/s DPSK Payload

In this section, we report an experimental investigation of the performance and transmission property of the in-band SCM labeling scheme. The presented scheme uses 40 Gbit/s DPSK payload and 25 Mbit/s NRZ SCM label signal.

3.2.1 Experimental Setup

Figure 3.2 shows the experimental setup used for investigation of the in-band SCM labeling scheme [30]. The baseband NRZ label signal generated from the 25 Mbit/s pattern generator is first up-converted to the subcarrier frequency. This is done by mixing the signal with a clock signal at the subcarrier frequency in the SCM label signal generator. The resulting 25 Mbit/s SCM label signal is then used to drive an electroabsorption modulator (EAM). In order to impose the label signal onto the optical carrier, the output of a continuous wave (CW) laser at 1554.9 nm is intensity modulated by the EAM. The signal is then amplified in an erbium doped fiber amplifier (EDFA) and phase modulated in a $LiNbO_3$ phase modulator driven with a 40 Gbit/s 2^{31}-1 pseudo random bit sequence (PRBS) payload, resulting in an in-band

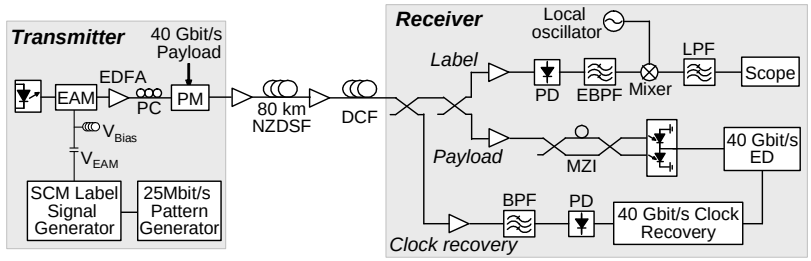

Figure 3.2: Experimental setup for in-band SCM labeling with 40 Gbit/s DPSK payload. EAM: electroabsorption modulator; PC: polarization controller; PM: phase modulator; EDFA: erbium doped fiber amplifier; NZDSF: non-zero dispersion shifted fiber; DCF: dispersion compensation fiber; PD: photodiode; EBPF: electrical bandpass filter; BPF: optical bandpass filter; LPF: electrical lowpass filter; MZI: Mach-Zehnder interferometer; ED: error detector [30].

SCM labeled 40 Gbit/s DPSK signal. The transmission span includes 80 km of NZDSF with a dispersion parameter of 5.7 ps/km/nm, and a matching length of dispersion compensation fiber (DCF) in a post-compensation configuration. The total fiber span loss is 23.5 dB, and is compensated for by two EDFAs. At the receiver, a small part of the signal is tapped for clock recovery. Phase-to-intensity modulation conversion is performed through an optical bandpass filter, the signal is then detected and sent to the clock recovery module to extract the 40 GHz clock. The main part of the received signal is split between the payload and label receivers. The balanced pre-amplified DPSK payload receiver consists of an EDFA, a one bit delay Mach-Zehnder interferometer (MZI) for demodulation, two 45 GHz photodiodes in a balanced configuration, and a 40 Gbit/s error detector (ED) for measurement. The label signal is pre-amplified, detected, and filtered by an electrical bandpass filter. The filtered SCM label signal is envelope recovered (down-converted to the baseband) by mixing the signal with a local oscillator operating at the subcarrier frequency. The envelope recovered signal is then lowpass filtered and visualized on an oscilloscope.

3.2.2 Results

In this experiment, the EAM driving voltage is chosen to vary from 0 to 150 mV, corresponding to modulation depths between $\eta = 0$ and

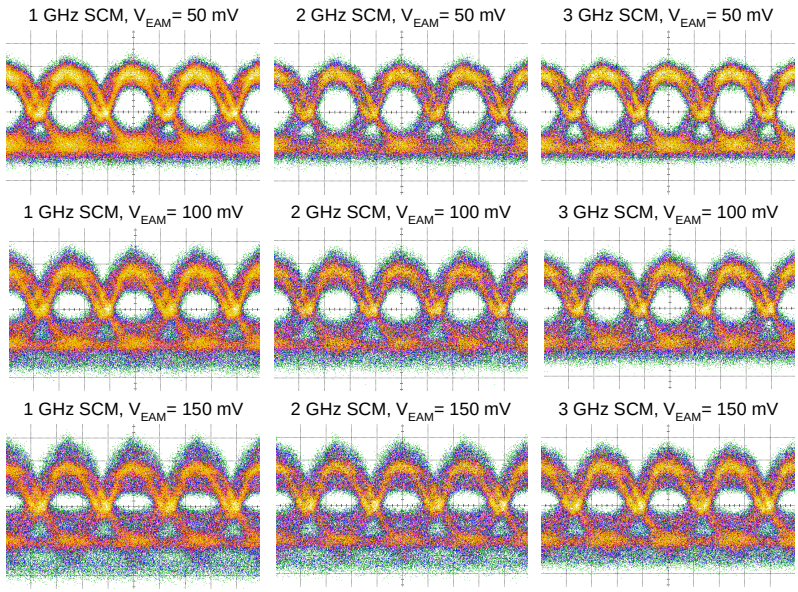

Figure 3.3: 40 Gbit/s DPSK payload eye diagrams for nine combinations of subcarrier frequencies (1, 2, and 3 GHz) and EAM driving voltages (50, 100, and 150 mV, corresponding to modulation depths η of 0.17, 0.33 and 0.45, respectively). Horizontal scale: 10 ps/div [30].

$\eta = 0.45$. The modulation depth is defined as $\eta = (I_0 - I)/I_0$, where I is the output intensity and I_0 is the value of I with no EAM driving signal applied. The subcarrier frequency of the 25 Mbit/s SCM label signal is chosen to be 1, 2 or 3 GHz.

In the back-to-back case (i.e. when the output of the transmitter is directly connected to the receiver), the DPSK payload eye diagrams and the corresponding detected SCM label signals (both before and after down-conversion to the baseband) for nine combinations of subcarrier frequencies (1, 2, and 3 GHz) and EAM driving voltages (50, 100, and 150 mV, leading to modulation depths η of 0.17, 0.33 and 0.45, respectively) are shown in Figure 3.3 [30] and Figure 3.4 [25], respectively. An increase of the EAM driving voltage corresponds to an increase of the SCM label modulation depth. Therefore, as seen in the figures, as the EAM driving voltage increases, the DPSK payload eye closes and the detected label signal amplitude increases. Furthermore, it can be

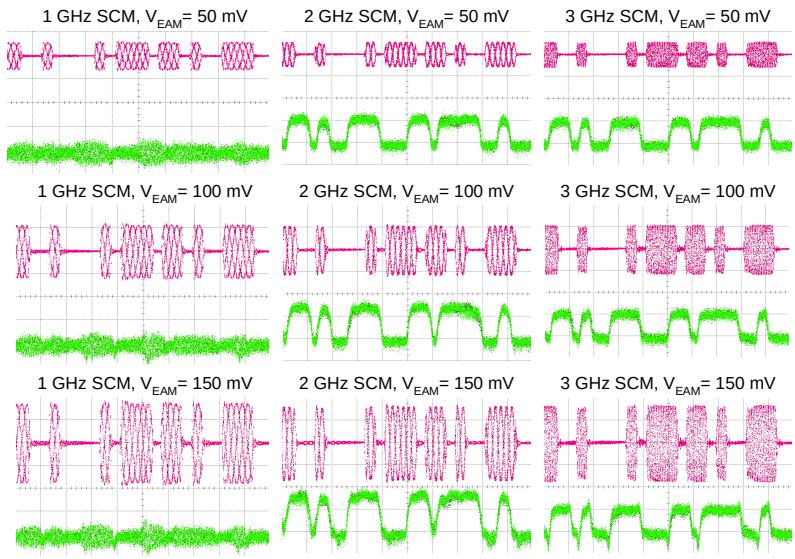

Figure 3.4: Detected 25 Mbit/s SCM label signal before (red) and after (green) down-conversion to the baseband, for nine combinations of subcarrier frequencies (1, 2, and 3 GHz) and EAM driving voltages (50, 100, and 150 mV, corresponding to modulation depths η of 0.17, 0.33 and 0.45, respectively). Horizontal scale: 100 ns/div [25].

seen that, as the subcarrier frequency decreases, due to the more severe interaction between the payload and label, the DPSK payload eye closes. More recent work [31] has shown that, the effect of the superimposed SCM label on the performance of the DPSK payload can be minimized when the label is centered at a subcarrier frequency equal to half the bit rate of the DPSK signal. For the label signal, the envelope of the detected SCM label appears unaffected as the subcarrier frequency decreases, while the pattern of the envelope recovered signal cannot be distinguished at 1 GHz, because of the limited received power after down-conversion.

Bit error rate (BER) measurements are performed on the 40 Gbit/s DPSK payload signal, while the 25 Mbit/s label signal is monitored on an oscilloscope before and after down-conversion to the baseband. The label signal quality is only qualitatively assessed due to the performance of the suboptimal label receiver.

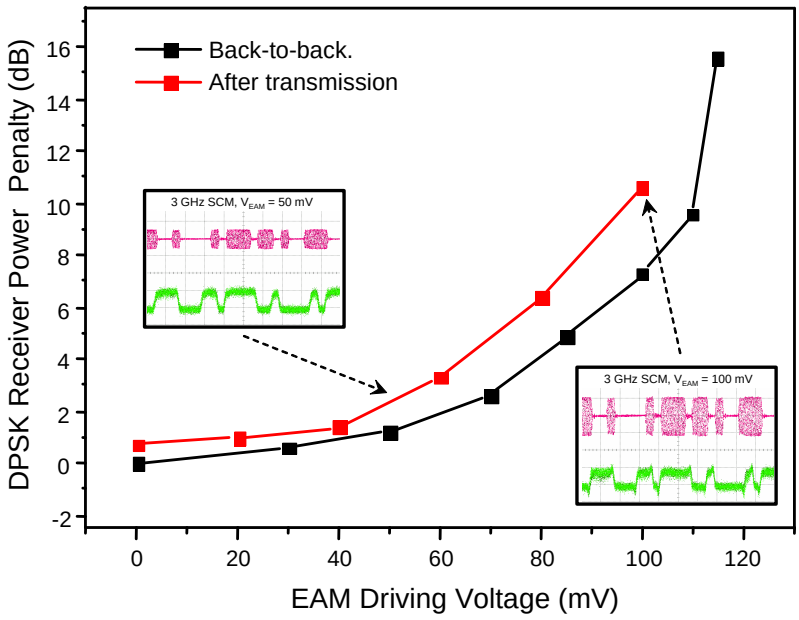

Figure 3.5: DPSK payload receiver penalty as a function of EAM driving voltage, in the back-to-back case (black line), and after transmission over 80 km of post-compensated NZDSF (red line). The insets show the detected 25 Mbit/s SCM label signal after 80 km transmission, before (red) and after (green) down-conversion to the baseband, for a subcarrier frequency of 3 GHz and EAM driving voltages of 50 and 100 mV (corresponding to modulation depths η of 0.17 and 0.33, respectively). Horizontal scale: 100 ps/div [30].

Figure 3.5 [30] (black line) shows the back-to-back DPSK payload receiver penalty as a function of the EAM driving voltage for a 3 GHz subcarrier frequency. The 0 dB penalty reference is the back-to-back receiver sensitivity at a BER of 10^{-9} without any EAM driving voltage, which is -24.0 dBm. When increasing the EAM driving voltage, additional power penalty appears. However, at an EAM driving voltage of 50 mV (corresponding to a modulation depth of $\eta = 0.17$), the penalty is only 1.2 dB.

The transmission feasibility of the in-band SCM labeling of a 40 Gbit/s DPSK payload is investigated by transmitting the signal over 80 km of post-compensated NZDSF using a subcarrier frequency of 3 GHz. The

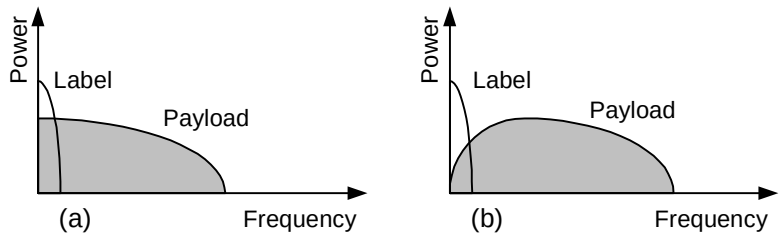

Figure 3.6: Illustration of RF frequency spectra for orthogonal ASK/DPSK labeled signal with (a) payload in PRBS pattern and (b) DC-null encoded payload [32].

DPSK payload receiver penalty as a function of the EAM driving voltage is also presented in Figure 3.5 (red line). Without label imposing (corresponding to an EAM driving voltage of 0 mV), the transmission penalty is 0.7 dB. At an EAM driving voltage of 50 mV, the additional transmission penalty is only 1.1 dB. Therefore, the in-band SCM labeled signal is demonstrated to be generated and transmitted over an 80 km NZDSF span without introducing significant penalty on the 40 Gbit/s DPSK payload, thus demonstrating the feasibility of this labeling scheme.

3.3 Transmission and Label Swapping of a 4×40 Gbit/s WDM Signals

In this section, we present an experimental investigation of an amplitude shift keying/differential phase shift keying (ASK/DPSK) labeling scheme using 40 Gbit/s RZ payload and 2.5 Gbit/s DPSK label. By employing 8B10B coding for the payload, the crosstalk between the two orthogonal modulation formats is significantly suppressed through spectrum shaping. The transmission and label swapping functionality are demonstrated for a 4×40 Gbit/s WDM labeled Signal.

3.3.1 Benefits of Using 8B10B Coding

As discussed in section 3.1.2, for the orthogonal labeling scheme, a limited ER of the payload is necessary to minimize the crosstalk between the two modulation formats used for the payload and label. In case of

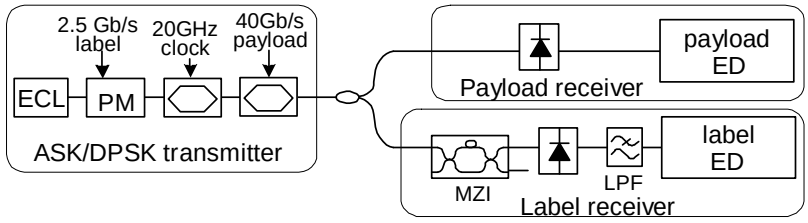

Figure 3.7: Experimental setup used to verify the performance of 8B10B coding applied in an ASK/DPSK labeling system. ECL: external cavity laser; PM: phase modulator; MZI: Mach-Zehnder interferometer; LPF: lowpass filter; ED: error detector [32].

ASK/DPSK labeling, where the payload is in RZ format and the label is in DPSK format, sufficient optical power for the payload is essential in order for the ASK signal to be able to carry the phase information of the label. In the RF domain, the crosstalk between the payload and label is generated by the spectra overlap of the payload and label. If the payload spectrum can be shaped to have a null at DC, the crosstalk will be suppressed significantly, as illustrated in Figure 3.6 [32]. Several coding techniques have been used to generate a DC-null spectrum, such as Manchester coding [33, 34] and 8B10B coding [35]. Manchester coding has advantages of enabling a simple clock extraction operation and robust burst mode data reception [34]. It is a 1B2B coding scheme and requires double bandwidth compared to NRZ coding [36]. Therefore, in this experiment, 8B10B coding is chosen as the coding technique because of its relatively high bandwidth efficiency (80%) [36].

In order to verify the effectiveness of the 8B10B coding scheme when it is applied to ASK/DPSK labeling, the setup shown in Figure 3.7 is used [32]. The output from an external cavity laser (ECL) operating at 1550 nm is sent through three consecutive modulators. The phase modulator driven with a 2.5 Gbit/s 2^{23}-1 PRBS is used to generate the 2.5 Gbit/s DPSK label signal. Two Mach-Zehnder modulators (MZMs), both in push-pull configuration, are used to generate the 40 Gbit/s RZ payload. The first MZM is biased at a peak of its transfer function and driven with a 20 GHz clock to generate RZ pulse train with 33% duty cycle. The second MZM is driven with a 40 Gbit/s 8B10B encoded data. The data is generated through encoding a 2^7-1 PRBS, thus yields a pe-

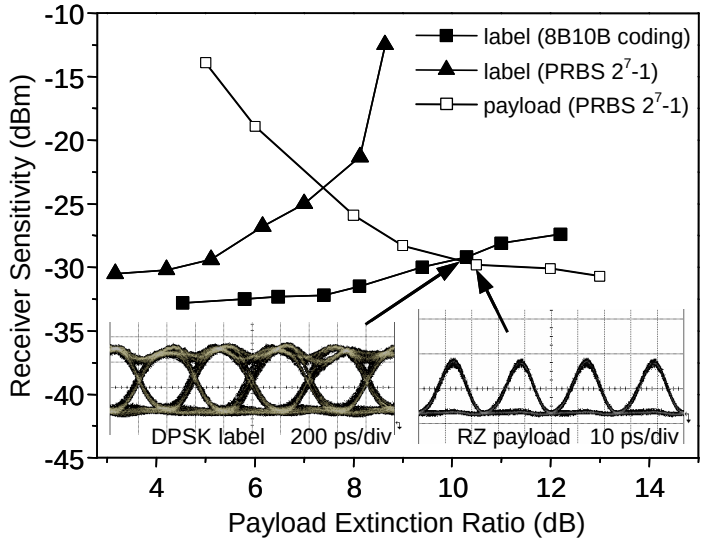

Figure 3.8: Measured receiver sensitivity for the payload and label vs. input extinction ratio of the payload. The insets show the eye diagrams of the 40 Gbit/s RZ payload and demodulated 2.5 Gbit/s DPSK label for an 8B10B encoded payload with an ER of 10.3 dB [32].

riod data pattern of 160 bits. The generated ASK/DPSK signal is split by a 3 dB coupler between the payload and label receivers. The payload receiver consists of a 50 GHz photodiode for detection and a 40 Gbit/s ED for measurement. The label receiver consists of a one bit delay MZI for demodulation, a 10 GHz photodiode for detection, a 1.8 GHz lowpass filter for out-of-band noise reduction, and a 2.5 Gbit/s ED for measurement. The MZI has a delay of approximately 8 cm, corresponding to one bit duration (400 ps) of the DPSK signal at 2.5 Gbit/s.

Figure 3.8 [32] shows the measured sensitivities of the payload and label as a function of the payload ER. The label is a 2.5 Gbit/s DPSK 2^{23}-1 PRBS signal. The payload is a 40 Gbit/s RZ signal, in 2^7-1 PRBS pattern in one case, and 8B10B encoded in another case. As shown in the figure, when the payload is a 2^7-1 PRBS, the balanced performance of the label and payload is obtained with a payload ER of ~ 7 dB. With this ER value, the label and payload receiver sensitivities at a BER of 10^{-9} are ~ -23 dBm. When the payload is 8B10B encoded, the balanced

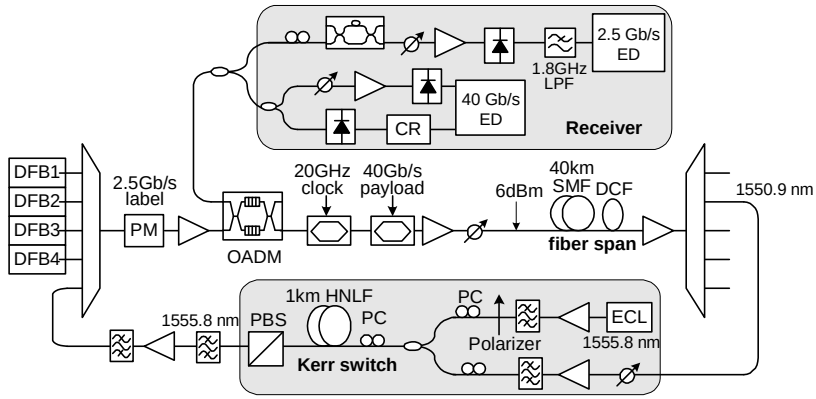

Figure 3.9: Experimental setup for WDM transmission and label swapping. DFB: distributed feedback laser; PM: phase modulator; OADM: optical add-drop multiplexer; SMF: standard single mode fiber; DCF: dispersion compensation fiber; ECL: external cavity laser; PC: polarization controller; HNLF: highly nonlinear fiber; PBS: polarization beam splitter; CR: clock recovery; LPF: lowpass filter; ED: error detector [32].

point is moved to a payload ER of 10.3 dB, and the label and payload receiver sensitivities are improved to ~ -30 dBm. It is clear that by using 8B10B coding for the payload, the limitation on the payload ER is overcome and the system performance is significantly improved. The insets of Figure 3.8 show the eye diagrams of the 40 Gbit/s RZ payload and demodulated 2.5 Gbit/s DPSK label for an 8B10B encoded payload with an ER of 10.3 dB.

3.3.2 WDM Transmission and Optical Label Swapping

Figure 3.9 shows the experimental setup for WDM transmission and label swapping [32]. The WDM source consists of four distributed feedback (DFB) lasers spaced 200 GHz, the outputs of which are combined in a WDM multiplexer. The wavelengths of the lasers are 1549.3 nm, 1550.9 nm, 1552.5 nm, and 1554.1 nm, respectively. All CW signals are simultaneously modulated by a phase modulator and two MZMs in a configuration similar to the one described above to generate a 4×40 Gbit/s WDM ASK/DPSK signal. The payload is 8B10B encoded with an initial ER of 12 dB. The WDM signal is then amplified to

an average power of 6 dBm and injected into the transmission span. The transmission span consists of 40 km of standard single mode fiber (SMF) with a matching length of DCF in a post-compensation scheme. The transmitted WDM signal is then demultiplexed and detected in the payload and label receivers, respectively. The receiver configurations are similar to the ones used to verify the performance of the 8B10B coding scheme, with an additional clock recovery circuit for payload BER measurements.

After transmission, label swapping is demonstrated for channel 2 signal at 1550.9 nm. The demultiplexed signal is combined with a CW pump at 1555.8 nm in a 3 dB coupler before being fed into the highly nonlinear fiber (HNLF) and subsequent polarization beam splitter (PBS), where wavelength conversion and label erasure are realized. Three polarization controllers are used to fine adjust the states of polarization (SOPs) of the CW pump light and the ASK/DPSK signal. At the HNLF input, the signal power is 20 dBm and the pump power is 15 dBm. At the PBS output, the demultiplexed ASK/DPSK signal at 1550.9 nm is converted to a pure ASK signal at 1555.8 nm. This method of label erasure making use of a Kerr switch [37] is based on a polarizer that, for proper adjustment, blocks the incoming signal in the absence of the pump. In the presence of the pump, cross phase modulation (XPM) will induce a polarization rotation of the CW signal that will align its SOP with that of the polarizer. As a result, the ASK payload data is copied onto the new optical carrier, while the DPSK label information is erased. In this experiment, the PBS is used as a polarizer. Because there is only one phase modulator available in the setup, the label-erased signal is first multiplexed with the four DFB lasers and then injected into the same phase modulator for the new label insertion. In this case, an optical add-drop multiplexer (OADM) is used to extract the signal at 1555.8 nm after transmission and label swapping. The ER of the label erased signal is slightly degraded to about 9 dB due to the residual phase shift induced by the Kerr switch. However, this value of ER is sufficient for payload and label detection.

Figure 3.10 shows the measured optical spectra at the output of the phase modulator, of the initial 4×40 Gbit/s WDM ASK/DPSK signals, and the spectra before and after wavelength conversion and label erasure. Figure 3.11 shows the eye diagrams for the demultiplexed 40 Gbit/s

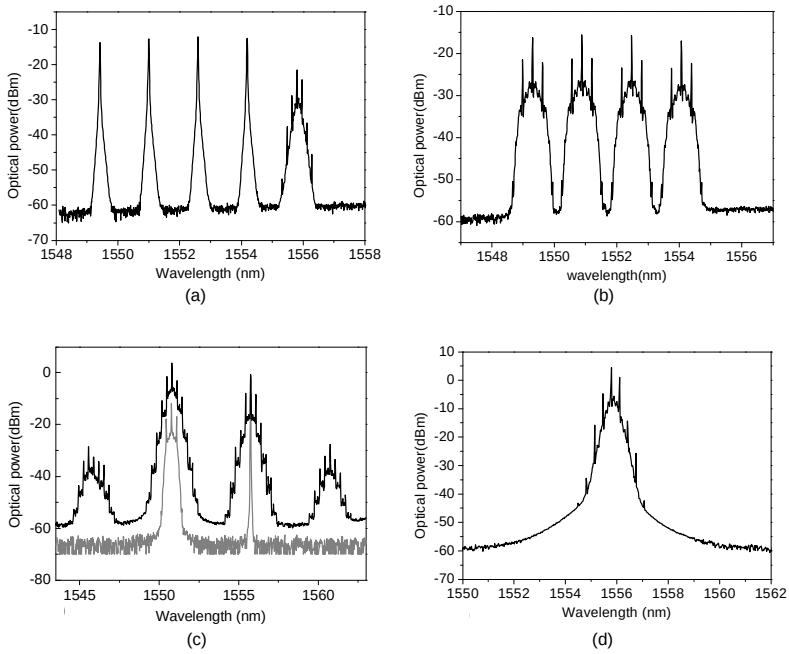

Figure 3.10: Measured optical spectra (a) at the output of the phase modulator, (b) of the initial 4×40 Gbit/s WDM ASK/DPSK signals, (c) at the input (gray line) and output (black line) of HNLF, (d) of received signal after transmission and label swapping. Resolution bandwidth: 0.01 nm.

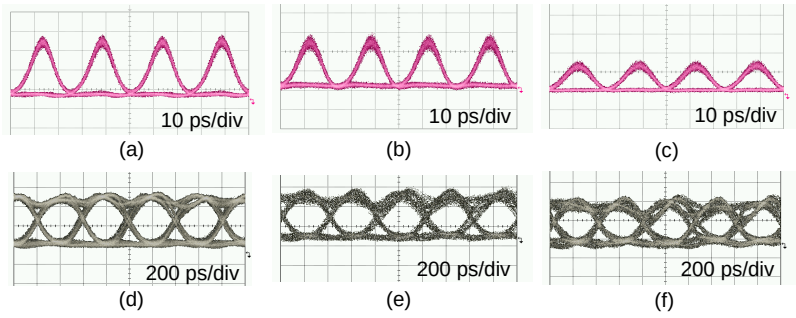

Figure 3.11: Eye diagrams of the demultiplexed 40 Gbit/s RZ payload in the back-to-back case (a), after 40 km transmission (b), and after label swapping (c); and 2.5 Gbit/s DPSK label in the back-to-back case (d), after 40 km transmission (e), and after label swapping (f).

RZ payload and 2.5 Gbit/s DPSK label in the back-to-back case, after 40 km transmission and after label swapping. Clear and open eyes can be obtained for both the payload and label after transmission and label swapping. These results indicate that the WDM transmission and label swapping utilizing the Kerr switch have very little detrimental effect on the signal.

The measured BER curves for payload and label in the back-to-back case and after transmission are shown in Figure 3.12. The results show that error free operation of all four channels can be achieved after 40 km transmission. For the payload the transmission penalty is less than 1 dB, while for the label it is less than 1.5 dB.

Figure 3.13 shows the measured BER curves for the demultiplexed channel payload and label after label swapping. For comparison, BER curves in the back-to-back case are also presented in the figure. The total power penalty induced by transmission and label swapping is 3.3 dB for the payload and 0.3 dB for the label. The high degradation of the payload sensitivity is mainly due to the reduction of the ER after label swapping. These results demonstrate successful transmission of 4×40 Gbit/s ASK/DPSK signals and label updating of one of the WDM channels.

3.4 Summary

We experimentally investigated the feasibility of in-band SCM labeling using 40 Gbit/s DPSK payload and 25 Mbit/s NRZ SCM label. We compared both the payload and label signal quality using different label modulation indices and subcarrier frequencies. With a label modulation depth of $\eta = 0.17$ and a subcarrier frequency of 3 GHz, 1.2 dB payload receiver power penalty was measured compared to the back-to-back sensitivity without in-band SCM labeling. This labeled signal was transmitted over 80 km post-compensated NZDSF span. The additional transmission penalty was only 1.1 dB. We therefore show that the subcarrier frequency can be reduced to only a few GHz with very small payload receiver penalty compared to a pure DPSK signal without any label. Operating at such relatively low subcarrier frequencies makes the subcarrier label signal processing simple and cost effective.

The performance of the ASK/DPSK labeling scheme, where the payload was a 40 Gbit/s RZ signal and the label was a 2.5 Gbit/s DPSK

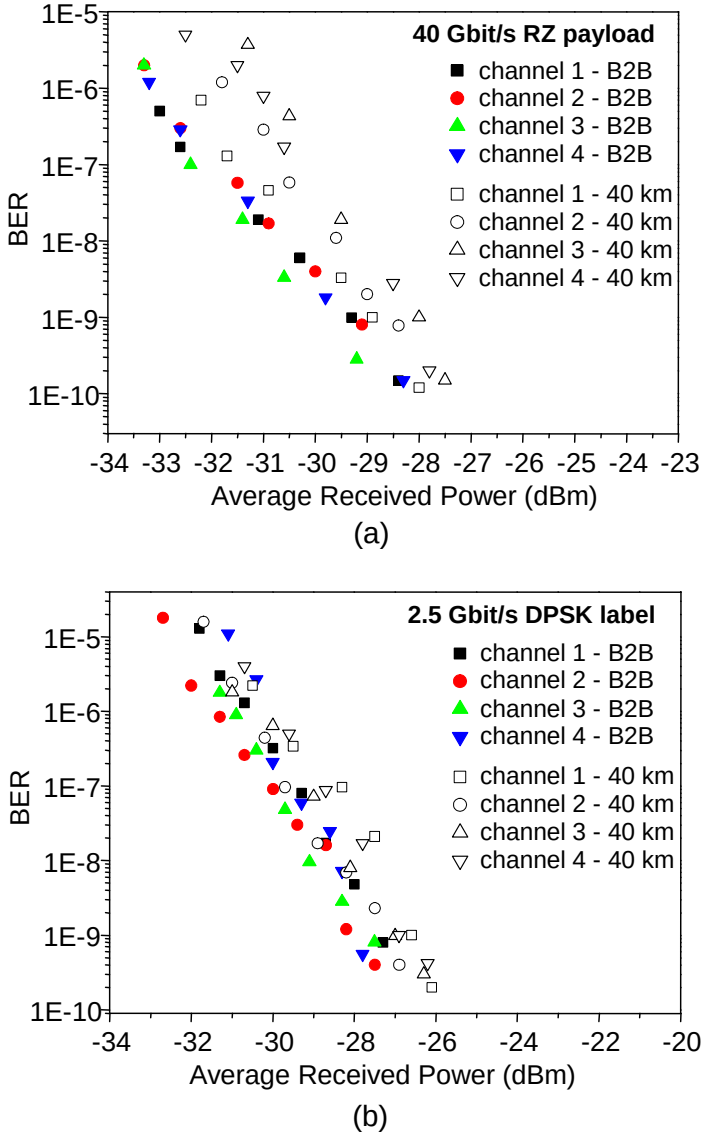

Figure 3.12: Measured BER curves for the 40 Gbit/s RZ payload (a) and the 2.5 Gbit/s DPSK label (b) in the back-to-back case and after 40 km SMF transmission.

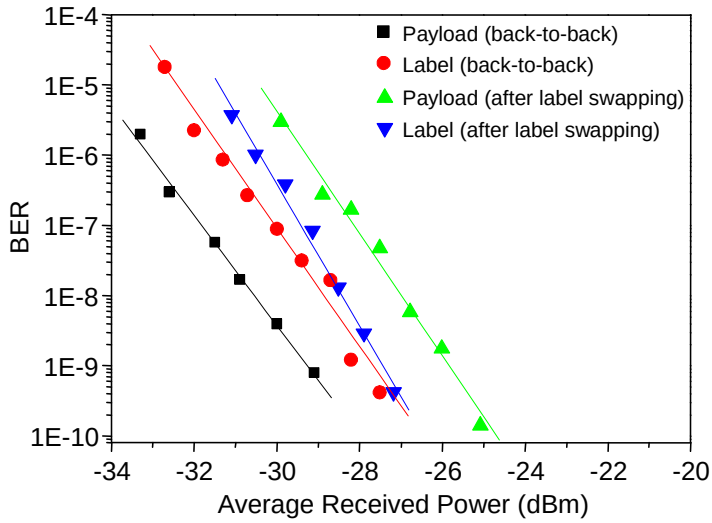

Figure 3.13: Measured BER curves for the demultiplexed channel 40 Gbit/s RZ payload and 2.5 Gbit/s DPSK label in the back-to-back case and after label swapping.

signal, was improved by using 8B10B encoding of the ASK payload. By using this method, 3.3 dB payload ER improvement was achieved for a balanced performance between the label and payload. WDM transmission for 4×40 Gbit/s ASK/DPSK signals, including label swapping of one of the channels using Kerr switching was successfully demonstrated. After 40 km SMF transmission, the payload experienced a transmission penalty of less than 1 dB, and the label showed a penalty of less than 1.5 dB. The cascaded transmission and label swapping of one of the channels induced an overall penalty of 3.3 dB for the payload and 0.3 dB for the label. We therefore show successful transmission and label updating for ASK/DPSK labeled signals in a WDM system.

By moving the subcarrier frequency inside the payload spectrum, in-band SCM labeling provides better spectral efficiency compared to the conventional SCM labeling scheme. However, the addition of the SCM label requires up-conversion to subcarrier frequency and down-conversion to baseband at the transmitter side and receiver side, respectively. These processes require more equipment in the system. Moreover, for optimal payload performance, the label needs to be centered at

a subcarrier frequency equal to half the bit rate of the payload signal. For high bit rate payload, this requirement will reduce the simplicity and cost effectiveness of the label processing in the electronic domain.

The orthogonal labeling scheme has been suggested as a competing scheme to SCM labeling, due to the compact spectrum, simple label swapping and high scalability to high bit rate. However, studies have shown that a limited ER of the payload is necessary to minimize the crosstalk and maintain the balanced performance between the payload and label. Alternatively, line coding techniques can be used to release the ER requirement of the payload, but at a cost of additional transmitter and/or receiver bandwidths.

References to Chapter 3

[1] N. Ghani. "Lambda-labeling: A framework for IP-over-WDM using MPLS", *Optical Networks Magazine*, vol. 1, no. 2, pp. 45–58, April 2000.

[2] N. Ghani, S. Dixit, and T.-S. Wang. "On IP-over-WDM integration", *IEEE Communications Magazine*, vol. 38, no. 3, pp. 72–84, March 2000.

[3] D. J. Blumenthal, B.-E. Olsson, G. Rossi, T. E. Dimmick, L. Rau, M. Mašanović, O. Lavrova, R. Doshi, O. Jerphagnon, J. E. Bowers, V. Kaman, L. A. Coldren, and J. Barton. "All-optical label swapping networks and technologies", *Journal of Lightwave Technology*, vol. 18, no. 12, pp. 2058–2075, December 2000.

[4] Z. Zhu, V. J. Hernandez, M. Y. Jeon, J. Cao, Z. Pan, and S. J. Ben Yoo. "RF photonics signal processing in subcarrier multiplexed optical-label switching communication systems", *Journal of Lightwave Technology*, vol. 21, no. 12, pp. 3155–3166, December 2003.

[5] C. Guillemot, M. Renaud, P. Gambini, C. Janz, I. Andonovic, R. Bauknecht, B. Bostica, M. Burzio, F. Callegati, M. Casoni, D. Chiaroni, F. Clérot, S. L. Danielsen, F. Dorgeuille, A. Dupas, A. Franzen, P. B. Hansen, D. K. Hunter, A. Kloch, R. Krähenbühl, B. Lavigne, A. L. Corre, C. Raffaelli, M. Schilling, J.-C. Simon, and

L. Zucchelli. “Transparent optical packet switching: The European ACTS KEOPS project approach”, *Journal of Lightwave Technology*, vol. 16, no. 12, pp. 2117–2134, December 1998.

[6] C. Bintjas, N. Pleros, K. Yiannopoulos, G. Theophilopoulos, M. Kalyvas, H. Avramopoulos, and G. Guekos. “All-optical packet address and payload separation”, *IEEE Photonics Technology Letters*, vol. 14, no. 12, pp. 1728–1730, December 2002.

[7] B.-E. Olsson, P. Öhlén, L. Rau, G. Rossi, O. Jerphagnon, R. Doshi, D. S. Humphries, D. J. Blumenthal, V. Kaman, and J. E. Bowers. “Wavelength routing of 40 Gbit/s packets with 2.5 Gbit/s header erasure/rewriting using all-fibre wavelength converter”, *Electronics Letters*, vol. 36, no. 4, pp. 345–347, February 2000.

[8] N. Chi, P. V. Holm-Nielsen, L. Xu, J. Zhang, T. Tokle, and P. Jeppesen. “Cascaded transmission, packet switching and all-optical wavelength conversion for 40 Gbit/s RZ payload with 10 Gbit/s serial-bit label”, *Electronics Letters*, vol. 40, no. 21, pp. 1366–1367, October 2004.

[9] A. Okada. “All-optical packet routing in AWG-based wavelength routing networks using an out-of-band optical label”, in *Technical Digest Optical Fiber Communication Conference, OFC’02,* Anaheim, California, U.S.A., vol. 1, pp. 213–215, Paper WG1, March 2002.

[10] K. Shrikhande, I. M. White, M. S. Rogge, F.-T. An, A. Srivatsa, E. S. Hu, S. S.-H. Yam, and L. G. Kazovsky. “Performance demonstration of a fast-tunable transmitter and burst-mode packet receiver for HORNET”, in *Technical Digest Optical Fiber Communication Conference, OFC’01,* Anaheim, California, U.S.A., Paper ThG2, March 2001.

[11] N. Wada, H. Harai, W. Chujo, and F. Kubota. “Multi-hop, 40 Gbit/s variable length photonic packet routing based on multi-wavelength label switching, waveband routing, and label swapping”, in *Technical Digest Optical Fiber Communication Conference, OFC’02,* Anaheim, California, U.S.A., vol. 1, pp. 216–217, Paper WG3, March 2002.

[12] S. F. Su, A. R. Bugos, V. Lanzisera, and R. Olshansky. "Demonstration of a multiple-access WDM network with subcarrier-multiplexed control channels", *IEEE Photonics Technology Letters*, vol. 6, no. 3, pp. 461–463, March 1994.

[13] D. J. Blumenthal, A. Carena, L. Rau, V. Curri, and S. Humphries. "All-optical label swapping with wavelength conversion for WDM-IP networks with subcarrier multiplexed addressing", *IEEE Photonics Technology Letters*, vol. 11, no. 11, pp. 1497–1499, November 1999.

[14] B. Meagher, G. K. Chang, G. Ellinas, Y. M. Lin, W. Xin, T. F. Chen, X. Yang, A. Chowdhury, J. Young, S. J. Yoo, C. Lee, M. Z. Iqbal, T. Robe, H. Dai, Y. J. Chen, and W. I. Way. "Design and implementation of ultra-low latency optical label switching for packet-switched WDM networks", *Journal of Lightwave Technology*, vol. 18, no. 12, pp. 1978–1987, December 2000.

[15] N. Chi, B. Carlsson, J. Zhang, P. V. Holm-Nielsen, C. Peucheret, and P. Jeppesen. "Transmission performance of all-optically labelled packets using ASK/DPSK orthogonal modulation", in *Technical Digest IEEE Lasers and Electro-Optics Society Annual Meeting, LEOS'02,* Glasgow, Scotland, vol. 1, pp. 51–52, Paper MF3, November 2002.

[16] T. Koonen, Sulur, I. Tafur Monroy, J. Jennen, and H. de Waardt. "Optical labeling of packets in IP-over-WDM networks", in *Proceedings European Conference on Optical Communication, ECOC'02,* Copenhagen, Denmark, vol. 2, Paper 5.5.2, September 2002.

[17] E. N. Lallas, N. Skarmoutsos, and D. Syvridis. "An optical FSK-based label coding technique for the realization of the all-optical label swapping", *IEEE Photonics Technology Letters*, vol. 14, no. 10, pp. 1472–1474, October 2002.

[18] N. Chi, J. Zhang, P. V. Holm-Nielsen, C. Peucheret, and P. Jeppesen. "Transmission and transparent wavelength conversion of an optically labeled signal using ASK/DPSK orthogonal modulation", *IEEE Photonics Technology Letters*, vol. 15, no. 5, pp. 760–762, May 2003.

[19] J. Zhang, N. Chi, P. V. Holm-Nielsen, C. Peucheret, and P. Jeppesen. "A novel optical labeling scheme using a FSK modulated DFB laser integrated with an EA modulator", in *Technical Digest Optical Fiber Communication Conference, OFC'03,* Atlanta, Georgia, U.S.A., vol. 1, pp. 279–280, Paper TuQ5, March 2003.

[20] I. Tafur Monroy, E. J. M. Verdurmen, S. Sulur, A. M. J. Koonen, H. de Waardt, G. D. Khoe, N. Chi, P. V. Holm-Nielsen, J. Zhang, and C. Peucheret. "Performance of a SOA-MZI wavelength converter for label swapping using combined FSK/IM modulation format", *Optical Fiber Technology*, vol. 10, no. 1, pp. 31–49, 2004.

[21] N. Chi, P. V. Holm-Nielsen, P. Jeppesen, C. Peucheret, J. Zhang, J. J. Vegas Olmos, and I. Tafur Monroy. "Optical label swapping of payloads up to 40 Gb/s using an orthogonally modulated label", in *Technical Digest IEEE Lasers and Electro-Optics Society Annual Meeting, LEOS'04,* Rio Grande, Puerto Rico, vol. 2, pp. 851–852, Paper ThM4, November 2004, Invited paper.

[22] N. Chi, L. Xu, J. Zhang, P. V. Holm-Nielsen, C. Peucheret, C. Mikkelsen, H. Ou, J. Seoane, and P. Jeppesen. "Orthogonal optical labeling based on a 40 Gbit/s DPSK payload and a 2.5 Gbit/s IM label", in *Technical Digest Optical Fiber Communication Conference, OFC'04,* Los Angeles, California, U.S.A., Paper FO6, February 2004.

[23] N. Chi, L. Xu, J. Zhang, P. V. Holm-Nielsen, C. Peucheret, S. Yu, and P. Jeppesen. "Improve the performance of orthogonal ASK/DPSK optical label switching by DC-balanced line encoding", *Journal of Lightwave Technology*, vol. 24, no. 3, pp. 1082–1092, March 2006.

[24] I. Tafur Monroy, E. van Breusegem, T. Koonen, J. J. Vegas Olmos, J. van Berkel, J. Jennen, C. Peucheret, and E. Zouganeli. "Optical label switched networks: Laboratory trial and network emulator in the IST-STOLAS project", *IEEE Communication Magazine*, vol. 44, no. 8, pp. 43–51, August 2006.

[25] T. Flarup. *Optical labelling of DPSK modulated signals at 40 Gbit/s.* Master's thesis, COM•DTU, Department of Commu-

nications, Optics & Materials, Technical University of Denmark, Kgs. Lyngby, Denmark, July 2004.

[26] R. Hui, B. Zhu, R. Huang, C. T. Allen, K. R. Demarest, and D. Richards. "Subcarrier multiplexing for high-speed optical transmission", *Journal of Lightwave Technology*, vol. 20, no. 3, pp. 417–427, 2002.

[27] I. Tafur Monroy, J. J. Vegas Olmos, A. M. J. Koonen, F. M. Huijskens, H. de Waardt, and G.-D. Khoe. "Optical label switching by using differential phase shift keying and in-band subcarrier multiplexing modulation format", *Optical Engineering*, vol. 43, no. 7, pp. 1476–1477, 2004.

[28] J. J. Vegas Olmos, I. Tafur Monroy, and A. M. J. Koonen. "Optical packet marking for fast discarding in an OLS scheme", in *Proceedings European Conference on Optical Communication, ECOC'04,* Stockholm, Sweden, vol. 3, pp. 650–651, Paper We4.P.091, September 2004.

[29] S. B. Jun, H. Kim, P. K. J. Park, J. H. Lee, and Y. C. Chung. "Pilot-tone-based WDM monitoring technique for DPSK systems", *IEEE Photonics Technology Letters*, vol. 18, no. 20, pp. 2171–2173, October 2006.

[30] T. Flarup, C. Peucheret, J. J. Vegas Olmos, Y. Geng, J. Zhang, I. Tafur Monroy, and P. Jeppesen. "Labeling of 40 Gbit/s DPSK payload using in-band subcarrier multiplexing", in *Technical Digest Optical Fiber Communication Conference, OFC'05,* Anaheim, California, U.S.A., Paper OWB7, March 2005.

[31] I. Tafur Monroy, J. J. Vegas Olmos, M. G. Larrode, T. Koonen, and C. D. Jiménez. "In-band 16-QAM and multi-carrier SCM modulation to label DPSK payload signals for IP packet routing", *Optics Express*, vol. 14, no. 3, pp. 1000–1005, February 2006.

[32] N. Chi, L. Xu, J. Zhang, P. V. Holm-Nielsen, C. Peucheret, Y. Geng, and P. Jeppesen. "Transmission and optical label swapping for 4 × 40 Gb/s WDM signals deploying orthogonal ASK/DPSK labeling",

IEEE Photonics Technology Letters, vol. 17, no. 6, pp. 1325–1327, June 2005.

[33] M. C. Ho, C. L. Lu, R. T. Hofmeister, and L. G. Kazovsky. "Nonlinear cross-talk reduction by spectrum shaping in subcarrier signalling WDM networks", in *Technical Digest Conference on Lasers and Electro-Optics, CLEO'98,* San Francisco, California, U.S.A., pp. 29–30, Paper CMG6, May 1998.

[34] J. Zhang, N. Chi, P. V. Holm-Nielsen, C. Peucheret, and P. Jeppesen. "Method for high-speed Manchester encoded optical signal generation", in *Technical Digest Optical Fiber Communication Conference, OFC'04,* Los Angeles, California, U.S.A., Paper MF76, February 2004.

[35] J. Zhang, P. V. Holm-Nielsen, N. Chi, C. Peucheret, and P. Jeppesen. "DC-balanced line encoding for optical labeling scheme using orthogonal modulation", in *Technical Digest Optical Fiber Communication Conference, OFC'04,* Los Angeles, California, U.S.A., Paper WF2, February 2004.

[36] F. Xiong. *Digital Modulation Techniques.* Artech House, 2000. ISBN 0-89006-970-0.

[37] V. Marembert, C. Schubert, C. Weinert, H. G. Weber, K. Schulze, F. Futami, and S. Watanabe. "Investigations of fiber Kerr switch: nonlinear phase shift measurements and optical time-division demultiplexing of 320 Gbit/s DPSK signals", in *Technical Digest Conference on Lasers and Electro-Optics, CLEO'05,* Baltimore, Maryland, U.S.A., vol. 2, pp. 1432–1434, Paper CWK7, May 2005.

Chapter 4

Wavelength Conversion of DPSK Signals

In future all-optical wavelength division multiplexing (WDM) networks, wavelength conversion is an essential functionality to implement, in order to provide wavelength flexibility and thus avoid wavelength blocking [1]. Considerable interest has been shown in the development of practical high-speed wavelength converter [2–4]. Wavelength converter based on electro-absorption has been demonstrated at 10 Gbit/s [5] and 40 Gbit/s [6]. Wavelength conversion realized in semiconductor optical amplifiers (SOAs) using cross gain modulation (XGM) [7, 8] or cross phase modulation (XPM) [9, 10] have been reported. XPM in a nonlinear optical loop mirror (NOLM) [11–13] has also been investigated and utilized to achieve wavelength conversion of signals at 10 and 40 Gbit/s. A tunable WDM wavelength converter based on XPM in a highly nonlinear normal dispersion holey fiber [14] has been proposed. However, the above mentioned schemes disregard the signal phase information, thus are not suitable for wavelength conversion of phase modulated signals, for example, signals using differential phase shift keying (DPSK) modulation format.

Four-wave fixing (FWM) in a fiber is a phase and intensity modulation preserving process that furthermore is independent of the signal bit rate due to the instantaneous response of the Kerr nonlinearity of fused silica, therefore satisfying the major requirements for transparent wavelength conversion in all-optical systems [2, 15]. FWM in a dis-

persion shifted fiber (DSF) has been used to implement optical phase conjugation (OPC), and its capability of compensating pulse shape distortion has been demonstrated in a transmission experiment [16]. In another demonstration, OPC based on FWM in a SOA has been used to reduce the phase noise of a DPSK based transmission system [17]. Wavelength conversion of phase modulated signals has been demonstrated using FWM in a nonlinear fiber for a 2.5 Gbit/s DPSK signal [18], and in a SOA for a 10 Gbit/s return-to-zero differential phase shift keying (RZ-DPSK) signal [19].

The design freedom offered by the crystal fiber technology makes highly nonlinear photonic crystal fibers (HNL-PCFs) very suitable for special applications where the fiber parameters should be tailored to satisfy specific demands, namely a flat dispersion profile and a high nonlinear coefficient. The dispersion of HNL-PCFs can be tailored to satisfy the phase matching requirements for FWM. Wavelength conversion using FWM in a HNL-PCF has been reported for nonreturn-to-zero (NRZ) signals at 10 Gbit/s [20,21], as well as for phase conjugation at 40 Gbit/s [22]. A widely tunable wavelength conversion scheme has been demonstrated lately, using this fiber in a NOLM structure [23].

In this chapter, we report wavelength conversion of high-speed phase modulated optical signals using FWM in a HNL-PCF. In section 4.1, we give a brief introduction to the FWM process in a nonlinear medium and the properties of the HNL-PCF used in the following presented experiments. In section 4.2, we describe wavelength conversion of a 40 Gbit/s RZ-DPSK signal. In section 4.3, we present wavelength conversion a 6×40 Gbit/s DPSK WDM signal. Finally, in section 4.4, we report wavelength conversion of an 80 Gbit/s RZ-DPSK-ASK signal. These experiments were carried out in cooperation with Torger Tokle from COM•DTU, and Peter Andreas Andersen who worked formerly at COM•DTU.

4.1 Introduction

This section gives a brief introduction to the FWM process in a nonlinear medium, and the properties of the HNL-PCF used in the experiments presented in the following sections.

4.1.1 Four-Wave Mixing

FWM is one of the nonlinear effects in optical fibers [24,25]. The refractive index of silica, n, becomes power dependent with increasing optical power P,

$$n = n_0 + n_2 \frac{P}{A_{\text{eff}}}, \tag{4.1}$$

where n_0 is the linear refractive index at low power, n_2 is the nonlinear index coefficient, and A_{eff} is the effective area of the optical mode in the fiber. Due to this nonlinear effect, three co-propagating waves at frequencies f_i, f_j, and f_k will give rise to a new optical wave at f_{FWM}

$$f_{\text{FWM}} = f_i + f_j - f_k. \tag{4.2}$$

The power of the new generated signal is given by

$$P_{\text{FWM}}(L) = \gamma^2 L_{\text{eff}}^2 P_i(0) P_j(0) P_k(0) e^{-\alpha L} \eta, \tag{4.3}$$

where $P_i(0)$, $P_j(0)$, and $P_k(0)$ are the input powers of the three waves, α is the fiber attenuation, L_{eff} is the effective interaction length defined as

$$L_{\text{eff}} = \frac{1 - e^{-\alpha L}}{\alpha},$$

γ is the fiber nonlinear coefficient defined as

$$\gamma = \frac{2\pi n_2}{\lambda A_{\text{eff}}}$$

with λ being the optical signal wavelength, and η is the conversion efficiency described as

$$\eta = \frac{\alpha^2}{\alpha^2 + \Delta\beta^2} \left(1 + \frac{4 e^{-\alpha L} \sin^2\left(\frac{\Delta\beta L}{2}\right)}{\left(1 - e^{-\alpha L}\right)^2} \right). \tag{4.4}$$

It can be seen from (4.3) and (4.4) that, the power of the FWM product is maximized when the FWM efficiency is largest which occurs when the phase matching condition $\Delta\beta = 0$ is satisfied, where $\Delta\beta = \beta_i + \beta_j - \beta_k - \beta_{\text{FWM}}$ is the difference in the propagation constants between the channels due to the fiber dispersion.

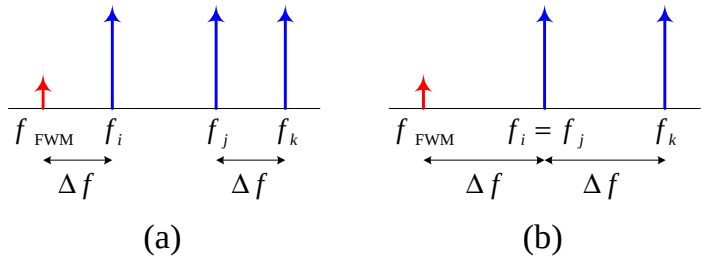

Figure 4.1: Illustration of (a) nondegenerate FWM case when $f_i \neq f_j \neq f_k$ and (b) degenerate FWM case when $f_i = f_j \neq f_k$, where f_i, f_j, and f_k are the frequencies of the incident waves, and f_{FWM} is the frequency of the generated FWM wave [28].

In a WDM system, FWM causes interchannel crosstalk by transferring signal power to neighboring channels, and thus degrades system performance. However, FWM can be quite efficient in generating new waves, and has been studied extensively [26–28].

When the three waves have different frequencies (where $f_i \neq f_j \neq f_k$) FWM occurs in a nondegenerate case, while when there are only two copropagating waves (where $f_i = f_j \neq f_k$) FWM occurs in a degenerate case. These two cases are illustrated in Figure 4.1 [28].

4.1.2 Properties of the HNL-PCF

Photonic crystal fibers are highly attractive as nonlinear media as they combine a large nonlinear coefficient and a highly controllable zero dispersion wavelength [30]. The combination of a high nonlinearity and a flat dispersion profile makes HNL-PCF a promising medium for wavelength conversion utilizing FWM [31]. All the experimental work presented in this chapter is based on a 50 m long HNL-PCF that was kindly provided by Crystal Fibre A/S. The inset of Figure 4.2 [29] shows microscopic picture of the microstructured region of this fiber. The fiber has a three-fold symmetric hybrid core region comprising a germanium doped center element surrounded by three fluorine doped regions embedded in a standard triangular cladding structure. This is an index-guiding microstructured fiber, where light is guided in the principle of modified total internal reflection. This means that, the holes act to lower the effective refractive index in the cladding region, so that light is confined

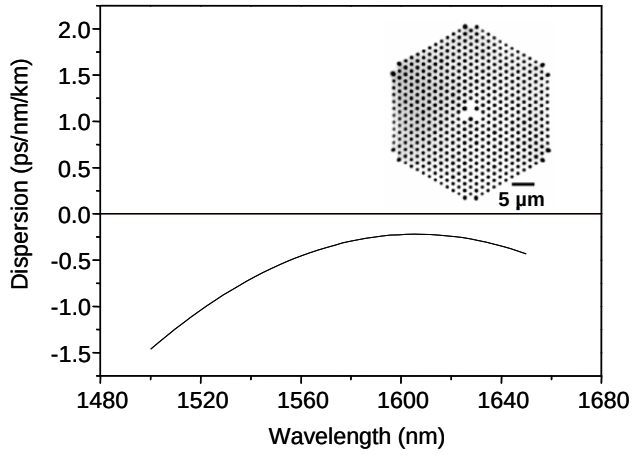

Figure 4.2: Measured dispersion curve of the 50 m long HNL-PCF used in the experiments presented in the chapter. The inset shows the microscopic picture of the microstructure region of the fiber [29].

to the solid core that has a relatively higher index. Due to the shape of the core, the nearfield is three fold symmetric resulting in a mode field diameter of approximately 3.5 μm [32]. The nonlinear coefficient of the fiber is $\gamma = 11.2$ W^{-1}·km^{-1} [30]. The dispersion profile is shown in Figure 4.2. The fiber has negative dispersion between 1500 nm and 1650 nm, with a dispersion variation of less than 1.5 ps/km/nm and a dispersion slope of less than 1.0×10^{-3} ps/km/nm^2 at 1550 nm. The attenuation of the fiber is $\sim$ 8 dB/km in the 1550 nm range, and the total insertion loss is $\sim$ 3 dB for this 50 m long HNL-PCF. Stimulated Brillouin scattering (SBS) measurements performed on the HNL-PCF show a SBS threshold of 21 dBm.

4.2 Wavelength Conversion of a 40 Gbit/s RZ-DPSK Signal

In this section, we present wavelength conversion of a 40 Gbit/s RZ-DPSK signal using FWM in the above mentioned 50 m long HNL-PCF [33].

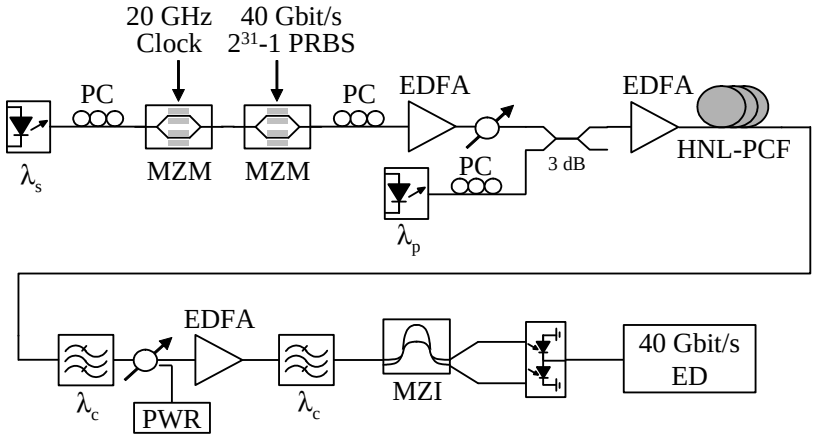

Figure 4.3: Experimental setup for wavelength conversion of a 40 Gbit/s RZ-DPSK signal using a HNL-PCF. λ_s: signal wavelength; λ_p: pump wavelength; λ_c: wavelength converted signal wavelength; PC: polarization controller; MZM: Mach-Zehnder modulator; PRBS: pseudo random bit sequence; EDFA: erbium doped fiber amplifier; HNL-PCF: highly nonlinear photonic crystal fiber; PWR: optical power meter; MZI: Mach-Zehnder interferometer; ED: error detector.

4.2.1 Experimental Setup

Figure 4.3 shows the experimental setup used for wavelength conversion of a 40 Gbit/s RZ-DPSK signal. Light from a continuous wave (CW) laser is modulated using a Mach-Zehnder modulator (MZM) biased at a peak in the transmission function, driven with a 20 GHz clock signal to generate a 40 GHz pulse train with a pulse width of 33% of the time slot, or 8.3 ps. A second MZM biased at null point and driven with a 40 Gbit/s 2^{31}-1 pseudo random bit sequence (PRBS) adds phase modulation resulting in a 40 Gbit/s RZ-DPSK signal. The signal is combined with a pump signal from a CW laser using a 3 dB coupler before amplification and entering the HNL-PCF with a pump power of 20 dBm and a total power of 25 dBm. The states of polarization (SOPs) of both the signal and the pump are optimized in order to ensure the highest conversion efficiency. At the fiber output the converted signal is filtered out using a tunable optical bandpass filter (OBPF) with a 3 dB bandwidth of 0.9 nm. After filtering, the converted signal is detected in a balanced pre-amplified receiver consisting of an erbium doped fiber

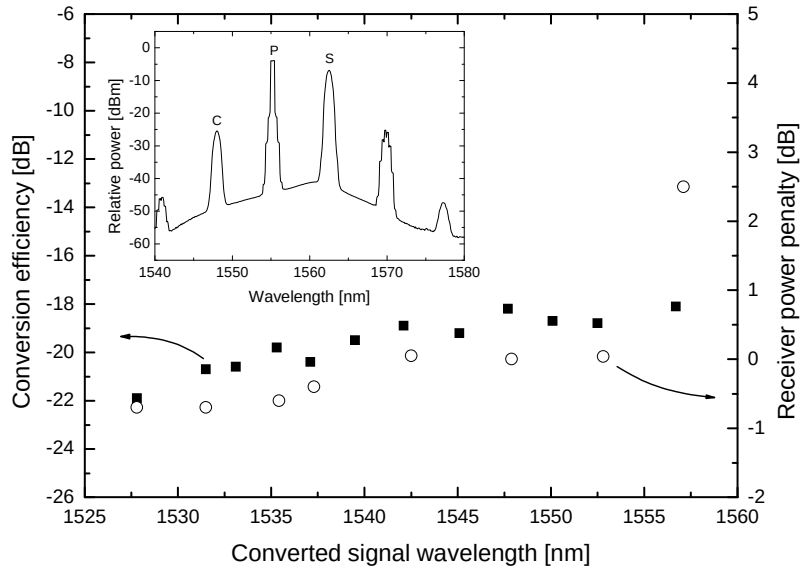

Figure 4.4: Conversion efficiency and receiver power penalty as a function of the converted signal wavelength, when the signal (S) is fixed at 1562.5 nm and the pump (P) is swept on the short wavelength side from 1559.8 nm to 1545.2 nm. The inset shows the spectrum at the output of the HNL-PCF when the signal is at 1562.5 nm, the converted signal (C) is at 1548.0 nm and the pump is at 1555.2 nm (Resolution bandwidth 1 nm).

amplifier (EDFA), a tunable OBPF with a 3 dB bandwidth of 0.9 nm, a one bit delay interferometer for demodulation, and two 45 GHz bandwidth photodiodes in a balanced configuration.

4.2.2 Results

The inset in Figure 4.4 shows the spectrum at the output of the HNL-PCF when the signal is located at 1562.5 nm, the pump at 1555.2 nm and the converted signal at 1548.0 nm. The first and second sidebands of the FWM process are clearly seen. The optical signal-to-noise ratio (OSNR) of the converted signal is found to be better than 25 dB measured in a 1 nm resolution bandwidth. Figure 4.4 shows the conversion efficiency (defined as the ratio between the power of the converted signal and the original signal at the output of the HNL-PCF) versus wavelength when

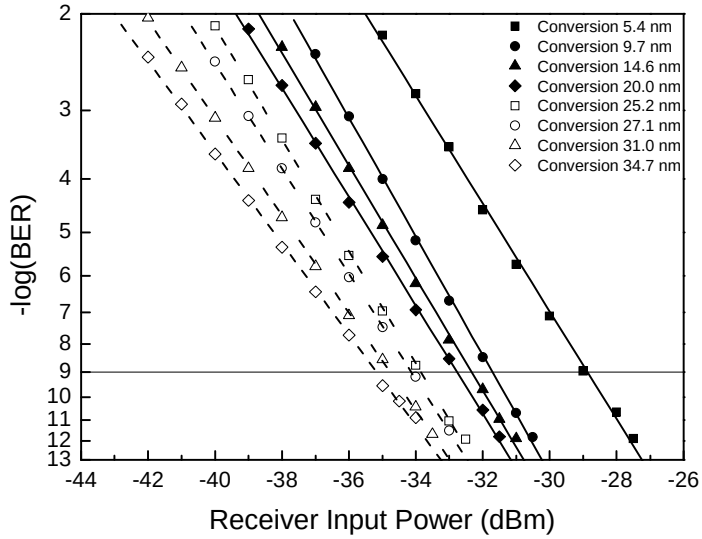

Figure 4.5: Measured BER curves for signal to converted signal wavelength separation between 5.4 and 34.7 nm.

the signal is fixed at 1562.5 nm and the pump wavelength is swept from 1559.8 nm to 1545.2 nm, allowing wavelength conversion of the signal to shorter wavelengths. These results demonstrate a conversion efficiency better than −20 dB with a 3 dB conversion bandwidth as broad as 31 nm.

We measure the bit error rate (BER) for several signals that are converted to shorter wavelengths, and define the receiver sensitivity as the average received power at a BER of 10^{-9}. The results are plotted in Figure 4.5. We see that the receiver sensitivity is −28.4 dBm for a signal to converted signal separation of 5.4 nm, and −34.6 dBm at 34.7 nm. The receiver power penalty is summarized in Figure 4.4. For small pump signal separation, the power penalty is high, due to overlapping between the converted signal and the pump spectrum that has been broadened by XPM. As the wavelength of the converted signal becomes shorter, smaller power penalties are observed.

Figure 4.6 shows the waveforms of the generated signal at 1562.5 nm and the converted signal at 1537.4 nm and 1531.5 nm. The single-ended

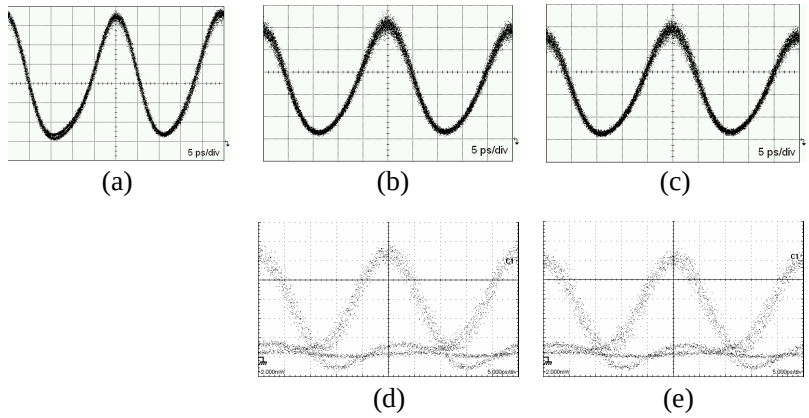

Figure 4.6: Waveforms of the generated signal (a) at 1562.5 nm, for the converted signal at (b) 1537.4 nm and (c) 1531.5 nm, and the corresponding single-ended detected eye diagrams at (d) 1537.4 nm and (e) 1531.5 nm. Horizontal scale: 5 ps/div.

detected eye diagrams are also shown in the figure for the two converted signals. It can be seen that the signal waveform is very well preserved after wavelength conversion, and the demodulated eye diagrams show very little deterioration. The conversion efficiency and the wide conversion band show that the 50 m long HNL-PCF is a suitable candidate for wavelength conversion of 40 Gbit/s RZ-DPSK signals using FWM across the C-band.

4.3 Wavelength Conversion of a 6 × 40 Gbit/s DPSK WDM Signal

In this section, we describe wavelength conversion of a 6 × 40 Gbit/s DPSK WDM signal using FWM in the same HNL-PCF as above [34].

4.3.1 Experimental Setup

Figure 4.7 shows the experimental setup used for wavelength conversion of a 6 × 40 Gbit/s DPSK WDM signal. The WDM source consists of six distributed feedback (DFB) lasers spaced 200 GHz apart, the outputs of which are combined in an arrayed waveguide grating (AWG) multi-

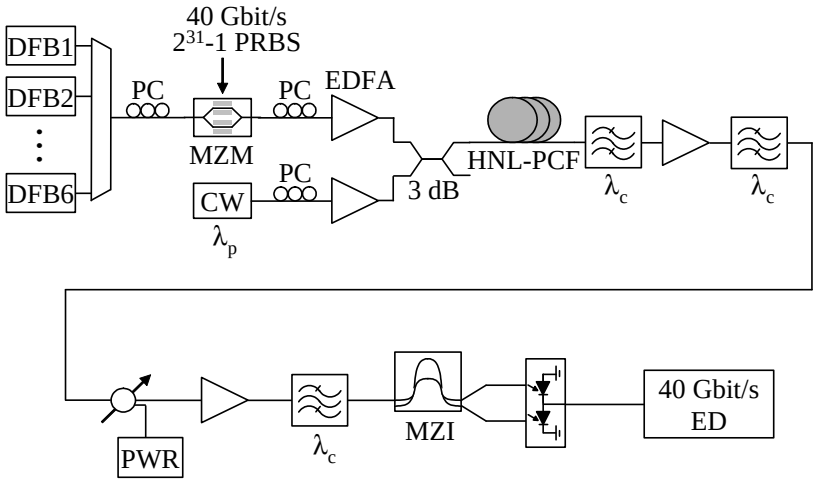

Figure 4.7: Experimental setup for wavelength conversion of a 6×40 Gbit/s DPSK WDM signal using a HNL-PCF. DFB: distributed feedback laser; λ_p: pump wavelength; λ_c: wavelength converted signal wavelength; PC: polarization controller; MZM: Mach-Zehnder modulator; PRBS: pseudo random bit sequence; EDFA: erbium doped fiber amplifier; HNL-PCF: highly nonlinear photonic crystal fiber; PWR: optical power meter; MZI: Mach-Zehnder interferometer; ED: error detector.

plexer. The wavelengths of the lasers are in the range from 1552.0 nm to 1560.0 nm. All CW signals are simultaneously modulated using a MZM biased at null transmission and driven with a 40 Gbit/s 2^{31}-1 PRBS, resulting in a 6×40 Gbit/s DPSK WDM signal. The WDM signal is combined with a CW pump at 1544.4 nm using a 3 dB coupler before being fed into the HNL-PCF, where wavelength conversion is realized. In order to achieve the best conversion efficiency for all six channels, both the WDM signal and the pump are polarization controlled and amplified before entering the 3 dB coupler. At the HNL-PCF input, the total WDM signal power is 18 dBm and the pump power is 25 dBm. At the HNL-PCF output, two consecutive tunable OBPFs, both with a 3 dB bandwidth of 0.9 nm, are used to select the desired wavelength converted channel. The signal is then detected in a balanced pre-amplified receiver consisting of an EDFA, a tunable OBPF with a 3 dB bandwidth of 0.9 nm, a one bit delay interferometer for demodulation, and two 45 GHz photodiodes in a balanced configuration.

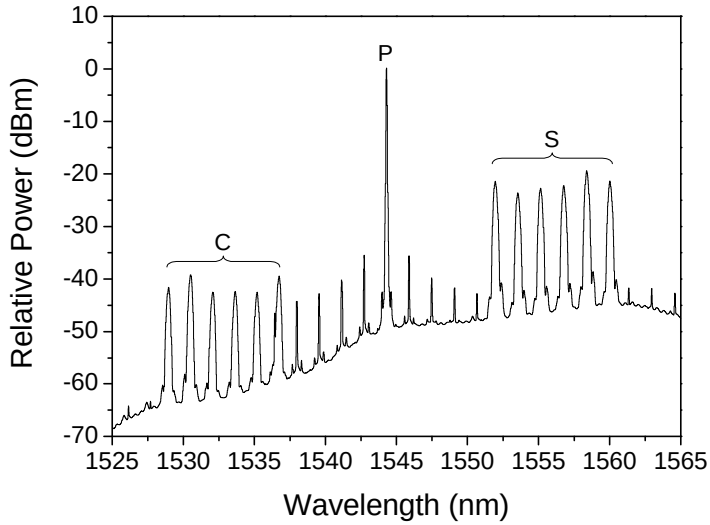

Figure 4.8: Measured spectrum at the output of the HNL-PCF when the WDM signals (S) are located in the wavelength range of 1552.0–1560.0 nm, the pump (P) is fixed at 1544.4 nm, and the wavelength converted WDM signals (C) are at 1528.8–1536.8 nm. Resolution bandwidth 0.1 nm.

4.3.2 Results

Figure 4.8 shows the spectrum measured at the HNL-PCF output. It is clearly seen that all six channels have been successfully converted to the wavelength range from 1528.8 nm to 1536.8 nm. Also, narrow peaks located at $\lambda \approx \lambda_p \pm n \cdot \Delta\lambda$ are found in the spectrum, where λ_p is the pump signal wavelength, n = 1, 2,..., 5, and $\Delta\lambda \approx 1.6$ nm is the WDM signal channel spacing. These components are due to nondegenerate FWM between the pump and signals at two different wavelengths. The inset in Figure 4.9 shows that the peak located at $\lambda_p - 5 \cdot \Delta\lambda$ overlaps with the spectrum of the converted channel at 1536.8 nm. This peak component has a random phase and varying intensity, hence deteriorating the converted signal. Figure 4.9 shows the conversion efficiency for each of the WDM channels as a function of the converted signal wavelength. These results demonstrate conversion efficiencies better than −20.3 dB for all six channels, and deviation from channel to channel of less than 2.3 dB.

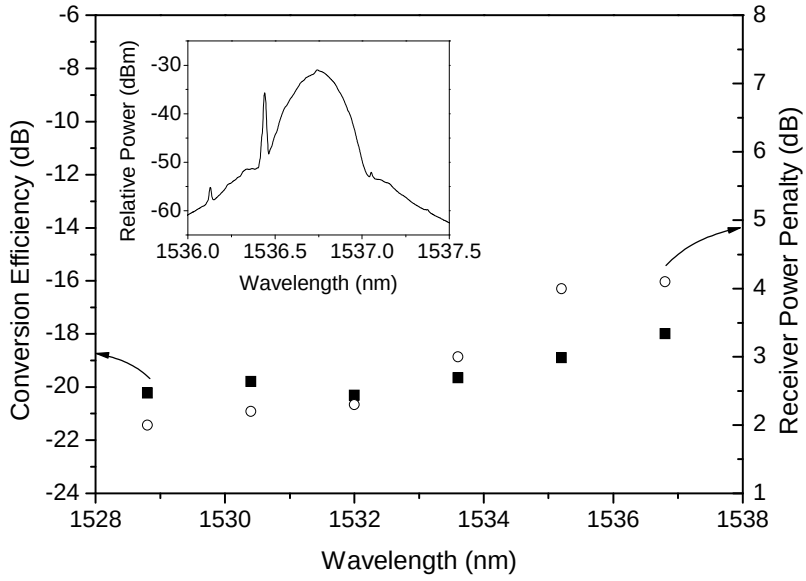

Figure 4.9: Conversion efficiency and receiver power penalty as a function of the wavelength for each of the wavelength converted WDM channels. The inset shows the spectrum overlap between one of the nondegenerate FWM products at $\lambda_p - 5 \cdot \Delta\lambda$ and the converted channel at 1536.8 nm.

Figure 4.10 shows measured BER curves for three out of the six WDM channels at 1552.0, 1555.2, and 1560.0 nm, and their corresponding wavelength converted signals at 1536.8, 1533.6, and 1528.8 nm. The receiver power penalty, defined as the degradation in receiver sensitivity due to the wavelength conversion process, is plotted in Figure 4.9 for all six converted channels. Power penalties between 2 dB and 4.1 dB are obtained. The highest receiver power penalty of 4.1 dB for the converted signal at 1536.8 nm is due to its spectrum overlapping with the nondegenerate FWM product, as explained in the previous paragraph.

Figure 4.11 shows the demodulated eye diagrams (after single-ended detection) of one of the WDM channels at 1556.8 nm and the corresponding converted signal at 1532.0 nm. It can be seen that after wavelength conversion the demodulated eye diagram shows little degradation. Though only two eye diagrams are presented in the figure, other channels show similar performance. These results suggest that the 50 m long

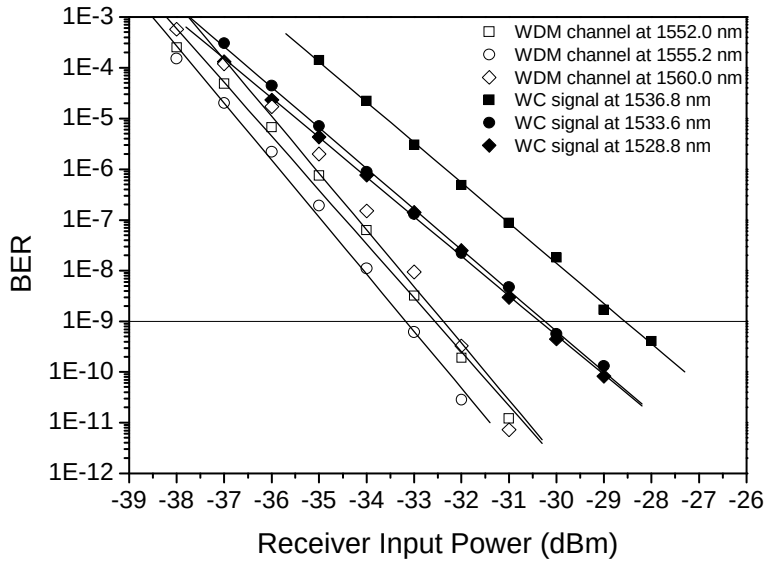

Figure 4.10: Measured BER curves for three out of the six WDM channels at 1552.0, 1555.2, and 1560.0 nm, and their corresponding wavelength converted signals at 1536.8, 1533.6, and 1528.8 nm.

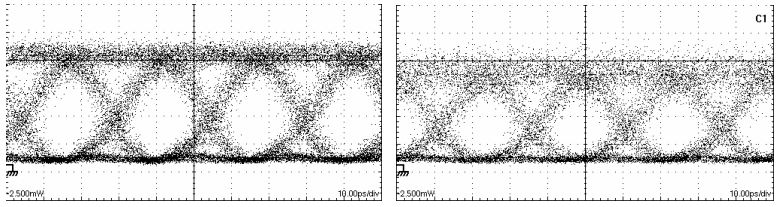

Figure 4.11: Single-ended detection eye diagrams of one of the WDM channels at 1556.8 nm (left) and the corresponding converted signal at 1532.0 nm (right). Horizontal scale: 10 ps/div.

HNL-PCF is a good candidate for multichannel wavelength conversion of phase modulated signals at 40 Gbit/s.

4.4 Wavelength Conversion of an 80 Gbit/s RZ-DPSK-ASK Signal

In Chapter 3, we presented orthogonal modulation as one way of adding the optical label onto a data payload in an optical label switched network. The use of orthogonal phase and amplitude modulation has also been proposed to increase the signal bit rate of optical communication systems [35]. By combining various forms of phase and amplitude modulation, 30 Gbit/s [36] and 40 Gbit/s [37] signals have been generated using only 10 Gbit/s equipments. By doing this, it becomes possible to generate signals at higher bit rates than state-of-the-art electronic and opto-electronic equipment can provide, and without the complexity of optical time division multiplexing (OTDM) techniques [38].

In the following, we report generation and wavelength conversion of an 80 Gbit/s signal using a combination of DPSK, amplitude shift keying (ASK) and return-to-zero (RZ) pulse carving at a symbol rate of 40 Gbaud [38].

4.4.1 Experimental Setup

Figure 4.12 shows the experimental setup used for wavelength conversion of an 80 Gbit/s RZ-DPSK-ASK signal. Light from a CW laser at 1556.4 nm is modulated in three consecutive MZMs. The first MZM is biased at a peak in the transmission function, driven with a 20 GHz clock signal to generate a 40 GHz pulse train with a pulse width of 33% of the time slot, or 8.3 ps. The second MZM is biased at null point and driven with a 40 Gbit/s 2^{31}-1 PRBS, to generate a 40 Gbit/s RZ-DPSK signal. Finally, the third MZM driven with a 40 Gbit/s 2^{23}-1 PRBS adds amplitude modulation on the 40 Gbit/s RZ-DPSK signal, resulting in an 80 Gbit/s RZ-DPSK-ASK signal. The bias voltage and the driving signal amplitude of the third MZM are adjusted to achieve the desired extinction ratio of the ASK signal. Certain optical power of a '0' level in the ASK signal is necessary to maintain the phase information of the RZ-DPSK signal. Therefore, the extinction ratio of the ASK signal is a

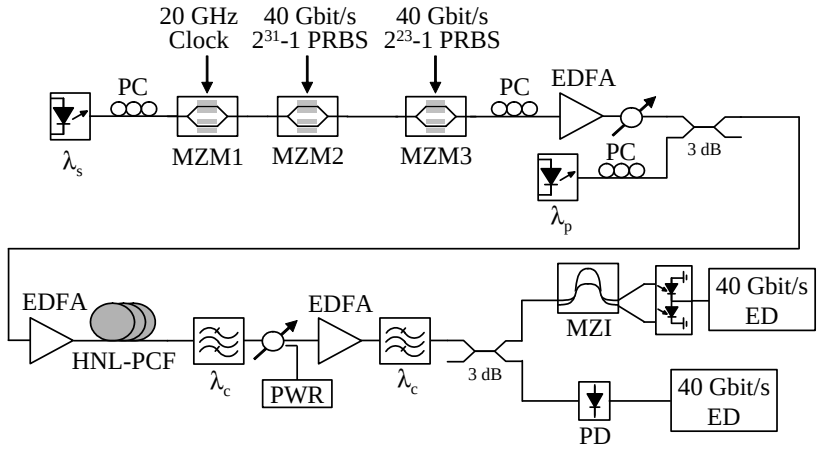

Figure 4.12: Experimental setup for wavelength conversion of an 80 Gbit/s RZ-DPSK-ASK signal using a HNL-PCF. λ_s: signal wavelength; λ_p: pump wavelength; λ_c: wavelength converted signal wavelength; PC: polarization controller; MZM: Mach-Zehnder modulator; PRBS: pseudo random bit sequence; EDFA: erbium doped fiber amplifier; HNL-PCF: highly nonlinear photonic crystal fiber; PWR: optical power meter; MZI: Mach-Zehnder interferometer; PD: photodiode; ED: error detector.

trade-off between good eye opening for the ASK signal and sufficient eye opening of the demodulated DPSK signal. An extinction ratio of 6 dB results in equal BER for the ASK and DPSK tributaries, thus leads to the best overall performance. Hence an extinction ratio of 6 dB is used throughout all the measurements.

The generated RZ-DPSK-ASK signal is combined with a pump signal from a CW laser at 1550.6 nm using a 3 dB coupler before amplification and entering the HNL-PCF with a total power of 25 dBm. The SOPs of both the signal and pump are optimized in order to obtain the highest conversion efficiency. At the fiber output, the converted signal at 1544.8 nm is filtered out using a tunable OBPF with a 3 dB bandwidth of 0.9 nm. Then the signal is amplified in an EDFA and filtered by an OBPF with a 3 dB bandwidth of 0.9 nm, and split into two branches for the DPSK and ASK signal detections. The DPSK detection is realized in a one bit delay interferometer for demodulation, a balanced receiver consisting of two 45 GHz photodiodes, and a 40 Gbit/s error detector (ED). The ASK detection is realized in a 50 GHz photodiode

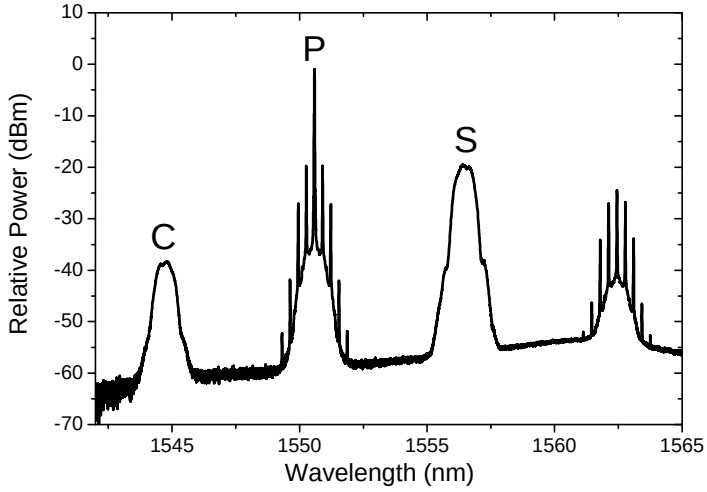

Figure 4.13: Measured spectrum at the output of the HNL-PCF, when the signal (S) is at 1556.4 nm, the pump is at 1550.6 nm, and the converted signal is at 1544.8 nm. Resolution bandwidth 0.01 nm.

followed by another 40 Gbit/s ED, so that the BER evaluations for the DPSK and ASK signals can be carried out simultaneously.

4.4.2 Results

Figure 4.13 shows the spectrum measured at the HNL-PCF output. Conversion efficiency of −19 dB is obtained. Figure 4.14 shows the measured BER curves for the DPSK and ASK signals in the back-to-back case, and after wavelength conversion. As shown in the figure, the receiver sensitivity (defined as average received power at a BER of 10^{-9}, when the BER is averaged over the DPSK and ASK tributaries) is $\sim$−22.5 dBm in the back-to-back case, and is $\sim$−13.6 dBm after wavelength conversion. We believe that the large penalty can be attributed to the reduced OSNR after wavelength conversion process; note that at low BER, little or no receiver penalty compared to the back-to-back case is found.

Figure 4.15 shows the eye diagrams of the generated RZ-DPSK-ASK signal at 1556.4 nm and the wavelength converted signal at 1544.8 nm.

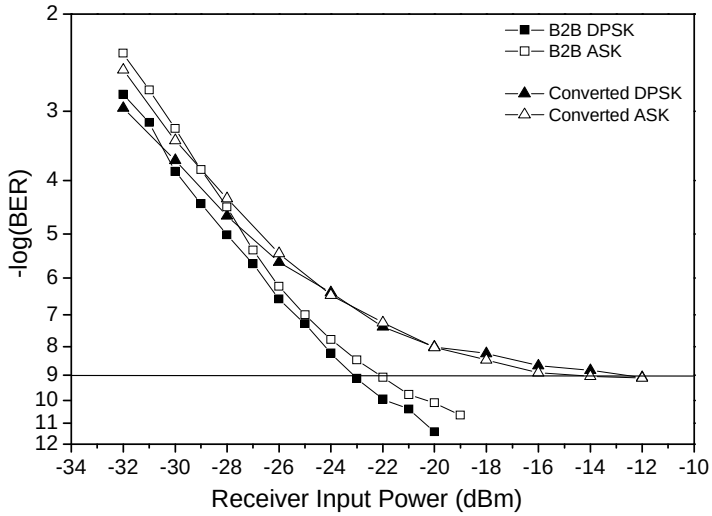

Figure 4.14: Measured BER curves for the DPSK and ASK signals in the back-to-back case, and after wavelength conversion.

The demodulated eye diagrams (after balanced detection) of the DPSK tributary in the back-to-back case and after wavelength conversion are also presented in the figure. The eye diagram of the back-to-back RZ-DPSK-ASK signal shows the limited extinction ratio used for the ASK signal generation. The demodulated DPSK signal exhibits six distinct traces as shown in the figure. This is due to the differential demodulation of combined high-high, high-low, and low-low amplitude signals with either 0 or π relative phase shift. The results also indicate that the signal waveform is very well preserved after wavelength conversion. These results show that the 50 m long HNL-PCF is suitable for wavelength conversion of high speed multilevel modulated signals implemented by combining phase and amplitude modulation.

4.5 Summary

We successfully demonstrated wavelength conversion of a 40 Gbit/s RZ-DPSK signal using FWM in a 50 m long HNL-PCF. A conversion efficiency better than -20 dB for a pump power of 20 dBm, and a wide

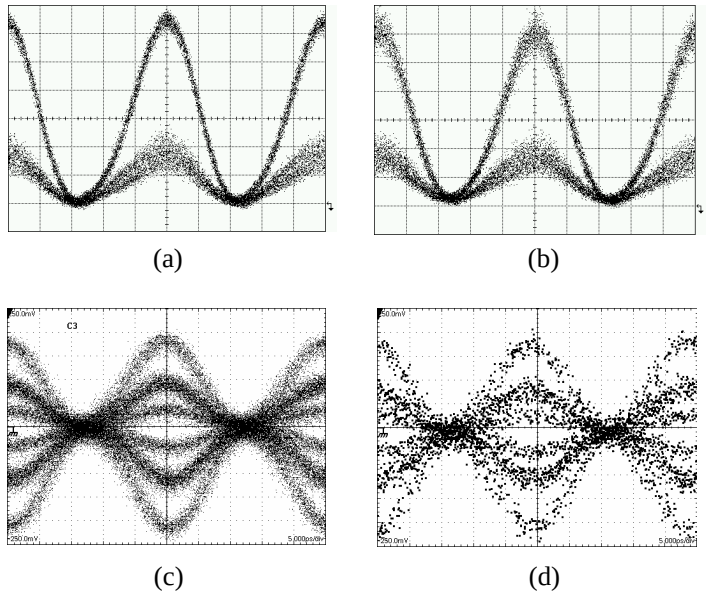

Figure 4.15: Eye diagrams of the generated RZ-DPSK-ASK signal at 1556.4 nm (a), and the wavelength converted RZ-DSPK-ASK signal at 1544.8 nm (b). The demodulated eye diagrams (after balanced detection) of the DPSK signal in the back-to-back case (c) and after wavelength conversion (d) are also presented. Horizontal scale: 5 ps/div.

conversion bandwidth of 31 nm only limited by the bandwidths of amplifiers and tunability of optical bandpass filters, were achieved. Using the same fiber, simultaneous wavelength conversion of a 6×40 Gbit/s DPSK WDM signal was successfully performed. Conversion efficiencies better than -20.3 dB for all six channels for a pump power of 25 dBm, and with deviation from channel to channel of less than 2.3 dB, were demonstrated. A receiver power penalty due to the wavelength conversion process of less than 4.1 dB was obtained. And finally, we reported generation of an 80 Gbit/s signal using a combination of phase and amplitude modulation at a symbol rate of 40 Gbaud. Wavelength conversion of the generated 80 Gbit/s RZ-DPSK-ASK signal was demonstrated. A conversion efficiency of -19 dB, and well preserved signal waveforms after wavelength conversion, were obtained.

The fiber used in the above mentioned experiments was a 50 m long

HNL-PCF. The fiber had a high nonlinear coefficient with a flat dispersion profile, thus satisfying the phase matching requirement for FWM. FWM in a fiber is a phase and intensity modulation preserving process that furthermore is independent of the signal bit rate, therefore satisfying the major requirements for transparent high-speed wavelength conversion. It has been shown that, in future all-optical networks, with a simple FWM scheme wavelength conversion functionality can be implemented for high speed signals with phase modulation and multilevel modulation, even combined with WDM technology.

References to Chapter 4

[1] K. K. Chow, C. Shu, C. Lin, and A. Bjarklev. "Polarization-insensitive widely tunable wavelength converter based on Four-Wave Mixing in a dispersion-flattened nonlinear photonic crystal fiber", *IEEE Photonics Technology Letters*, vol. 17, no. 3, pp. 624–626, March 2005.

[2] K. Inoue and H. Toba. "Wavelength conversion experiment using fiber Four-Wave Mixing", *IEEE Photonics Technology Letters*, vol. 4, no. 1, pp. 69–72, January 1992.

[3] S. J. B. Yoo. "Wavelength conversion technologies for WDM network applications", *Journal of Lightwave Technology*, vol. 14, no. 6, pp. 955–966, June 1996.

[4] K. E. Stubkjær. "Semiconductor optical amplifier-based all-optical gates for high-speed optical processing", *IEEE Journal of Selected Topics in Quantum Electronics*, vol. 6, no. 6, pp. 1428–1435, November/December 2000.

[5] L. K. Oxenloewe, A. T. Clausen, and H. N. Poulsen. "Wavelength conversion in an electroabsorption modulator", in *Proceedings European Conference on Optical Communication, ECOC'00,* Munich, Germany, vol. 3, pp. 303–304, Paper 9.4.4, September 2000.

[6] T. Otani, T. Miyzaki, and S. Yamamoto. "40 Gbit/s signal transmission using optical 3R regenerator based on electroabsorption modulators", in *Technical Digest Optical Fiber Communication*

Conference, OFC'00, Baltimore, Maryland, U.S.A., vol. 3, pp. 226–228, Paper ThP3, March 2000.

[7] J. M. Wiesenfeld, B. Glance, J. S. Perino, and A. H. Gnauck. "Wavelength conversion at 10 Gb/s using a semiconductor optical amplifier", *IEEE Photonics Technology Letters*, vol. 5, no. 11, pp. 1300–1303, November 1993.

[8] C. Joergensen, S. L. Danielsen, M. Vaa, B. Mikkelsen, K. E. Stubkjaer, P. Doussiere, F. Pommerau, L. Goldstein, and M. Goix. "40 Gbit/s all-optical wavelength conversion by semiconductor optical amplifiers", *Electronics Letters*, vol. 32, no. 4, pp. 367–368, February 1996.

[9] B. Mikkelsen, M. Vaa, H. N. Poulsen, S. L. Danielsen, C. Joergensen, A. Kloch, P. B. Hansen, K. E. Stubkjaer, K. Wunstel, K. Daub, E. Lach, G. Laube, W. Idler, M. Schilling, and S. Bouchoule. "40 Gbit/s all-optical wavelength converter and RZ-to-NRZ format adapter realised by monolithic integrated active Michelson interferometer", *Electronics Letters*, vol. 33, no. 2, pp. 133–134, January 1997.

[10] T. Fjelde, D. Wolfson, P. B. Hansen, A. Kloch, C. Janz, A. Coquelin, I. Guillemot, F. Gaborit, F. Poingt, B. Dagens, and M. Renaud. "20 Gbit/s optical wavelength conversion in all-active Mach-Zehnder interferometer", *Electronics Letters*, vol. 35, no. 11, pp. 913–914, May 1999.

[11] K. J. Blow, N. J. Doran, B. K. Nayar, and B. P. Nelson. "Two-wavelength operation of the nonlinear fiber loop mirror", *Optics Letters*, vol. 15, no. 4, pp. 248–250, February 1990.

[12] K. A. Rauschenbach, K. L. Hall, J. C. Livas, and G. Raybon. "All-optical pulse width and wavelength conversion at 10 Gb/s using a nonlinear optical loop mirror", *IEEE Photonics Technology Letters*, vol. 6, no. 9, pp. 1130–1132, September 1994.

[13] P. Öhlén, B.-E. Olsson, and D. J. Blumenthal. "Wavelength dependence and power requirements of a wavelength converter based on

XPM in a dispersion-shifted optical fiber", *IEEE Photonics Technology Letters*, vol. 12, no. 5, pp. 522–524, May 2000.

[14] J. H. Lee, Z. Yusoff, W. Belardi, M. Ibsen, T. M. Monro, and D. J. Richardson. "A tunable WDM wavelength converter based on cross-phase modulation effects in normal dispersion holey fiber", *IEEE Photonics Technology Letters*, vol. 15, no. 3, pp. 437–439, March 2003.

[15] O. Aso, S.-I. Arai, T. Yagi, M. Tadakuma, Y. Suzuki, and S. Namiki. "Broadband Four-Wave Mixing generation in short optical fibers", *Electronics Letters*, vol. 36, no. 8, pp. 709–711, April 2000.

[16] S. Watanabe, G. Ishikawa, T. Naito, and T. Chikama. "Generation of optical phase-conjugate waves and compensation for pulse shape distortion in a single-mode fiber", *Journal of Lightwave Technology*, vol. 15, no. 3, pp. 440–442, March 2003.

[17] S. L. Jansen, D. van den Borne, G. D. Khoe, H. de Waardt, C. Climent Monsalve, S. Spälter, and P. M. Krummrich. "Reduction of phase noise by mid-link spectral inversion in a DPSK based transmission system", in *Technical Digest Optical Fiber Communication Conference, OFC'05,* Anaheim, California, U.S.A., Paper OThO5, March 2005.

[18] N. Chi, J. Zhang, P. V. Holm-Nielsen, C. Peucheret, and P. Jeppesen. "Transmission and transparent wavelength conversion of an optically labeled signal using ASK/DPSK orthogonal modulation", *IEEE Photonics Technology Letters*, vol. 15, no. 5, pp. 760–762, May 2003.

[19] Z. Li, Y. Dong, J. Mo, Y. Wang, and C. Lu. "Cascaded all-optical wavelength conversion for RZ-DPSK signal based on four-wave mixing in semiconductor optical amplifier", *IEEE Photonics Technology Letters*, vol. 16, no. 7, pp. 1685–1687, July 2004.

[20] J. H. Lee, W. Belardi, K. Furusawa, P. Petropoulos, Z. Yusoff, T. M. Monro, and D. J. Richardson. "Four-Wave Mixing based 10-Gb/s tunable wavelength conversion using a holey fiber with a

high SBS threshold", *IEEE Photonics Technology Letters*, vol. 15, no. 3, pp. 440–442, March 2003.

[21] K. K. Chow, C. Shu, C. Lin, and A. Bjarklev. "Widely tunable wavelength converter by Four Wave Mixing in a dispersion-flattened nonlinear photonic crystal fiber", in *Proceedings European Conference on Optical Communication, ECOC'04,* Stockholm, Sweden, vol. 2, pp. 188–189, Paper Tu3.3.6, September 2004.

[22] C. Peucheret, B. Zsigri, P. A. Andersen, K. S. Berg, A. Tersigni, P. Jeppesen, K. P. Hansen, and M. D. Nielsen. "40 Gbit/s transmission over photonic crystal fibre using mid-span spectral inversion in highly nonlinear photonic crystal fibre", *Electronics Letters*, vol. 39, no. 12, pp. 919–921, June 2003.

[23] C. H. Kwok, S. H. Lee, K. K. Chow, C. Shu, C. Lin, and A. Bjarklev. "Widely tunable wavelength conversion with extinction ratio enhancement using PCF-based NOLM", *IEEE Photonics Technology Letters*, vol. 17, no. 12, pp. 2655–2657, December 2005.

[24] G. P. Agrawal. *Nonlinear Fiber Optics*. Academic Press, Second edition, 1995. ISBN 0-12-045142-5.

[25] P. Bayvel and R. Killey. *Nonlinear Optical Effects in WDM Transmission*, In I. Kaminow and T. Li, editors, *Optical Fiber Telecommunications IVB Components,* Chapter 13, pp. 611–641, Academic Press, March 2002. ISBN 0-12-395173-9.

[26] E. Lichtman, A. A. Friesem, R. G. Waarts, and H. H. Yaffe. "Exact solution of Four-Wave Mixing of copropagating light beams in a Kerr medium", *Journal of the Optical Society of America B*, vol. 4, no. 11, pp. 1801–1805, November 1987.

[27] G. Cappellini and S. Trillo. "Third-order three-wave mixing in single-mode fibers: Exact solutions and spatial instability effects", *Journal of the Optical Society of America B*, vol. 8, no. 4, pp. 824–838, April 1991.

[28] K. Inoue. "Four-Wave Mixing in an optical fiber in the zero-dispersion wavelength region", *Journal of Lightwave Technology*, vol. 10, no. 11, pp. 1553–1561, November 1992.

[29] P. A. Andersen, T. Tokle, Y. Geng, C. Peucheret, and P. Jeppesen. "Wavelength conversion of a 40 Gbit/s RZ-DPSK signal using Four-Wave Mixing in a dispersion flattened highly nonlinear photonic crystal fiber", *IEEE Photonics Technology Letters*, vol. 17, no. 9, pp. 1908–1910, September 2005.

[30] T. P. Hansen. "Dispersion flattened hybrid-core nonlinear photonic crystal fiber", *Optics Express*, vol. 11, no. 13, pp. 1503–1509, June 2003.

[31] T. Okuno, M. Hirano, T. Kato, M. Shigematsu, and M. Onishi. "Highly nonlinear and perfectly dispersion-flattened fibres for efficient optical signal processing applications", *Electronics Letters*, vol. 39, no. 13, pp. 972–974, June 2003.

[32] K. P. Hansen, J. R. Folkenberg, C. Peucheret, and A. Bjarklev. "Fully dispersion controlled triangular-core nonlinear photonic crystal fiber", in *Technical Digest Optical Fiber Communication Conference, OFC'03,* Atlanta, Georgia, U.S.A., Paper PD2, March 2003, Post-deadline paper.

[33] Y. Geng, P. A. Andersen, T. Tokle, C. Peucheret, and P. Jeppesen. "Broadband wavelength conversion of a 40 Gbit/s RZ-DPSK signal using dispersion flattened highly nonlinear photonic crystal fiber", in *Proceedings OptoElectronics and Communications Conference, OECC'05,* Seoul, Korea, pp. 796–797, Paper 8B3-4, July 2005.

[34] Y. Geng, P. A. Andersen, T. Tokle, C. Peucheret, and P. Jeppesen. "Wavelength conversion of a 6×40 Gb/s DPSK WDM signal using FWM in a highly non-linear photonic crystal fiber", in *Proceedings European Conference on Optical Communication, ECOC'05,* Glasgow, Scotland, vol. 2, pp. 205–206, Paper Tu3.3.4, September 2005.

[35] M. Ohm and J. Speidel. "Quaternary optical ASK-DPSK and receivers with direct detection", *IEEE Photonics Technology Letters*, vol. 15, no. 1, pp. 159–161, January 2004.

[36] T. Miyazaki and F. Kubota. "Superposition of QPSK over inverse-RZ for 3 bit/symbol transmission", in *Proceedings European Con-*

ference on Optical Communication, ECOC'04, Stockholm, Sweden, vol. 3, pp. 428–429, Paper We3.4.7, September 2004.

[37] K. Sekine, N. Kikuchi, S. Sasaki, S. Hayase, C. Hasegawa, and T. Sugawara. "Proposal and demonstration of 10-Gsymbol/sec 16-ary (40 Gbit/s) optical modulation/demodulation scheme", in *Proceedings European Conference on Optical Communication, ECOC'04,* Stockholm, Sweden, vol. 3, pp. 424–425, Paper We3.4.5, September 2004.

[38] T. Tokle, P. A. Andersen, Y. Geng, B. Zsigri, C. Peucheret, and P. Jeppesen. "Generation, transmission and wavelength conversion of an 80 Gbit/s RZ-DBPSK-ASK signal", in *Technical Digest Conference on Lasers and Electro-Optics, CLEO'05,* Baltimore, Maryland, U.S.A., vol. 1, pp. 294–296, Paper CMQ4, May 2005.

Chapter 5

Amplitude Equalization of RZ-DPSK Signals

Amplitude fluctuations of return-to-zero differential phase shift keying (RZ-DPSK) signals induced by amplified spontaneous emission (ASE) noise and the interaction between optical fiber nonlinearity and dispersion (such as e.g. intra-channel four wave mixing) might degrade the quality of the received signal [1]. Those amplitude fluctuations will moreover be converted into nonlinear phase noise that has been shown to be a major source of impairments for differential phase shift keying (DPSK) systems [2]. Consequently, all-optical amplitude regeneration of RZ-DPSK signals will be needed to achieve improved signal quality in ultra long-haul transmission systems.

An extra requirement compared to conventional on-off keying (OOK) regeneration methods is that the process involved should not affect the phase of the signal, or should even provide phase regeneration [3]. So far, only a few regenerative mechanisms suitable for RZ-DPSK signals have been presented. Amplitude regeneration with phase preserving RZ-DPSK signal regeneration has been numerically studied at 40 Gbit/s in a nonlinear optical loop mirror (NOLM) setup including an additional directional attenuator [4], and demonstrated at 10 Gbit/s in a similar setup [5] and in a nonlinear amplifying loop mirror (NALM) [6]. An implementation of a newer design of NOLM based on distributed Raman amplification in a loop (RA-NOLM) combined with spectral filtering has been shown to result in amplitude regeneration with negligible phase dis-

tortion [7,8]. Phase regeneration using phase-sensitive amplifiers (PSAs) has been numerically investigated at 40 Gbit/s [9] and experimentally demonstrated at 10 Gbit/s [10,11]. Reduction of phase noise can also be realized by converting phase information to amplitude information and performing the regeneration operation on the amplitude [12, 13]. This scheme has been implemented in semiconductor optical amplifier (SOA) based structures [14–19], and more recently in a fiber-based regenerator [20].

Four-wave mixing (FWM) is a phase and intensity modulation preserving process that has already been used for wavelength conversion of DPSK signals both in single channel [21] and wavelength division multiplexing (WDM) systems [22]. Amplitude noise reduction of DPSK signal has been demonstrated at 10 Gbit/s using the nonlinear transfer function of pump-modulated FWM in a SOA [23]. Using saturation of FWM in an optical fiber, amplitude equalization has been reported for OOK signals at 2 Gbit/s [24]. The amplitude regeneration capabilities of FWM for DPSK signals have been proposed and numerically investigated [25–27]. The enhancement of DPSK transmission performance through the reduction of nonlinear phase noise using a FWM-based equalizer has been demonstrated for short ($\sim$ 7 ps) pulses at 10 Gbit/s [28]. However, the use of FWM for amplitude equalization of realistic RZ-DPSK signals with larger duty cycles at 40 Gbit/s has not been demonstrated so far.

In this chapter, we describe amplitude equalization of 40 Gbit/s RZ-DPSK signals using saturation of FWM in a highly nonlinear fiber (HNLF). In section 5.1, we present the principle of the RZ-DPSK amplitude equalization process and simulation results that suggest the amplitude regeneration capabilities of FWM in a HNLF. In section 5.2, we report, to the best of our knowledge, the first experimental demonstration of amplitude equalization of 40 Gbit/s RZ-DPSK signals using a 500 m long HNLF. Experimental setup, results and further discussions are presented. And finally, the chapter is summarized.

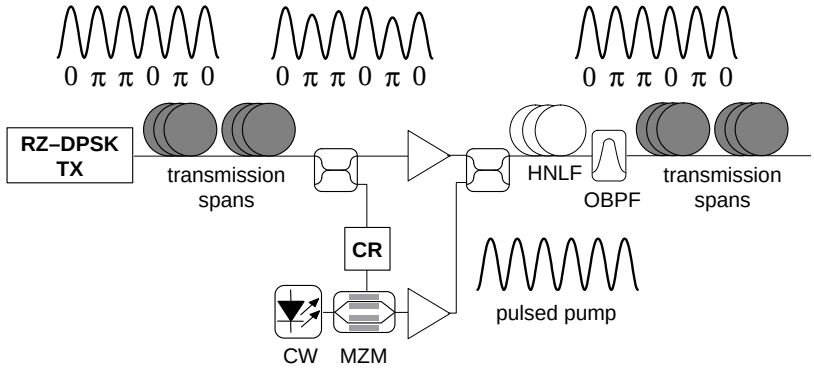

Figure 5.1: Principle of RZ-DPSK amplitude regeneration using saturation of FWM in a HNLF. TX: transmitter; CR: clock recovery; CW: continuous wave laser; MZM: Mach-Zehnder modulator; HNLF: highly nonlinear fiber; OBPF: optical bandpass filter.

5.1 FWM Based Amplitude Equalization Process

In this section, we first describe the principle of RZ-DPSK amplitude regeneration using saturation of FWM in a HNLF, and then we present simulation results that verify the amplitude equalization capability of FWM.

5.1.1 Principle of RZ-DPSK Amplitude Equalization

Figure 5.1 illustrates the principle of the RZ-DPSK amplitude equalization process. At the output of the transmitter, an RZ-DPSK signal is generated. After several fiber spans, a certain amount of intensity fluctuation is accumulated. The amplitude distorted RZ-DPSK signal is input to a piece of HNLF together with a pulsed optical pump obtained by modulating a continuous wave with a sinusoidal electrical clock recovered from the transmitted signal. Due to saturation of FWM in the HNLF, the amplitude of the wavelength converted RZ-DPSK signal is equalized, while the phase information is preserved. Ideally, one would expect the wavelength conversion process to induce a phase distortion that is insignificant. In the present scheme, no phase regeneration is

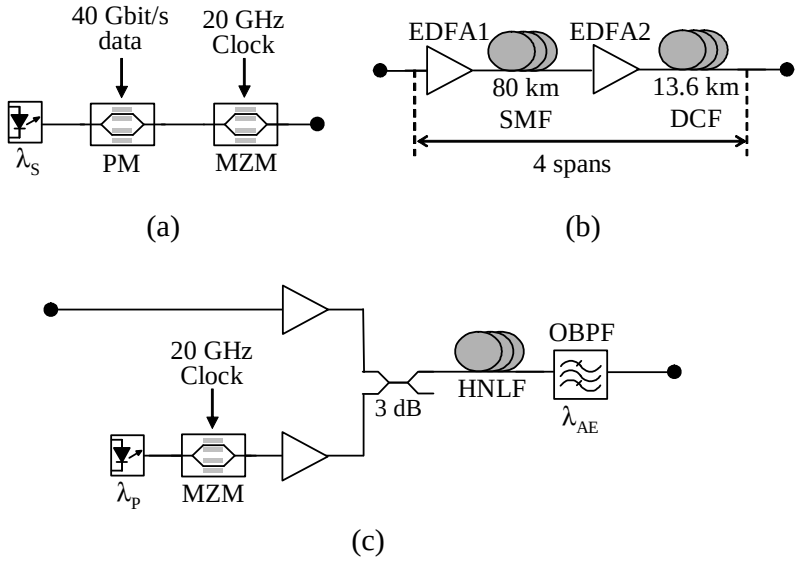

Figure 5.2: A schematic of the simulation setup used to verify the amplitude equalization capability of FWM in a HNLF for 40 Gbit/s RZ-DPSK signals. (a) RZ-DPSK transmitter, (b) transmission spans, and (c) amplitude equalizer based on a HNLF. λ_S: signal wavelength; λ_P: pump wavelength; λ_{AE}: amplitude equalized signal wavelength; PM: phase modulator; MZM: Mach-Zehnder modulator; EDFA: erbium doped fiber amplifier; SMF: standard single mode fiber; DCF: dispersion compensation fiber; HNLF: highly nonlinear fiber; OBPF: optical bandpass filter.

achieved. However, performance improvement will be realized by the reduction of nonlinear phase noise in the transmission spans following the amplitude equalizer.

5.1.2 Simulation Results

In order to verify the amplitude regeneration capability of FWM in a HNLF for RZ-DPSK signals, we simulate the system shown in Figure 5.2 using the commercial software VPItransmissionMaker^{TM}. Light from a continuous wave (CW) operating at 1553.6 nm is phase modulated using a phase modulator driven with a 40 Gbit/s data signal. Then the signal is pulse carved using a Mach-Zehnder modulator (MZM) driven with a 20 GHz clock, resulting in a 40 Gbit/s RZ-DPSK signal. The signal is

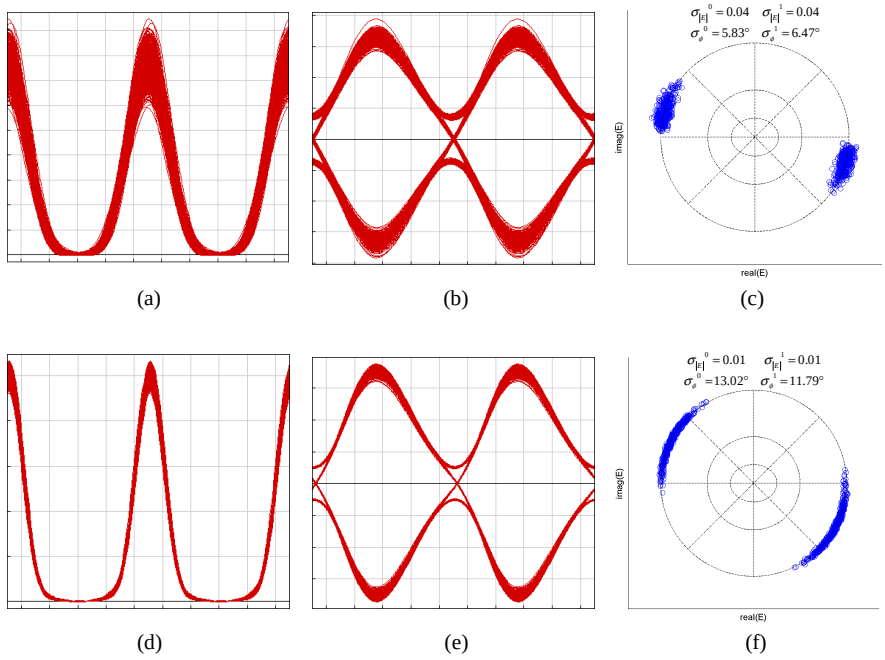

Figure 5.3: Simulation results that verify the amplitude regeneration capability of FWM in a HNLF for RZ-DPSK signals. Eye diagrams of the transmitted (a) and amplitude equalized (d) RZ-DPSK signal, and the corresponding balanced detected eye diagrams (b) and (e), and calculated constellation diagrams of the transmitted (c) and amplitude equalized (f) RZ-DPSK signal. ${\sigma_{|E|}}^0$: amplitude standard deviation of the electric field of bit '0', ${\sigma_{|E|}}^1$: amplitude standard deviation of the electric field of bit '1', ${\sigma_\phi}^0$: phase standard deviation of the electric field of bit '0', ${\sigma_\phi}^1$: phase standard deviation of the electric field of bit '1'. Horizontal scale: 5 ps/div.

transmitted through 4 spans, each consisting of 80 km standard single mode fiber (SMF) and a matching length of 13.6 km dispersion compensation fiber (DCF) and two erbium doped fiber amplifiers (EDFAs) for loss compensation. The transmitted signal is mixed with a pulsed pump at 40 GHz repetition rate—generated by pulse carving the output from the pump laser operating 600 GHz away from the signal on the shorter wavelength side—in a 1 km long HNLF. At the input of the HNLF, the signal and pump powers are 12 dBm and 15 dBm, respectively. At the HNLF output, the amplitude equalized signal is selected with an optical bandpass filter (OBPF) centered at the FWM product wavelength.

The HNLF used in the simulation has a fiber loss of $\alpha = 0.87$ dB/km. The nonlinear coefficient of the fiber is $\gamma = 10.6$ W^{-1}·km^{-1}. The fiber dispersion is $D = 0.031$ ps/km/nm at 1550 nm with a dispersion slope of $S = 0.022$ ps/km/nm^2.

Figure 5.3 shows the eye diagrams of the transmitted and amplitude equalized RZ-DPSK signal, and the corresponding balanced detected eye diagrams. The calculated constellation diagrams of the transmitted and amplitude equalized signals are also shown in the figure. The results indicate that the amplitude fluctuations accumulated over the transmission spans are suppressed after the equalization process. After 320 km transmission, the amplitude standard deviations of the electric fields of bit '1' and '0' ($\sigma_{|E|}{}^1$ and $\sigma_{|E|}{}^0$) are 4%. They are reduced to 1% after amplitude regeneration. The phase standard deviations of the electric fields ($\sigma_\phi{}^1$ and $\sigma_\phi{}^0$) are increased by a factor of two due to self phase modulation (SPM) and cross phase modulation (XPM) occurring associated with the FWM process. The influence of equalization induced phase distortion is discussed in section 5.2.2.

5.2 Amplitude Equalization of 40 Gbit/s RZ-DPSK Signals using Saturation of FWM in a HNLF

The simulation results presented in the previous section suggest the amplitude regeneration capability of FWM in a HNLF for a 40 Gbit/s RZ-DPSK signal. In this section, we report experimental work on amplitude equalization of 40 Gbit/s RZ-DPSK signals using saturation of FWM in a 500 m HNLF [29].

5.2.1 Experimental Setup and Fiber Properties

Figure 5.4 shows a schematic of the setup used for experimental investigation of amplitude equalization of a 40 Gbit/s RZ-DPSK signal. The equalization scheme relies on saturation of FWM between the degraded RZ-DPSK signal and a pulse train with the same duty cycle as the RZ-DPSK signal. In our demonstration, we generate two identical return-to-zero (RZ) pulse trains by simultaneously modulating two CW lasers at the pump and signal wavelengths in a single Mach-Zehnder

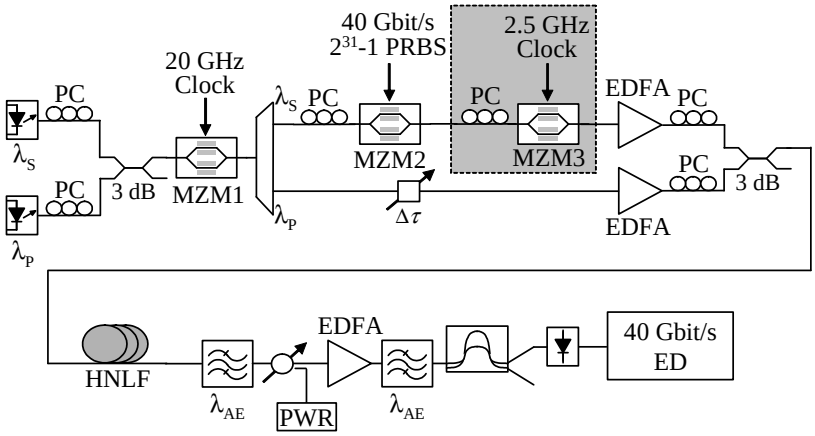

Figure 5.4: A schematic of the setup used for experimental investigation of amplitude equalization of a 40 Gbit/s RZ-DPSK signal. λ_S: signal wavelength; λ_P: pump wavelength; λ_{AE}: amplitude equalized signal wavelength; PC: polarization controller; MZM: Mach-Zehnder modulator; PRBS: pseudo-random bit sequence; EDFA: erbium doped fiber amplifier; HNLF: highly nonlinear fiber; PWR: optical power meter; ED: error detector.

modulator (MZM1) biased at a peak of its transfer function and driven with a 20 GHz clock. The two 40 GHz pulse trains with 33% duty cycle are then demultiplexed in an arrayed waveguide grating (AWG). The pulse train at the signal wavelength is phase modulated in the second MZM (MZM2) driven with a 40 Gbit/s 2^{31}-1 pseudo random bit sequence (PRBS), resulting in a 40 Gbit/s RZ-DPSK signal. To intentionally introduce amplitude distortion to the RZ-DPSK signal, a third MZM (MZM3) driven with a 2.5 GHz clock is used in this experiment. The demultiplexed pulse train at the pump wavelength is then synchronized using an optical delay line, amplified and combined with the amplified distorted RZ-DPSK signal before entering the HNLF. The polarization states of both signal and pump are optimized in order to ensure the best signal amplitude equalization. Alternatively, a polarization insensitive scheme such as e.g. the one presented in [30] could be used. At the input of the HNLF, the signal and pump powers are 19 dBm and 22 dBm, respectively. At the HNLF output, the amplitude equalized FWM product is selected with an OBPF. The signal is then

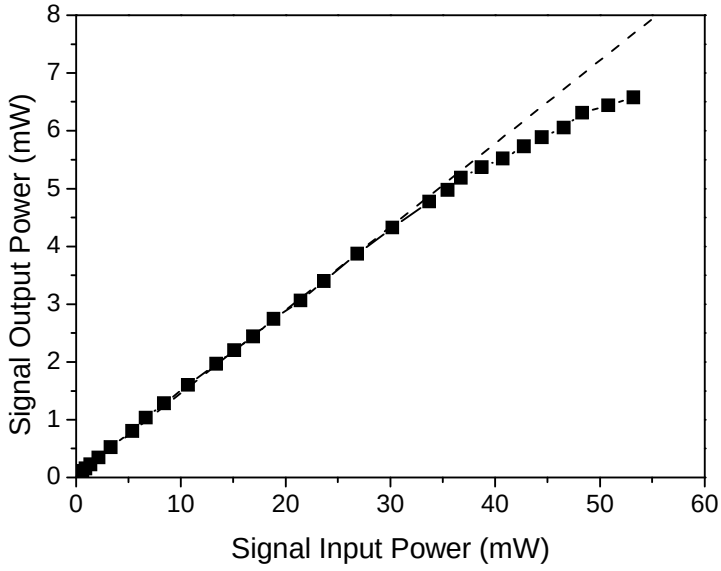

Figure 5.5: Average power transfer function of the amplitude equalizer for a pump average power of 160 mW (22 dBm) at the input of the HNLF.

detected in a single-ended pre-amplified receiver consisting of an EDFA, a tunable OBPF with a 3 dB bandwidth of 0.9 nm, a one bit delay interferometer for demodulation, and a 45 GHz photodiode.

The fiber used in this experiment is a 500 m long HNLF. The nonlinear coefficient of the fiber is $\gamma = 10.6\ \mathrm{W^{-1}{\cdot}km^{-1}}$. The fiber zero dispersion wavelength is $\lambda_0 = 1553.6$ nm, with a dispersion slope of $S = 0.022\ \mathrm{ps/km/nm^2}$. The wavelengths of the RZ-DPSK signal, pump, and amplitude equalized FWM signal are $\lambda_S = 1560.60$ nm, $\lambda_P = 1555.84$ nm, and $\lambda_{AE} = 1550.91$ nm, respectively. Here, the pump wavelength is set to be slightly detuned from the fiber zero dispersion wavelength on the longer wavelength side, in order to satisfy the phase-matching condition when taking the nonlinear refractive index into account [24].

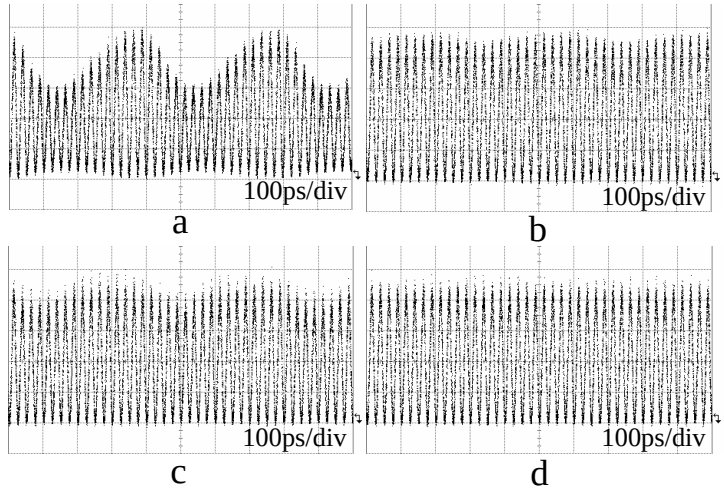

Figure 5.6: Waveforms of the distorted signal for different intensity distortion modulation indices of (a) 45% and (c) 5%. The corresponding amplitude equalized signals are shown in traces (b) and (d), respectively.

5.2.2 Results and Discussions

Figure 5.5 shows the power transfer function of the equalizer—defined as wavelength converted signal average power at the output of the HNLF as a function of signal average power at the HNLF input—for an average pump power at the HNLF input of 160 mW (22 dBm). Due to the limitation of the EDFA output power and the insertion loss of the optical attenuator, the transfer function shown in Figure 5.5 does not cover the operating region of the equalizer. However, it clearly shows the saturation behavior of the equalizer in the high signal input power regime.

The modulation index of the intensity distortion imposed on the RZ-DPSK signal depends on the bias voltage and the driving clock amplitude that are applied to MZM3. In the present experiment, the 2.5 GHz driving signal amplitude is kept constant while the bias point is changed to achieve different modulation indices in the range 5 to 45%. Figure 5.6 shows the waveforms of the distorted RZ-DPSK signals corresponding to modulation indices of 5 and 45%, as well as the corresponding amplitude equalized signals. It can be seen that the amplitude fluctuation is

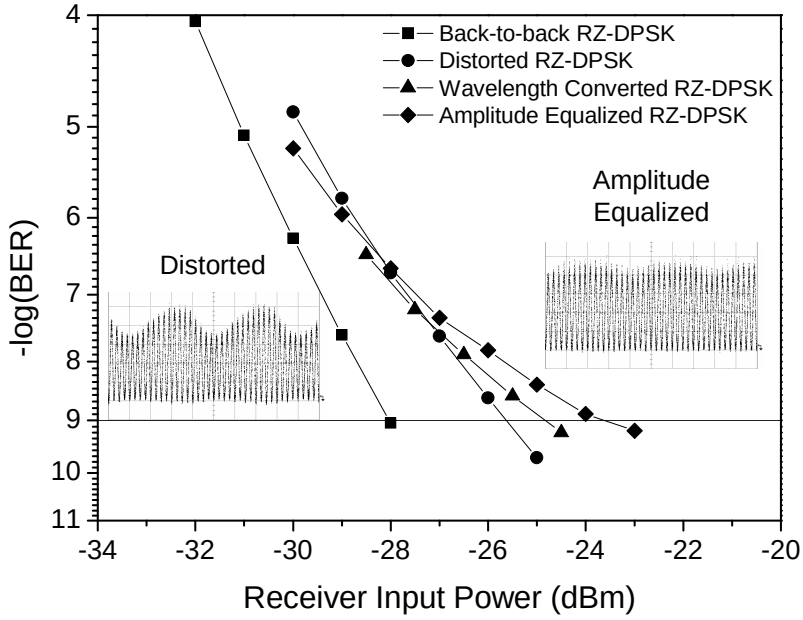

Figure 5.7: Measured BER curves for back-to-back, distorted, wavelength converted (corresponding to wavelength conversion of an RZ-DPSK signal without amplitude distortion), and amplitude equalized RZ-DPSK signals. The insets show the waveforms of the distorted and amplitude equalized signals under the same distortion condition as the one used for the BER measurements.

significantly reduced in both cases.

Bit error rate (BER) measurement results in the back-to-back case (i.e. when the signal at the output of MZM2 is directly connected to the receiver) and for the distorted and amplitude equalized RZ-DPSK signals for a modulation index of 32% are shown in Figure 5.7, together with the corresponding waveforms. The BER curve obtained after wavelength conversion of an RZ-DPSK signal without amplitude distortion is also presented in the figure. In our implementation, wavelength conversion of an RZ-DPSK signal without amplitude distortion induces a power penalty of 3 dB at a BER of 10^{-9}. This penalty is inherent to the wavelength conversion scheme, and consequently defines the reference to which the output of the equalizer should be compared when intensity distortion is introduced. This intrinsic power penalty is believed to

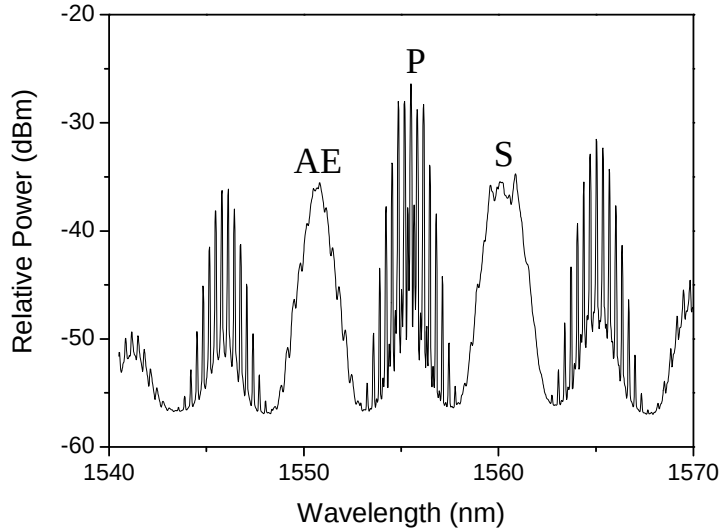

Figure 5.8: Spectrum measured at the output of the HNLF for a modulation index of 32% (resolution bandwidth 0.1 nm). P: pump, S: distorted RZ-DPSK signal, AE: amplitude equalized RZ-DPSK signal.

originate from the high power regime in which the wavelength converter is operated, where both SPM and XPM also take place. This is confirmed by the spectrum measured at the output of the HNLF shown in Figure 5.8, where the pump, distorted signal (for a modulation index of 32%), amplitude equalized signal, and other FWM products can be clearly seen. The pump spectrum has been broadened and the signal spectrum has been distorted due to nonlinearities. The amplitude distorted RZ-DPSK signal experiences a power penalty of 2.5 dB compared to the back-to-back case. After wavelength conversion, the equalized signal exhibits a power penalty of only 1 dB compared to the reference wavelength converted undistorted signal. Therefore the excess penalty due to intensity distortion is reduced from 2.5 dB to 1 dB after amplitude equalization. This 1 dB residual power penalty compared to the case of wavelength conversion of an undistorted RZ-DPSK signal is attributed to the fact that the intensity distortion is significantly reduced, but not totally suppressed by the equalizer.

The FWM process employed for equalization should preserve the

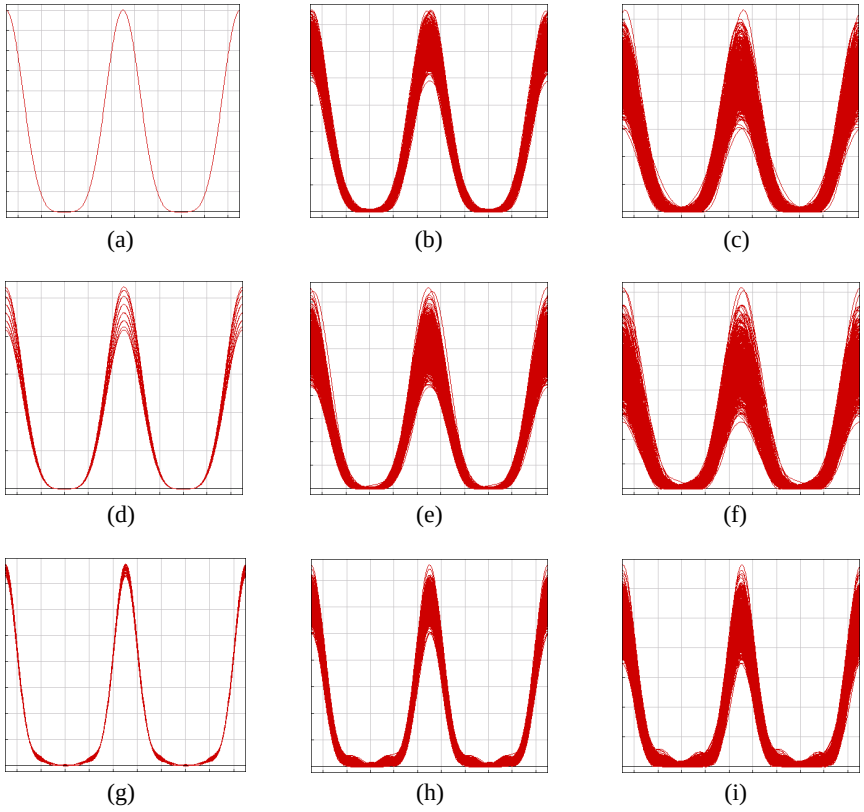

Figure 5.9: Calculated eye diagrams of (a) generated RZ-DPSK signal, (b) RZ-DPSK signal after 320 km transmission, (c) RZ-DPSK signal after 800 km transmission, (d) distorted RZ-DPSK signal, (e) distorted RZ-DPSK signal after 320 km transmission, (f) distorted RZ-DPSK signal after 800 km transmission, (g) amplitude equalized RZ-DPSK signal, (h) amplitude equalized RZ-DPSK signal after 320 km transmission, (f) amplitude equalized RZ-DPSK signal after 800 km transmission. Horizontal scale: 5 ps/div.

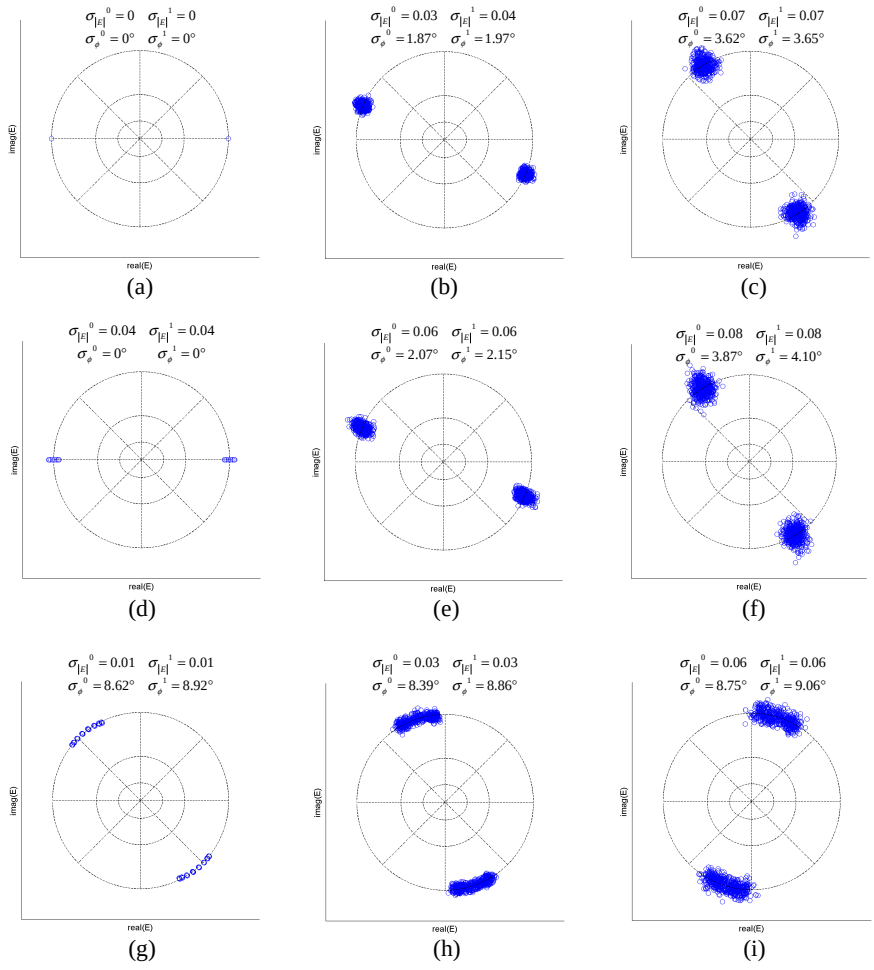

Figure 5.10: Calculated constellation diagrams of (a) generated RZ-DPSK signal, (b) RZ-DPSK signal after 320 km transmission, (c) RZ-DPSK signal after 800 km transmission, (d) distorted RZ-DPSK signal, (e) distorted RZ-DPSK signal after 320 km transmission, (f) distorted RZ-DPSK signal after 800 km transmission, (g) amplitude equalized RZ-DPSK signal, (h) amplitude equalized RZ-DPSK signal after 320 km transmission, (i) amplitude equalized RZ-DPSK signal after 800 km transmission. ${\sigma_{|E|}}^0$: amplitude standard deviation of the electric field of bit '0', ${\sigma_{|E|}}^1$: amplitude standard deviation of the electric field of bit '1', ${\sigma_\phi}^0$: phase standard deviation of the electric field of bit '0', ${\sigma_\phi}^1$: phase standard deviation of the electric field of bit '1'.

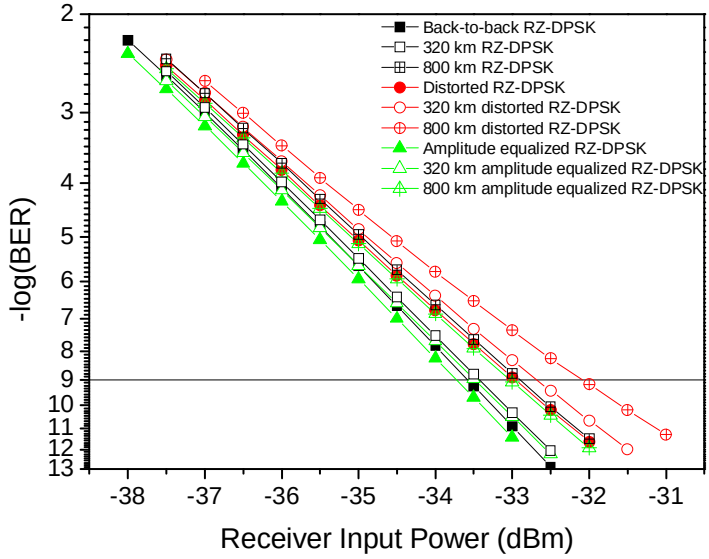

Figure 5.11: Calculated BER curves for the generated RZ-DPSK signal, distorted and amplitude equalized RZ-DPSK signals in the back-to-back case, and after transmission over 320 km and 800 km fiber spans.

phase information of the RZ-DPSK signal. It should be pointed out that the technique does not present phase regeneration, but only amplitude equalization. However, due to the high power levels involved, some nonlinear phase noise induced by SPM and XPM is expected at the output of the equalizer. In order to quantify the eventual phase distortion induced by the equalization process, we simulate the experiment using VPItransmissionMaker^{TM} again. An undistorted RZ-DPSK signal is generated and distorted using a MZM driven with a 2.5 GHz clock, as in the experiment. The distorted signal is then amplitude equalized in a piece of HNLF with the same properties as the fiber used in our experiment. In the simulations, amplitude equalization is achieved with a signal power of 18 dBm and a pump power of 17 dBm at the input of the HNLF. Polarization effects in the fiber are not taken into account in the simulations. We compare the transmission property of the distorted and amplitude equalized signals by transmitting them through 4 or 10 spans, each consisting of 80 km standard SMF and a match-

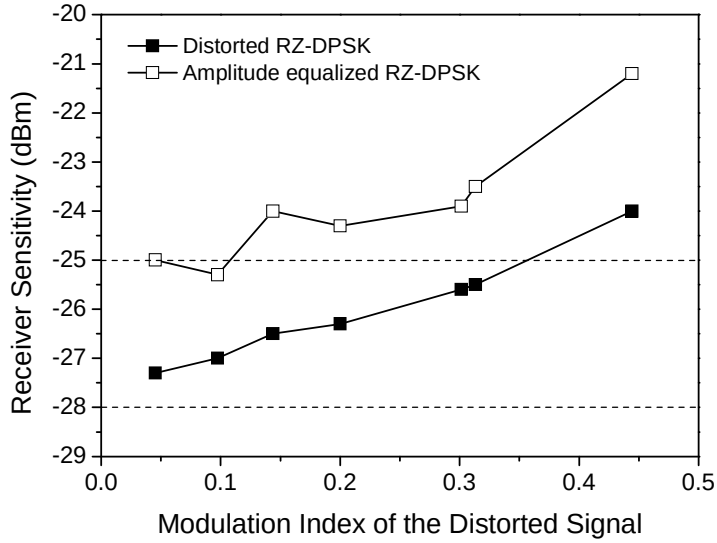

Figure 5.12: Measured receiver sensitivity for detection of the distorted and amplitude equalized RZ-DPSK signals as a function of the modulation index of the intensity distortion.

ing length of 13.6 km DCF. The eye diagrams, constellation diagrams, and BER measurements are shown in Figure 5.9, Figure 5.10, and Figure 5.11, respectively. The performance of an undistorted RZ-DPSK signal is also shown in the figures for comparison. The results show that the amplitude fluctuation is reduced by the equalization process, while the nonlinear phase noise introduced in the process does not have any significant influence on the BER performance. As shown in Figure 5.11, the receiver sensitivity of the distorted RZ-DPSK signal is −32.9 dBm, and it is −32.7 dBm and −32.1 dBm after 320 km and 800 km transmission, respectively. It is improved to −33.7 dBm after equalization, and −33.5 dBm and −33.0 dBm after 320 km and 800 km transmission, respectively. It can also be seen from the figure that the BER of the amplitude equalized signal after transmission is comparable with that of an undistorted signal, which verifies that performance improvement has been realized by the reduction of nonlinear phase noise in the transmission spans following the amplitude equalizer.

To further assess the amplitude equalization, the modulation index

of the amplitude distortion of the RZ-DPSK signal is varied from 5 to 45%. The measured receiver sensitivities for the distorted and equalized signals are shown in Figure 5.12. As expected, the sensitivities of both distorted and equalized RZ-DPSK signals degrade with increasing intensity distortion. It can be seen that, within the limited accuracy of the BER measurements, the receiver sensitivity of the distorted signal is limited by the back-to-back sensitivity of −28 dBm, while the sensitivity of the equalized signal is limited to −25 dBm which is the sensitivity of the wavelength converted RZ-DPSK signal without amplitude distortion.

5.3 Summary

We presented proof-of-principle numerical simulation results demonstrating the amplitude regeneration capability of FWM in a HNLF. We showed that, after amplitude equalization, the amplitude fluctuation accumulated over transmission spans was suppressed and the amplitude standard deviation of the electric fields were significantly reduced.

Using a 500 m long HNLF, we experimentally investigated amplitude equalization of 40 Gbit/s RZ-DPSK signals using saturation of FWM. We demonstrated that amplitude distortion could be efficiently suppressed, and the excess power penalty introduced by superimposed intensity fluctuations was reduced from 2.5 to 1 dB after wavelength conversion. We therefore confirmed experimentally the phase preserving suppression of intensity fluctuations of RZ-DPSK signals by the pump-saturation induced regenerative nature of the wavelength conversion process.

References to Chapter 5

[1] C. Xu, X. Liu, and X. Wei. “Differential phase-shift keying for high spectral efficiency optical transmissions”, *IEEE Journal of Selected Topics in Quantum Electronics*, vol. 10, no. 2, pp. 281–293, March/April 2004.

[2] A. H. Gnauck and P. J. Winzer. “Optical phase-shift-keyed transmission”, *Journal of Lightwave Technology*, vol. 23, no. 1, pp. 115–130, January 2005.

[3] A. Striegler and B. Schmauss. "All-optical DPSK signal regeneration based on cross-phase modulation", *IEEE Photonics Technology Letters*, vol. 16, no. 4, pp. 1083–1085, April 2004.

[4] A. G. Striegler, M. Meissner, K. Cveček, K. Sponsel, G. Leuchs, and B. Schmauss. "NOLM-based RZ-DPSK signal regeneration", *IEEE Photonics Technology Letters*, vol. 17, no. 3, pp. 639–641, March 2005.

[5] K. Cvecek, G. Onishchukov, K. Sponsel, A. G. Striegler, B. Schmauss, and G. Leuchs. "Experimental investigation of a modified NOLM for phase-encoded signal regeneration", *IEEE Photonics Technology Letters*, vol. 18, no. 17, pp. 1801–1803, September 2006.

[6] K. Cvecek, K. Sponsel, G. Onishchukov, B. Schmauss, and G. Leuchs. "2R-regeneration of an RZ-DPSK signal using a nonlinear amplifying loop mirror", *IEEE Photonics Technology Letters*, vol. 19, no. 3, pp. 146–148, February 2007.

[7] S. Boscolo, R. Bhamber, and S. K. Turitsyn. "Design of Raman-based NOLM for optical 2R regeneration of RZ-DPSK transmission", in *Technical Digest Optical Fiber Communication Conference, OFC'06,* Anaheim, California, U.S.A., Paper OWJ5, March 2006.

[8] S. Boscolo, R. Bhamber, and S. K. Turitsyn. "Design of Raman-based nonlinear loop mirror for all-optical 2R regeneration of differential phase-shift-keying transmission", *IEEE Journal of Quantum Electronics*, vol. 42, no. 7, pp. 619–624, July 2006.

[9] K. Croussore, C. Kim, and G. Li. "All-optical regeneration of differential phase-shift keying signals based on phase-sensitive amplification", *Optics Letters*, vol. 29, no. 20, pp. 2357–2359, October 2004.

[10] K. Croussore, I. Kim, Y. Han, C. Kim, G. Li, and S. Radic. "Demonstration of phase-regeneration of DPSK signals based on phase-sensitive amplification", *Optics Express*, vol. 13, no. 11, pp. 3945–3950, May 2005.

[11] K. Croussore, I. Kim, C. Kim, Y. Han, and G. Li. "Phase-and-amplitude regeneration of differential phase-shift keyed signals using a phase-sensitive amplifier", *Optics Express*, vol. 14, no. 6, pp. 2085–2094, March 2006.

[12] R. Elschner, A. M. de Melo, C.-A. Bunge, and K. Petermann. "Noise suppression properties of an interferometer-based regenerator for differential phase-shift keying data", *Optics Letters*, vol. 32, no. 2, pp. 112–114, January 2007.

[13] E. S. Awad, P. S. Cho, and J. Goldhar. "All-optical phase and amplitude regeneration of return-to-zero differential phase shift keying data", *Optics Letters*, vol. 32, no. 4, pp. 352–354, February 2007.

[14] P. S. Devgan, M. Shin, V. S. Grigoryan, J. Lasri, and P. Kumar. "SOA-based regenerative amplification of phase noise degraded DPSK signals", in *Technical Digest Optical Fiber Communication Conference, OFC'05,* Anaheim, California, U.S.A., Paper PDP34, March 2005, Post-deadline paper.

[15] V. S. Grigoryan, M. Shin, P. Devgan, and P. Kumar. "Mechanism of SOA-based regenerative amplification of phase-noise degraded DPSK signals", *Electronics Letters*, vol. 41, no. 18, pp. 1021–1022, September 2005.

[16] I. Kang, C. Dorrer, L. Zhang, M. Rasras, L. Buhl, A. Bhardwaj, S. Cabot, M. Dinu, X. Liu, M. Cappuzzo, L. Gomez, A. Wong-Foy, Y. F. Chen, S. Patel, D. T. Neilson, J. Jaques, and C. R. Giles. "Regenerative all optical wavelength conversion of 40-Gb/s DPSK signals using a semiconductor optical amplifier Mach-Zehnder interferometer", in *Proceedings European Conference on Optical Communication, ECOC'05,* Glasgow, Scotland, vol. 6, pp. 29–30, Paper Th4.3.3, September 2005.

[17] V. S. Grigoryan, M. Shin, P. Devgan, J. Lasri, and P. Kumar. "SOA-based regenerative amplification of phase-noise degraded DPSK signals: Dynamic analysis and demonstration", *Journal of Lightwave Technology*, vol. 24, no. 1, pp. 135–142, January 2006.

[18] P. Johannisson, G. Adolfsson, and M. Karlsson. "Suppression of phase error in differential phase-shift keying data by amplitude regeneration", *Optics Letters*, vol. 31, no. 10, pp. 1385–1387, May 2006.

[19] P. Vorreau, A. Marculescu, J. Wang, G. Böttger, B. Sartorius, C. Bornholdt, J. Slovak, M. Schlak, C. Schmidt, S. Tsadka, W. Freude, and J. Leuthold. "Cascadability and regenerative properties of SOA all-optical DPSK wavelength converters", *IEEE Photonics Technology Letters*, vol. 18, no. 18, pp. 1970–1972, September 2006.

[20] M. Matsumoto. "A fiber-based all-optical 3R regenerator for DPSK signals", *IEEE Photonics Technology Letters*, vol. 19, no. 5, pp. 273–275, March 2007.

[21] Y. Geng, P. A. Andersen, T. Tokle, C. Peucheret, and P. Jeppesen. "Broadband wavelength conversion of a 40 Gbit/s RZ-DPSK signal using dispersion flattened highly nonlinear photonic crystal fiber", in *Proceedings OptoElectronics and Communications Conference, OECC'05,* Seoul, Korea, pp. 796–797, Paper 8B3-4, July 2005.

[22] Y. Geng, P. A. Andersen, T. Tokle, C. Peucheret, and P. Jeppesen. "Wavelength conversion of a 6×40 Gb/s DPSK WDM signal using FWM in a highly non-linear photonic crystal fiber", in *Proceedings European Conference on Optical Communication, ECOC'05,* Glasgow, Scotland, vol. 2, pp. 205–206, Paper Tu3.3.4, September 2005.

[23] M. P. Fok and C. Shu. "All-optical amplitude noise reduction for DPSK signal using pump-modulated Four-Wave Mixing in a semiconductor optical amplifier", in *Proceedings European Conference on Optical Communication, ECOC'06,* Cannes, France, vol. 3, pp. 265–266, Paper We3.P.72, September 2006.

[24] K. Inoue. "Optical level equalisation based on gain saturation in fibre optical parametric amplifier", *Electronics Letters*, vol. 36, no. 12, pp. 1016–1017, June 2000.

[25] M. Matsumoto. "Regeneration of RZ-DPSK signals by fiber-based all-optical regenerators", *IEEE Photonics Technology Letters*, vol. 17, no. 5, pp. 1055–1057, May 2005.

[26] M. Matsumoto. "Performance improvement of phase-shift-keying signal transmission by means of optical limiters using Four-Wave Mixing in fibers", *Journal of Lightwave Technology*, vol. 23, no. 9, pp. 2696–2701, September 2005.

[27] M. Matsumoto. "Simultaneous reshaping of OOK and DPSK signals by a fiber-based all-optical regenerator", *Optics Express*, vol. 14, no. 4, pp. 1430–1438, February 2006.

[28] M. Matsumoto. "Nonlinear phase noise reduction of DPSK signals by an all-optical amplitude limiter using FWM in a fiber", in *Proceedings European Conference on Optical Communication, ECOC'06,* Cannes, France, vol. 2, pp. 11–12, Paper Tu1.3.5, September 2006.

[29] Y. Geng, C. Peucheret, and P. Jeppesen. "Amplitude equalization of 40 Gb/s RZ-DPSK signals using saturation of four-wave mixing in a highly non-linear fiber", in *Technical Digest IEEE Lasers and Electro-Optics Society Annual Meeting, LEOS'06,* Montreal, Quebec, Canada, pp. 158–159, Paper MP5, October 2006.

[30] K. K. Chow, C. Shu, C. Lin, and A. Bjarklev. "Polarization-insensitive widely tunable wavelength converter based on Four-Wave Mixing in a dispersion-flattened nonlinear photonic crystal fiber", *IEEE Photonics Technology Letters*, vol. 17, no. 3, pp. 624–626, March 2005.

Chapter 6

Wavelength Conversion and Transmission of Differential Quadrature Phase Shift Keying Signals

In 2002, Griffin et. al. proposed the use of differential quadrature phase shift keying (DQPSK) in direct detection optical communication systems [1, 2]. Since then, DQPSK has gained much attention and been intensively studied [3–12].

Instead of using two phase levels to carry the information as in the differential phase shift keying (DPSK) format, DQPSK uses four phase levels. Therefore, two bits are transmitted for each symbol, and the information is carried by the phase change between two consecutive symbols, resulting in a symbol rate that is half of the bit rate.

The use of DQPSK in optical communication systems enables generation of high speed signals at a per channel bit rate that is twice the operating speed of the electronics. The resulting signal has a spectral width half of the binary signal at the same bit rate, thus reducing the impact of transmission impairments. Recent demonstrations have suggested that DQPSK including its variants—such as return-to-zero DQPSK (RZ-DQPSK) and carrier suppressed return-to-zero DQPSK (CSRZ-DQPSK)—is a promising format for long-haul, high capacity

optical transmission systems, due to its doubling of spectral efficiency, larger dispersion tolerance and increased polarization-mode dispersion (PMD) limited transmission range [1]. By combining the optical time division multiplexing (OTDM) technique and polarization multiplexing, 160 km transmission of 2.56 Tbit/s DQPSK signal in a single wavelength channel has been demonstrated [13]. Employing optical phase conjugation (OPC), dense wavelength division multiplexing (DWDM) transmission of 22×20 Gbit/s DQPSK over 10,200 km [14] and 26×42.8 Gbit/s DQPSK transmission with 0.8 bit/s/Hz spectral efficiency over 4500 km standard single mode fiber (SMF) have been reported [15]. Using polarization multiplexing, 1.6 bit/s/Hz spectrally efficient 40×85.6 Gbit/s DQPSK wavelength division multiplexing (WDM) signals have been transmitted over 1700 km standard SMF, resulting in a total capacity of 3.2 Tbit/s [16]. This capacity has lately been increased to 12.3 Tbit/s using 77 WDM channels, each carrying 160 Gbit/s polarization multiplexed 85.4 Gbit/s RZ-DQPSK signals [17]. Moreover, by employing electrical time division multiplexing (ETDM), per channel bit rate of over 100 Gbit/s DQPSK transmission has been lately realized in both single channel [18] and WDM systems [19, 20], demonstrating the feasibility of DQPSK for future 100G Ethernet transport over wide area networks.

In this chapter, we present experimental study of wavelength conversion and transmission of DQPSK signals at a per channel bit rate of 80 Gbit/s and above. In section 6.1, we give a brief introduction to the DQPSK transmitter, precoding procedure, and receiver. In section 6.2, we report for the first time wavelength conversion of an 80 Gbit/s DQPSK signal using four-wave mixing (FWM) in a highly nonlinear fiber (HNLF). This work was done in cooperation with Torger Tokle from COM•DTU. In section 6.3, we describe an experimental investigation on transmission property of a 240 Gbit/s RZ-DQPSK-ASK signal generated by polarization multiplexing of 120 Gbit/s multilevel modulated signals using a combination of DQPSK with amplitude shift keying (ASK) and return-to-zero (RZ) pulse carving at a symbol rate of 40 Gbaud. This latter work was done in cooperation with Torger Tokle and Jesper Bevensee Jensen, both from COM•DTU, and Murat Serbay from University of Kiel, Germany.

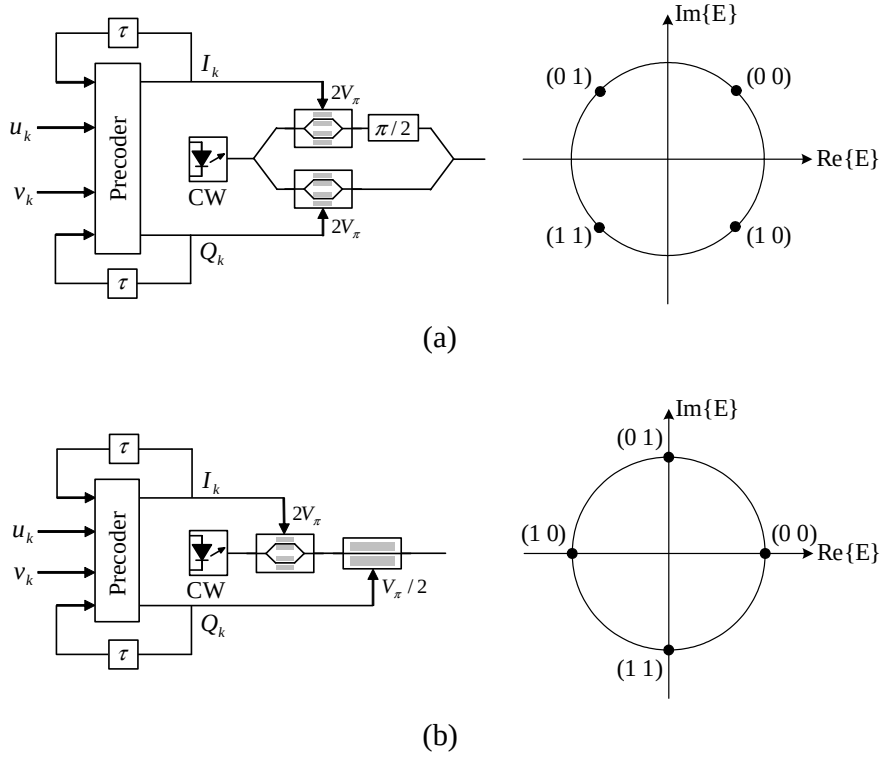

Figure 6.1: Two commonly used DQPSK transmitter structures. The first approach uses two MZMs in parallel (a), and the second approach uses a MZM and a phase modulator in series (b). The constellation diagrams of the corresponding generated DQPSK signals at the output of the transmitter are also presented, as well as the phase values assigned for the precoded pair (I_k, Q_k).

6.1 Introduction

In this section, a very brief introduction is given to the DQPSK transmitter and receiver structures and to the precoding procedure.

6.1.1 Transmitter and Precoding

Two transmitter structures commonly used to generate a DQPSK signal are illustrated in Figure 6.1. The first approach uses an electrical precoder that is capable of operating at half the bit rate, and two parallel

Mach-Zehnder modulators (MZMs) in a Mach-Zehnder interferometer structure with a phase shift of $\pi/2$ in one of the arms, as suggested in [2, 21]. The two MZMs are driven with the precoded in-phase (I) and quadrature (Q) components of the optical signal, respectively. The precoding procedure is as follows [22]:

$$I_k = \overline{(u_k \oplus v_k)}\,(u_k \oplus I_{k-1}) + (u_k \oplus v_k)\,(v_k \oplus Q_{k-1}) \quad (6.1)$$

$$Q_k = \overline{(u_k \oplus v_k)}\,(v_k \oplus Q_{k-1}) + (u_k \oplus v_k)\,(u_k \oplus I_{k-1}) \quad (6.2)$$

where $\oplus$ denotes exclusive OR operation. $u_k \in (0,1)$ and $v_k \in (0,1)$ are odd and even numbered original information bits, respectively; $I_k \in (0,1)$ and $Q_k \in (0,1)$ are coded I-channel and Q-channel bits, respectively. Pairs (u_k, v_k) and (I_{k-1}, Q_{k-1}) are used to calculate pair (I_k, Q_k) that in turn is used to control the absolute phase of the optical carrier. The amplitude of the driving signals to the two MZMs is adjusted to have $2V_\pi$ peak-to-peak voltage swing to add a π phase shift, and the resulting DQPSK signal at the transmitter output is a four-level phase modulated signal with phase values within $\left\{\frac{\pi}{4}, \frac{3\pi}{4}, \frac{5\pi}{4}, \frac{7\pi}{4}\right\}$, with the symbol allocation as shown in Figure 6.1(a).

The optical field at the output of the transmitter can be written as,

$$E(t_k) = E_0 \cos\left[\frac{\pi\,(I_k - Q_k) + \frac{\pi}{2}}{2}\right] e^{j\left[\frac{\pi(I_k+Q_k)+\frac{\pi}{2}}{2}\right]} \quad (6.3)$$

where $t = t_k$ indicates the sampling time at the center of the symbol.

The second approach uses a MZM and a phase modulator in series, as suggested in [3]. As shown in Figure 6.1, a MZM driven with the precoded signal I having an amplitude of $2V_\pi$ peak-to-peak voltage swing adds a π phase shift, and the following phase modulator driven with the precoded signal Q having an amplitude of $V_\pi/2$ adds a $\pi/2$ phase shift. The resulting DQPSK signal at the transmitter output is a four-level phase modulated signal with phase values within $\left\{0, \frac{\pi}{2}, \pi, \frac{3\pi}{2}\right\}$, with the symbol allocation as shown in Figure 6.1(b).

Using this transmitter structure, the precoding rules can be found as follows [23],

$$I_k = \overline{(v_k \oplus I_{k-1})} \cdot \overline{Q_{k-1}} + \overline{(u_k \oplus I_{k-1})} \cdot Q_{k-1} \quad (6.4)$$

$$Q_k = u_k \oplus v_k \oplus Q_{k-1} \quad (6.5)$$

and the optical field at the output of the transmitter can be written as,

$$E\left(t_k\right) = E_0 e^{j\pi\left(I_k + \frac{Q_k}{2}\right)}. \tag{6.6}$$

The two MZMs in parallel structure can be integrated on a single chip to provide suitable stability (i.e. to ensure a constant phase shift of $\pi/2$ between the two arms of the interferometer), as utilized in [24–26]. Nevertheless, it has been shown that similar performance is found for DQPSK transmitters using either two MZMs in parallel or a MZM and a phase modulator in series [27].

As described above, a differential precoder is required for DQPSK signal generation in order to map the input data onto the four possible phase states. Precoders without feedback paths—using delays and logic circuits instead, as suggested in [28, 29]—have been proposed to allow easier implementation for high speed DQPSK signal generation. For laboratory testing, precoding can be omitted if a pseudo random bit sequence (PRBS) is transmitted, since in this case the expected received data can be calculated and programmed into a programmable error detector (ED) for bit error rate (BER) measurements [3].

In the experiments presented in this chapter, the transmitter is realized using a MZM and a phase modulator in series. And due to the lack of an electrical precoder, two decorrelated PRBS signals are used to modulate the MZM and the phase modulator respectively, and the expected received data is programmed into a programmable ED for performance evaluations.

6.1.2 Receiver

The direct detection of a DQPSK signal requires phase to intensity modulation conversion in a demodulator at the receiver. The most commonly used DQPSK demodulator consists of two one symbol delay MZ interferometers made of 3 dB couplers and offset $\pm\frac{\pi}{4}$ from the transmission maximum respectively, and two balanced receivers. The basic structure is illustrated in Figure 6.2. The received signal is first split into two branches and sent to two MZ interferometers each with a delay of one symbol period, corresponding to twice the bit slot. Then each branch is detected in a balanced configuration to generate the demodulated sig-

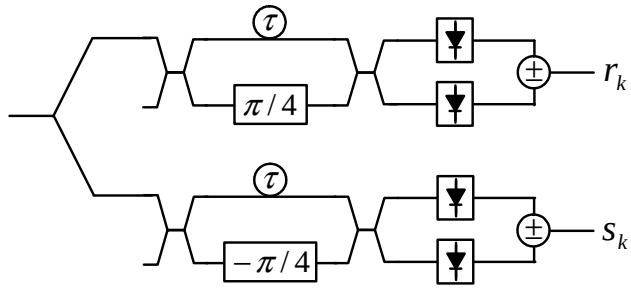

Figure 6.2: Illustration of the DQPSK receiver that consists of two one symbol delay MZ interferometers offset $\pm\frac{\pi}{4}$ from the transmission maximum respectively, and two balanced receivers.

nals r and s, respectively. It has been shown that balanced detection gives 3 dB better receiver sensitivity than single-ended detection [3].

Assuming the input signal to the demodulator has the form $E_0 e^{j\phi(t)}$, and assuming the same responsivity R for all the photodiodes, the output currents of the two balanced receivers can be written as,

$$r_k = -\frac{\sqrt{2}}{4} E_0^2 \left[\cos\left(\Delta\phi_k\right) + \sin\left(\Delta\phi_k\right)\right] \tag{6.7}$$

$$s_k = -\frac{\sqrt{2}}{4} E_0^2 \left[\cos\left(\Delta\phi_k\right) - \sin\left(\Delta\phi_k\right)\right] \tag{6.8}$$

where $\Delta\phi_k = \phi(t_k) - \phi(t_{k-1})$ is the optical phase difference between two consecutive symbols. By evaluating the demodulated bit sequence r_k and s_k, the original transmitted data sequence u_k and v_k can be recovered.

Integrated optical DQPSK receiver using silicon oxynitride (SiON) technology has been proposed to ease both thermal stabilization and active tuning [30, 31]. Moreover, a single MZ interferometer made of a 4×4 star coupler with an easier receiver construction has been reported [32, 33].

In the experiments presented in this chapter, only a single one symbol delay MZ interferometer made of 3 dB couplers is available. We therefore detect the two tributaries of the DQPSK signal one following the other by tuning the phase offset of the MZ interferometer to $\pi/4$ and $-\pi/4$, respectively.

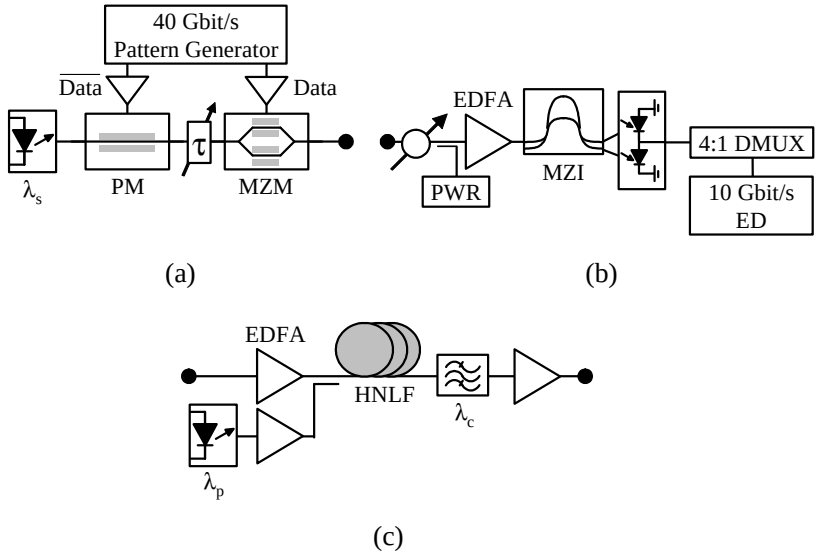

Figure 6.3: Experimental setup used for wavelength conversion of an 80 Gbit/s DQPSK signal using a HNLF. (a) DQPSK transmitter, (b) receiver, and (c) wavelength converter based on a 1 km long HNLF. λ_S: signal wavelength; λ_P: pump wavelength; λ_C: wavelength converted signal wavelength; PM: phase modulator; MZM: Mach-Zehnder modulator; EDFA: erbium doped fiber amplifier; HNLF: highly nonlinear fiber; PWR: optical power meter; MZI: Mach-Zehnder interferometer; DMUX: demultiplexer; ED: error detector [34].

6.2 Wavelength Conversion of 80 Gbit/s DQPSK Signals

In this section, we present an experimental investigation on wavelength conversion of an 80 Gbit/s DQPSK signal using FWM in a 1 km long HNLF.

6.2.1 Experimental Setup

Figure 6.3 [34] shows the experimental setup used for wavelength conversion of an 80 Gbit/s DQPSK signal. Light from a continuous wave (CW) laser operating at 1552.0 nm is first modulated by a phase modulator driven with a 40 Gbit/s inverted 2^7-1 PRBS data signal whose amplitude is adjusted to achieve a $\pi/2$ phase shift. After the phase modulator, a

MZM driven with a 40 Gbit/s 2^7-1 PRBS data signal of $2V_\pi$ peak-to-peak voltage swing is used to add π phase shift, resulting in an 80 Gbit/s DQPSK signal. The two data signals used to drive the phase modulator and the MZM are decorrelated by a relative delay of 48 bits. The generated DQPSK signal is combined with a CW pump at 1553.2 nm using a 3 dB coupler before being fed into a 1 km long HNLF with a nonlinear coefficient of $\gamma = 10.9\ \mathrm{W^{-1}{\cdot}km^{-1}}$. In order to achieve the highest conversion efficiency, both the signal and pump are polarization controlled and amplified before entering the 3 dB coupler. At the HNLF input, the power of the signal and pump is 14 and 17 dBm, respectively. At the HNLF output, the wavelength converted signal is selected by a tunable optical bandpass filter (OBPF) centered at 1554.4 nm, and amplified by an erbium doped fiber amplifier (EDFA). The signal is then detected in a balanced pre-amplified receiver consisting of an EDFA, a one symbol delay interferometer with a $\pm\pi/4$ phase shift in one arm for demodulation, and two 45 GHz photodiodes in a balanced configuration. As precoding is not applied at the transmitter side, the ED is programmed with the expected bit pattern. Due to the lack of a programmable 40 Gbit/s ED at the time of the experiment, the received signal is electrically demultiplexed to 10 Gbit/s, and the errors are then counted on a programmable 10 Gbit/s ED.

6.2.2 Results

Figure 6.4 shows the spectrum measured at the HNLF output, where the DQPSK signal, the pump and the wavelength converted signal are clearly seen. The spectrum recorded at the input of the HNLF is also presented in the figure. The conversion efficiency—defined as the ratio between the power of the converted signal and the original signal at the output of the HNLF—is found to be −12.4 dB.

Figure 6.5 shows the measured BER curves for the 80 Gbit/s DQPSK signal before and after wavelength conversion. A receiver sensitivity (at a BER of 10^{-9}) of −21.8 dBm for the 80 Gbit/s DQPSK signal in the back-to-back case is observed. A receiver sensitivity of −19.0 dBm is found after wavelength conversion, leading to a wavelength conversion induced power penalty of 2.8 dB. No indication of error floor is observed.

Figure 6.6 shows the eye diagrams of the generated DQPSK sig-

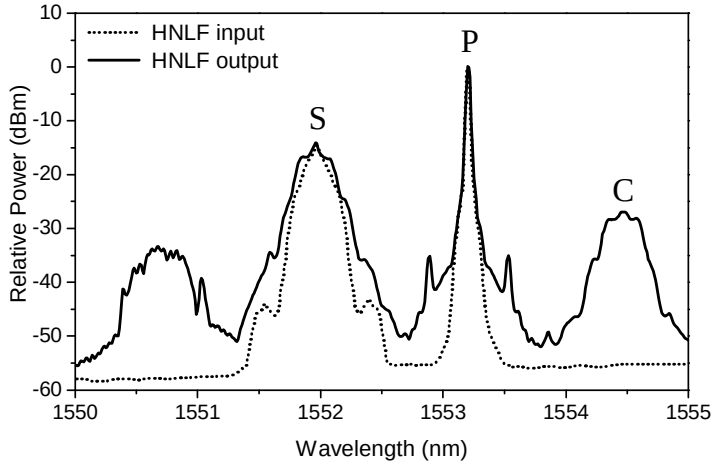

Figure 6.4: Measured spectrum at the input and output of the HNLF when the DQPSK signal (S) is located at 1552.0 nm, the pump (P) is at 1553.2 nm, and the wavelength converted signal (C) is at 1554.4 nm. Resolution bandwidth: 0.05 nm.

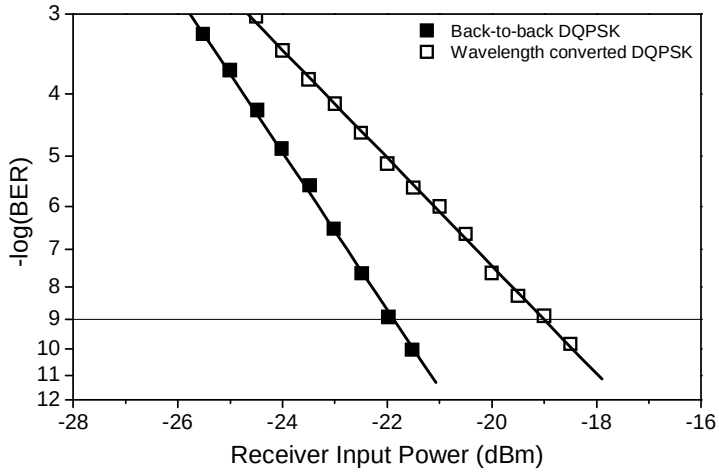

Figure 6.5: Measured BER curves for 80 Gbit/s DQPSK signal before and after wavelength conversion.

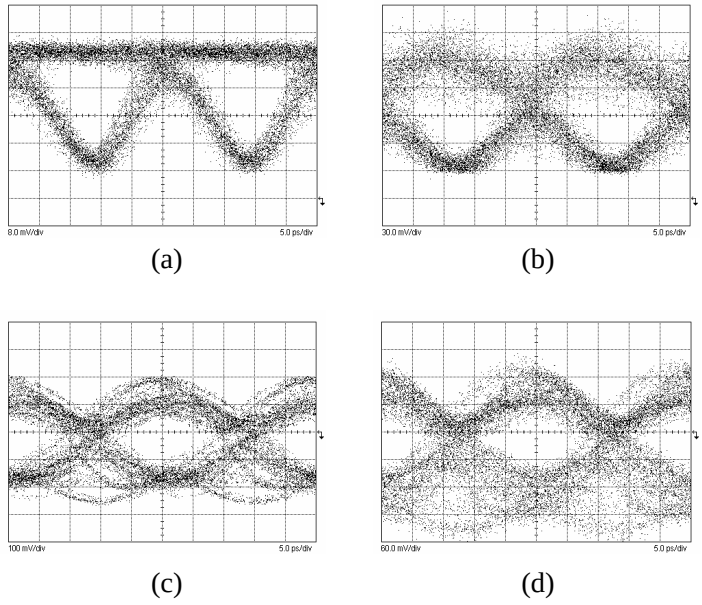

Figure 6.6: Eye diagrams of the generated DQPSK signal at 1552.0 nm (a), and the wavelength converted DQSPK signal at 1554.4 nm (b). The demodulated eye diagrams (after balanced detection) of the DQPSK signal in the back-to-back case (c) and after wavelength conversion (d) are also presented. Horizontal scale: 5 ps/div.

nal at 1552.0 nm and the wavelength converted signal at 1554.4 nm. The demodulated eye diagrams recorded after balanced detection of the DQPSK signal in the back-to-back case and after wavelength conversion are also presented in the figure. As we can see in the figure, the generated DQPSK signal has the typical feature of a DPSK signal that is generated using a MZM, as the phase modulator in front of the MZM in the setup does not add significant amplitude modulation. The eye diagram of the demodulated signal in the back-to-back case shows certain amount of inter-symbol interference (ISI), due to the relatively small 28 GHz bandwidth of the drive amplifier for the MZM and the 22 GHz limited bandwidth of the phase modulator. After wavelength conversion, certain distortions are observed in both the optical signal and the demodulated signal, mainly attributed to the reduced optical signal-to-noise ratio (OSNR) obtained after wavelength conversion process.

6.3 Transmission of 240 Gbit/s RZ-DQPSK-ASK Signals

In this section, we report an experimental investigation on generation of a 240 Gbit/s RZ-DQPSK-ASK signal by employing polarization multiplexing of 120 Gbit/s signals using a combination of DQPSK with ASK and RZ pulse carving at a symbol rate of 40 Gbaud. The transmission feasibility of such a multilevel modulated signal is demonstrated by transmitting the signal over a 50 km fiber span.

6.3.1 Experimental Setup

A schematic of the setup used for generation and transmission of a 240 Gbit/s RZ-DQPSK-ASK signal is shown in Figure 6.7 [35]. Light from a CW laser at 1550 nm is modulated by four consecutive modulators. The first MZM is biased at a middle point of its transmission function and driven with a 40 GHz clock signal to generate a 40 GHz pulse train with a pulse width of 50% of the time slot, or 12.5 ps. The second MZM is biased at null point and driven with a 40 Gbit/s 2^7-1 PRBS data signal of $2V_\pi$ peak-to-peak voltage swing to add π phase shift. The following phase modulator is driven with a 40 Gbit/s inverted 2^7-1 PRBS data signal whose amplitude is adjusted to achieve a $\pi/2$ phase shift. Finally, the third MZM driven with a 40 Gbit/s 2^7-1 PRBS adds amplitude modulation on the 80 Gbit/s RZ-DQPSK signal, resulting in a 120 Gbit/s RZ-DQPSK-ASK signal. The bias voltage and the driving signal amplitude of the third MZM are adjusted to achieve the desired extinction ratio of the ASK signal. Certain optical power of a '0' level in the ASK signal is necessary to maintain the phase information of the RZ-DQPSK signal. Therefore, the extinction ratio of the ASK signal is a trade-off between good eye opening for the ASK signal and sufficient eye opening of the demodulated DQPSK signal. An extinction ratio of 4.5 dB results in equal BER for the ASK and DQPSK tributaries, thus leading to the best overall performance. Hence an extinction ratio of 4.5 dB is used throughout all the measurements. Decorrelation of the driving data signals is obtained by applying appropriate time delays between all modulators.

The generated 120 Gbit/s RZ-DQPSK-ASK signal is then split into

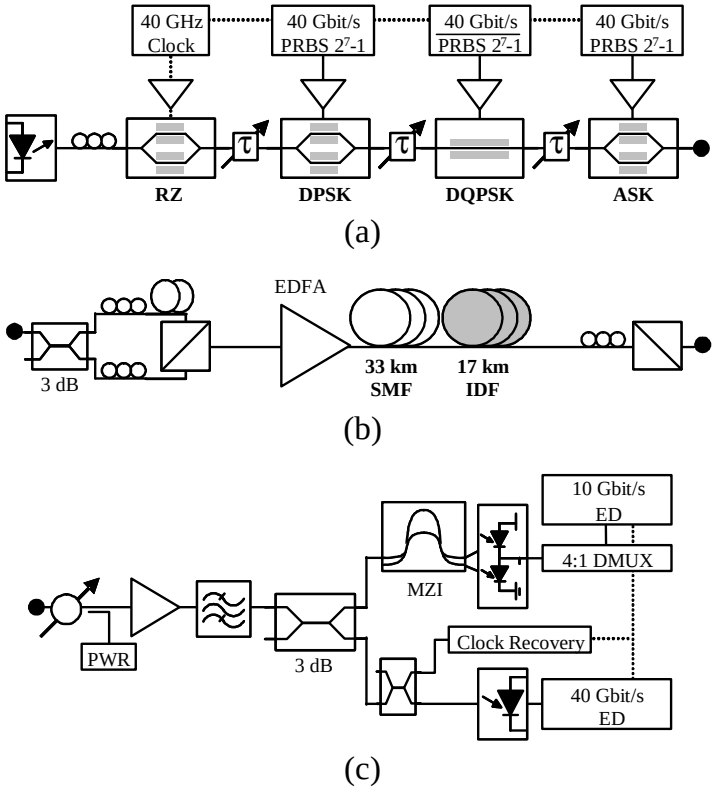

Figure 6.7: Simplified experimental setup used for generation and transmission of a 240 Gbit/s RZ-DQPSK-ASK signal. (a) RZ-DQPSK-ASK transmitter, (b) transmission span with polarization multiplexing, and (c) receiver. RZ: return-to-zero; DPSK: differential phase shift keying; DQPSK: differential quadrature phase shift keying; ASK: amplitude shift keying; PRBS: pseudo random bit sequence; SMF: standard single mode fiber; IDF: inverse dispersion fiber; EDFA: erbium doped fiber amplifier; PWR: optical power meter; MZI: Mach-Zehnder interferometer; DMUX: demultiplexer; ED: error detector [35].

two parts using a 3 dB coupler. The two signals are then delayed compared to each other to decorrelate the data patterns. The states of polarization (SOPs) of the two signals are adjusted to match the two orthogonal polarization axes of the following polarization beam splitter (PBS) used to combine the two signals before they are input to the transmission fiber span. The transmission span consists of 33 km standard SMF followed by 17 km inverse dispersion fiber (IDF). The dispersion is 17 ps/km/nm for the SMF and −36 ps/km/nm for the IDF, respectively, resulting in a residual dispersion of ~ -50 ps/nm at the signal wavelength of 1550 nm. After the transmission span, the signal is polarization demultiplexed using a polarization controller followed by a PBS. Then the signal is amplified in an EDFA and filtered by an OBPF with a 3 dB bandwidth of 1.3 nm, and split into two branches for the DQPSK and ASK signal detections. The DQPSK detection is realized in a one symbol delay interferometer with a $\pm\pi/4$ phase shift in one arm for demodulation, and two 45 GHz photodiodes in a balanced configuration. Precoding at the transmitter side is not applied in this demonstration, and due to the lack of a programmable 40 Gbit/s ED, the received signal is demultiplexed to 10 Gbit/s and the errors are then counted on a programmable 10 Gbit/s ED. The ASK detection is realized in a 50 GHz photodiode followed by a 40 Gbit/s ED, so that the BER evaluations for the DQPSK and ASK signals can be carried out simultaneously.

6.3.2 Results

Figure 6.8 [35] shows the eye diagrams of the generated 120 Gbit/s RZ-DQPSK-ASK signal and the signal after polarization multiplexing, 50 km fiber span transmission, and polarization demultiplexing. The corresponding demodulated eye diagrams recorded after balanced detection are also presented in the figure. The eye diagram of the back-to-back RZ-DQPSK-ASK signal shows the limited extinction ratio used for the ASK signal generation. The demodulated DQPSK signal exhibits multilevel traces as shown in the figure. This is due to the delay demodulation of pulses with different amplitudes. As shown in the figure, the polarization multiplexing, transmission, and polarization demultiplexing do not induce visible signal degradation.

Figure 6.9 [35] shows the BER curves for the 120 and 240 Gbit/s

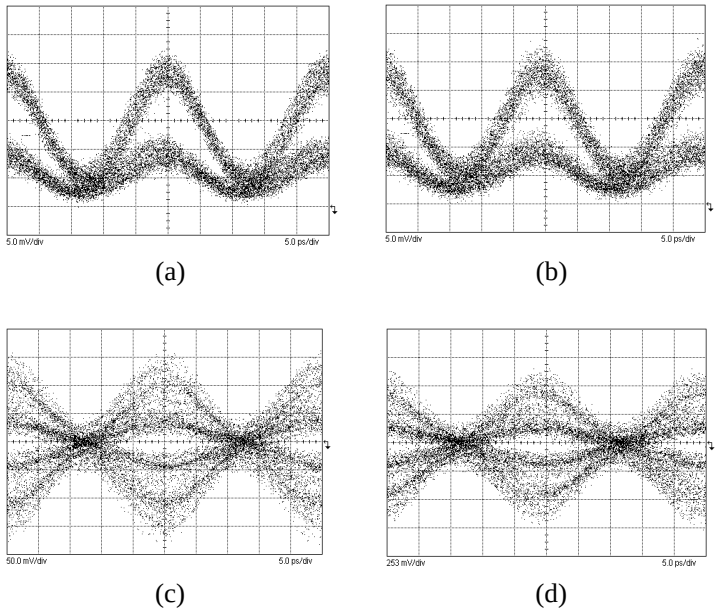

Figure 6.8: Eye diagrams of the generated 120 Gbit/s RZ-DQPSK-ASK signal (a), and the signal after polarization multiplexing, 50 km fiber span transmission, and polarization demultiplexing (b). The demodulated eye diagrams (after balanced detection) of the DQPSK signal in the back-to-back case (c) and after polarization multiplexing, transmission, and polarization demultiplexing (d) are also presented. Horizontal scale: 5 ps/div [35].

RZ-DQPSK-ASK signals in the back-to-back case and after 50 km fiber transmission. Measurements for all DQPSK and ASK tributaries and the two orthogonal tributaries are shown, as well as the calculated average BER values. It can be seen from the figure that a receiver sensitivity of -16.6 dBm is obtained for the 120 Gbit/s RZ-DQPSK-ASK signal in the back-to-back case for a BER of 10^{-9}. After polarization multiplexing, 50 km fiber transmission, and polarization demultiplexing, the receiver sensitivity doesn't change. We therefore demonstrate penalty-free transmission of multilevel 240 Gbit/s RZ-DQPSK-ASK signal employing polarization multiplexing.

The inset of Figure 6.9 shows the measured spectrum of a 40 Gbit/s RZ-DPSK signal and a 120 Gbit/s RZ-DQPSK-ASK signal. It indicates

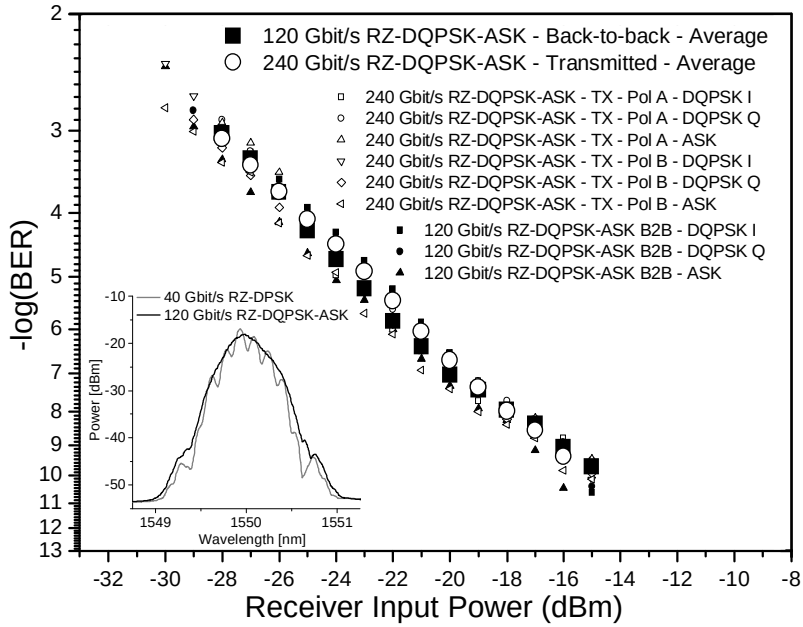

Figure 6.9: Measured BER curves for the 120 and 240 Gbit/s RZ-DQPSK-ASK signal in the back-to-back case, and after transmission. Measurements for all DQPSK and ASK tributaries and the two orthogonal tributaries are also presented, as well as the calculated average BER values. The inset shows the measured spectrum of a 40 Gbit/s RZ-DPSK signal and a 120 Gbit/s RZ-DQPSK-ASK signal [35].

that even the signal bit rate is increased by a factor of three, the symbol rate is the same for both formats, as well as the spectral width. Later investigations [36, 37] show that, increasing the data rate by a factor of three by using multilevel modulation formats, the reduction of the dispersion tolerance is much less than the nine times (3^2) reduction expected from binary modulation.

6.4 Summary

This chapter described the experimental investigation of wavelength conversion and transmission feasibility of high speed DQPSK signals.

Using a 1 km long HNLF, we successfully demonstrated for the first

time wavelength conversion of an 80 Gbit/s DQPSK signal in a simple FWM scheme. Conversion efficiency as high as −12.4 dB was achieved. A wavelength conversion induced power penalty of 2.8 dB was measured. No indication of error floor was observed.

Furthermore, using only 40 Gbit/s equipment, we successfully generated a high speed RZ-DQPSK-ASK signal at 240 Gbit/s by polarization multiplexing of 120 Gbit/s signals using a combination of DQPSK with ASK and RZ pulse carving at a symbol rate of 40 Gbaud. The transmission feasibility of such a multilevel modulated signal was demonstrated by transmitting the signal over a 50 km fiber span with no power penalty for a 2^7-1 PRBS data.

It has been shown that, using DQPSK modulation format, it becomes possible to generate high speed optical signal at a per channel bit rate that is much higher than the operating speed of existing electronics. Using 40 Gbit/s equipment, 80 Gbit/s DQPSK signals and 240 Gbit/s RZ-DQPSK-ASK signals can be generated. All-optical network functionality, such as wavelength conversion, can be implemented for an 80 Gbit/s DQPSK signal. Moreover, penalty-free transmission of ultra-high speed multilevel modulated signal combining phase and amplitude modulation formats demonstrates the suitability of RZ-DQPSK-ASK for future high speed, short range networks.

References to Chapter 6

[1] R. A. Griffin and A. C. Carter. "Optical differential quadrature phase-shift key (oDQPSK) for high capacity optical transmission", in *Technical Digest Optical Fiber Communication Conference, OFC'02,* Anaheim, California, U.S.A., pp. 367–368, Paper WX6, March 2002.

[2] R. A. Griffin, R. I. Johnstone, R. G. Walker, J. Hall, S. D. Wadsworth, K. Berry, A. C. Carter, M. J. Wale, P. A. Jerram, and N. J. Parsons. "10 Gb/s optical differential quadrature phase shift key (DQPSK) transmission using GaAs/AlGaAs integration", in *Technical Digest Optical Fiber Communication Conference, OFC'02,* Anaheim, California, U.S.A., Paper FD6, March 2002.

[3] C. Wree, J. Leibrich, J. Eick, and W. Rosenkranz. "Experimental investigation of receiver sensitivity of RZ-DQPSK modulation format using balanced detection", in *Technical Digest Optical Fiber Communication Conference, OFC'03,* Atlanta, Georgia, U.S.A., Paper ThE5, 2003.

[4] H. Kim and P. J. Winzer. "Robustness to laser frequency offset in direct-detection DPSK and DQPSK systems", *Journal of Lightwave Technology*, vol. 21, no. 9, pp. 1887–1891, September 2003.

[5] K.-P. Ho. "The effect of interferometer phase error on direct-detection DPSK and DQPSK signals", *IEEE Photonics Technology Letters*, vol. 16, no. 1, pp. 308–310, January 2004.

[6] S. Savory and A. Hadjifotiou. "Laser linewidth requirements for optical DQPSK systems", *IEEE Photonics Technology Letters*, vol. 16, no. 3, pp. 930–932, March 2004.

[7] T. Tokle, C. R. Davidson, M. Nissov, J.-X. Cai, D. G. Foursa, and A. Pilipetskii. "6500 km transmission of RZ-DQPSK WDM signals", *Electronics Letters*, vol. 40, no. 7, pp. 444–445, April 2004.

[8] T. Tokle, C. R. Davidson, M. Nissov, J.-X. Cai, D. G. Foursa, and A. Pilipetskii. "Transmission of RZ-DQPSK over 6500 km with 0.66 bit/s/Hz spectral efficiency", in *IEEE/LEOS 2004 Workshop on Advanced Modulation Formats,* San Francisco, California, U.S.A, pp. 3–4, Paper ThA2, July 2004.

[9] X. Huang, L. Zhang, M. Zhang, and P. Ye. "Impact of nonlinear phase noise on direct-detection DQPSK WDM systems", *IEEE Photonics Technology Letters*, vol. 17, no. 7, pp. 1423–1425, July 2005.

[10] H. Griesser and J.-P. Elbers. "Influence of cross-phase modulation induced nonlinear phase noise on DQPSK signals from neighbouring OOK channels", in *Proceedings European Conference on Optical Communication, ECOC'05,* Glasgow, Scotland, vol. 2, pp. 123–124, Paper Tu1.2.2, September 2005.

[11] G. Bosco and P. Poggiolini. "On the joint effect of receiver impairments on direct-detection DQPSK systems", *Journal of Lightwave Technology*, vol. 24, no. 3, pp. 1323–1333, March 2006.

[12] T. Tokle, M. Serbay, W. Rosenkranz, and P. Jeppesen. "32.1 Gbit/s InverseRZ-ASK-DQPSK modulation with low implementation penalty", in *Technical Digest IEEE Lasers and Electro-Optics Society Annual Meeting, LEOS'06,* Montreal, Quebec, Canada, pp. 490–491, Paper WH2, October 2006.

[13] H. G. Weber, S. Ferber, M. Kroh, C. Schmidt-Langhorst, R. Ludwig, V. Marembert, C. Boerner, F. Futami, S. Watanabe, and C. Schubert. "Single channel 1.28 Tbit/s and 2.56 Tb/s DQPSK transmission", in *Proceedings European Conference on Optical Communication, ECOC'05,* Glasgow, Scotland, vol. 6, pp. 3–4, Paper Th4.1.2, September 2005, Post-deadline paper.

[14] S. L. Jansen, D. van den Borne, C. Climent, M. Serbay, C.-J. Weiske, H. Suche, P. M. Krummrich, S. Spälter, S. Calabró, N. Hecker-Denschlag, P. Leisching, W. Rosenkranz, W. Sohler, G. D. Khoe, T. Koonen, and H. de Waardt. "10,200 km $22 \times 2 \times 10$ Gbit/s RZ-DQPSK dense WDM transmission without inline dispersion compensation through optical phase conjugation", in *Technical Digest Optical Fiber Communication Conference, OFC'05,* Anaheim, California, U.S.A., Paper PDP28, March 2005, Post-deadline paper.

[15] S. L. Jansen, D. van den Borne, A. Schöpflin, E. Gottwald, P. M. Krummrich, G. D. Khoe, and H. de Waardt. "26×42.8-Gbit/s DQPSK transmission with 0.8-bit/s/Hz spectral efficiency over 4,500-km SSMF using optical phase conjugation", in *Proceedings European Conference on Optical Communication, ECOC'05,* Glasgow, Scotland, vol. 6, pp. 9–10, Paper Th4.1.5, September 2005, Post-deadline paper.

[16] D. van den Borne1, S. L. Jansen, E. Gottwald, P. M. Krummrich, G. D. Khoe, and H. de Waardt. "1.6 b/s/Hz spectrally efficient 40×85.6 Gb/s transmission over 1,700 km of SSMF using

POLMUX-RZ-DQPSK", in *Technical Digest Optical Fiber Communication Conference, OFC'06,* Anaheim, California, U.S.A., Paper PDP34, March 2006, Post-deadline paper.

[17] A. H. Gnauck, P. J. Winzer, L. L. Buhl, T. Kawanishi, T. Sakamoto, M. Izutsu, and K. Higuma. "12.3-Tb/s C-band DQPSK transmission at 3.2 b/s/Hz spectral efficiency", in *Proceedings European Conference on Optical Communication, ECOC'06,* Cannes, France, Paper Th4.1.2, September 2006, Post-deadline paper.

[18] M. Daikoku, I. Morita, H. Taga, H. Tanaka, T. Kawanishi, T. Sakamoto, T. Miyazaki, and T. Fujita. "100 Gbit/s DQPSK transmission experiment without OTDM for l00G Ethernet transport", in *Technical Digest Optical Fiber Communication Conference, OFC'06,* Anaheim, California, U.S.A., Paper PDP36, March 2006, Post-deadline paper.

[19] A. Sano, H. Masuda, Y. Kisaka, S. Aisawa, E. Yoshida, Y. Miyamoto, M. Koga, K. Hagimoto, T. Yamada, T. Furuta, and H. Fukuyama. "14-Tb/s (140 × 111-Gb/s PDM/WDM) CSRZ-DQPSK transmission over 160 km using 7-THz bandwidth extended L-band EDFAs", in *Proceedings European Conference on Optical Communication, ECOC'06,* Cannes, France, Paper Th4.1.1, September 2006, Post-deadline paper.

[20] P. J. Winzer, G. Raybon, C. R. Doerr, L. L. Buhl, T. Kawanishi, T. Sakamoto, M. Izutsu, and K. Higuma. "2000-km WDM transmission of 10 × 107-Gb/s RZ-DQPSK", in *Proceedings European Conference on Optical Communication, ECOC'06,* Cannes, France, Paper Th4.1.3, September 2006, Post-deadline paper.

[21] R. A. Griffin, R. I. Johnstone, R. G. Walker, S. D. Wadsworth, A. C. Carter, and M. J. Wale. "Integrated DQPSK transmitter for dispersion-tolerant and dispersion-managed DWDM transmission", in *Technical Digest Optical Fiber Communication Conference, OFC'03,* Atlanta, Georgia, U.S.A., Paper FP6, March 2003, Post-deadline paper.

[22] F. Xiong. *Digital Modulation Techniques.* Artech House, 2000. ISBN 0-89006-970-0.

[23] T. Tokle. *Optimised Dispersion Management and Modulation Formats for High Speed Optical Communication Systems*. Ph.D. thesis, COM•DTU, Department of Communications, Optics & Materials, Technical University of Denmark, Kgs. Lyngby, Denmark, September 2004.

[24] R. A. Griffin, R. G. Walker, and R. I. Johnstone. "Integrated devices for advanced modulation formats", in *IEEE/LEOS 2004 Workshop on Advanced Modulation Formats,* San Francisco, California, U.S.A, pp. 39–40, Paper FC1, July 2004.

[25] R. A. Griffin. "Integrated DQPSK transmitters", in *Technical Digest Optical Fiber Communication Conference, OFC'05,* Anaheim, California, U.S.A., Paper OWE3, March 2005.

[26] T. Kawanishi, K. Higuma, T. Fujita, S. Mori, S. Oikawa, J. Ichikawa, T. Sakamoto, and M. Izutsu. "40 Gbit/s versatile $LiNbO_3$ lightwave modulator", in *Proceedings European Conference on Optical Communication, ECOC'05,* Glasgow, Scotland, vol. 4, pp. 855–856, Paper Th2.2.6, September 2005.

[27] M. Serbay, C. Wree, and W. Rosenkranz. "Comparison of six different RZ-DQPSK transmitter set-ups regarding their tolerance towards fibre impairments in 8×40 Gb/s WDM-systems", in *IEEE/LEOS 2004 Workshop on Advanced Modulation Formats,* San Francisco, California, U.S.A, pp. 9–10, Paper ThB3, July 2004.

[28] M. Serbay, C. Wree, and W. Rosenkranz. "Implementation of differential precoder for high-speed optical DQPSK transmission", *Electronics Letters*, vol. 40, no. 20, pp. 1288–1289, September 2004.

[29] Y. Konishi, K. Ishida, K. Kubo, and T. Mizuochi. "True PRBS transmission of DQPSK by differential precoder employing parallel prefix network", in *Technical Digest Optical Fiber Communication Conference, OFC'06,* Anaheim, California, U.S.A., Paper OThR3, March 2006.

[30] F. Morichetti, R. Costa, G. Cusmai, A. Cabas, M. Ferè, M. C. Ubaldi, A. Melloni, and M. Martinelli. "Integrated optical receiver for RZ-DQPSK transmission systems", in *Technical Digest Optical*

Fiber Communication Conference, OFC'04, Los Angeles, California, U.S.A, Paper FC8, February 2004.

[31] F. Morichetti, R. Siano, A. Boletti, and A. Melloni. "Optical integrated receiver for DQPSK systems", in *Proceedings of 7th IEEE International Conference on Transparent Optical Networks, (ICTON2005),* Barcelona, Spain, vol. 2, pp. 213–216, Paper Th.B1.2, July 2005.

[32] C. R. Doerr, D. M. Gill, A. H. Gnauck, L. L. Buhl, P. J. Winzer, M. A. Cappuzzo, A. Wong-Fay, E. Y. Chen, and L. T. Gomez. "Simultaneous reception of both quadratures of 40-Gb/s DQPSK using a simple monolithic demodulator", in *Technical Digest Optical Fiber Communication Conference, OFC'05,* Anaheim, California, U.S.A., Paper PDP12, March 2005, Post-deadline paper.

[33] C. R. Doerr, D. M. Gill, A. H. Gnauck, L. L. Buhl, P. J. Winzer, M. A. Cappuzzo, A. Wong-Foy, E. Y. Chen, and L. T. Gomez. "Monolithic demodulator for 40-Gb/s DQPSK using a star coupler", *Journal of Lightwave Technology*, vol. 24, no. 1, pp. 171–174, January 2006.

[34] T. Tokle, Y. Geng, C. Peucheret, and P. Jeppesen. "Wavelength conversion of 80 Gbit/s optical DQPSK using FWM in a highly nonlinear fibre", in *Technical Digest Conference on Lasers and Electro-Optics, CLEO'05,* Baltimore, Maryland, U.S.A., vol. 3, pp. 1708–1710, Paper JThE50, May 2005.

[35] T. Tokle, M. Serbay, Y. Geng, J. B. Jensen, W. Rosenkranz, and P. Jeppesen. "Penalty-free transmission of multilevel 240 Gbit/s RZ-DQPSK-ASK using 40 Gbit/s equipment", in *Proceedings European Conference on Optical Communication, ECOC'05,* Glasgow, Scotland, vol. 6, pp. 11–12, Paper Th4.1.6, September 2005, Post-deadline paper.

[36] T. Tokle, M. Serbay, J. B. Jensen, Y. Geng, W. Rosenkranz, and P. Jeppesen. "Investigation of multilevel phase and amplitude modulation formats in combination with polarisation multiplexing up to 240 Gbit/s", *IEEE Photonics Technology Letters*, vol. 18, no. 20, pp. 2090–2092, October 2006.

[37] J. B. Jensen, T. Tokle, Y. Geng, P. Jeppesen, M. Serbay, and W. Rosenkranz. "Dispersion tolerance of 40 Gbaud multilevel modulation formats with up to 3 bits per symbol", in *Technical Digest IEEE Lasers and Electro-Optics Society Annual Meeting, LEOS'06,* Montreal, Quebec, Canada, pp. 494–495, Paper WH4, October 2006.

Chapter 7

Conclusion

This thesis has addressed demodulation in direct detection systems and signal processing of high-speed phase modulated signals in future all-optical networks where differential phase shift keying (DPSK) or differential quadrature phase shift keying (DQPSK) format will be used to carry the information. Network functionalities have been investigated include optical labeling, wavelength conversion and signal regeneration.

DPSK Demodulation

Two alternative ways of DPSK demodulation were investigated.

A Michelson interferometer using waveguide gratings as reflective elements was fabricated by direct ultra-violet (UV) writing technique. Successful demodulation of DPSK signals up to 40 Gbit/s was demonstrated using this device. As only one coupler was used, the device leads to a compact and inherently stable DPSK demodulator. However, the limited bandwidth of the gratings requires the device to be customized for a given wavelength channel.

A polarization MZ delay interferometer was implemented by using a 2.4 m long air-guiding photonic bandgap (PBG) fiber. The large birefringence of the fiber allowed phase-to-intensity modulation conversion for DPSK demodulation at 10 and 40 Gbit/s. Due to the large value of the fiber birefringence, an order of magnitude shorter air-guiding PBG fiber can be used instead of a conventional polarization maintaining fiber, if the latter would be used to realize the same interferometer delay. How-

ever, the large birefringence observed at the fiber bandgap edge limited the tunability of the demodulator to different signal wavelengths.

Both structures can be used at the transmitter side to generate optical return-to-zero alternate mark inversion (RZ-AMI) signals with desired pulse widths. Various signal duty cycles can be realized by tailoring the relative positions of the gratings in each arm of the coupler in the Michelson interferometer based structure, or by tuning the operating wavelength in the PBG fiber based structure.

Optical Labeling

Two optical labeling schemes were investigated in this work, namely, the optical in-band subcarrier multiplexing (SCM) method and the orthogonal modulation method.

The feasibility of in-band SCM labeling using 40 Gbit/s DPSK payload and 25 Mbit/s nonreturn-to-zero (NRZ) SCM label, was experimentally investigated. A receiver power penalty of 1.2 dB was measured for a labeled signal using label modulation depth of $\eta = 0.17$ and subcarrier frequency of 3 GHz. Transmission penalty of 1.1 dB was found after 80 km post-compensated non-zero dispersion shifted fiber (NZDSF) span. Compared to the conventional SCM labeling scheme, in-band SCM labeling offers better spectral efficiency, as the subcarrier frequency is located inside the payload spectrum. Additional equipment at both transmitter and receiver side is required for the implementation of the scheme. Moreover, for high bit rate payload, the simplicity and cost effectiveness of label processing in the electronic domain, will be reduced in order to maintain the optimal payload performance.

The performance of orthogonal labeling using 40 Gbit/s return-to-zero (RZ) payload and 2.5 Gbit/s DPSK label, was experimentally studied. By using 8B10B encoding of the amplitude shift keying (ASK) payload, 3.3 dB payload extinction ratio (ER) improvement was observed for a balanced performance between the label and payload. Transmission of 4×40 Gbit/s ASK/DPSK signals was successfully demonstrated with a payload penalty of less than 1 dB and label penalty of less than 1.5 dB, after a 40 km standard single mode fiber (SMF) span. An overall penalty of 3.3 dB for the payload and 0.3 dB for the label were achieved after cascaded transmission and label swapping of one of the wavelength division multiplexing (WDM) channels. Due to the compact spectrum,

simple label swapping and good scalability to high bit rate, orthogonal labeling is considered a serious competitor to SCM labeling. Line coding techniques are useful to improve the limited ER of the payload to maintain the balanced performance between the payload and label, at a price of additional transmitter and/or receiver bandwidths.

Wavelength Conversion

Using four-wave mixing (FWM) realized in a 50 m long highly nonlinear photonic crystal fiber (HNL-PCF), wavelength conversion of high-speed phase modulated signals were reported in Chapter 4.

Wavelength conversion of a 40 Gbit/s RZ-DPSK signal was performed. A conversion efficiency of -20 dB for a pump power of 20 dBm and a conversion bandwidth of 31 nm, were obtained. Multichannel wavelength conversion was also investigated using 6×40 Gbit/s DPSK WDM signals. Conversion efficiencies better than -20.3 dB for a pump power of 25 dBm and wavelength conversion power penalties less than 4.1 dB, were achieved for all six channels. Using the same fiber, wavelength conversion of an 80 Gbit/s RZ-DPSK-ASK signal generated by combining phase and amplitude modulation, was presented. A conversion efficiency of -19 dB and well preserved signal waveforms after wavelength conversion were obtained.

HNL-PCF can be a good candidate for transparent high-speed wavelength converters, as the phase matching requirement for FWM is realized by combination of high nonlinear coefficient and flat dispersion profile of the fiber. With a simple FWM scheme, the possibility of wavelength conversion of high speed signals with both phase modulation and multilevel modulation, and even combined with WDM technology, was demonstrated.

Amplitude Equalization

The amplitude regeneration capability of FWM in a highly nonlinear fiber (HNLF) was numerically studied. It was showed that, after amplitude equalization, the amplitude distortions accumulated over transmission spans could be suppressed and the amplitude standard deviation of the electrical fields were reduced.

The first experimental demonstration of amplitude equalization of 40 Gbit/s RZ-DPSK signals using a 500 m long HNLF was reported. Using saturation of FWM, it was shown that amplitude distortion was efficiently suppressed, and the excess power penalty introduced by intentionally superimposed intensity fluctuations was reduced from 2.5 to 1 dB after wavelength conversion.

In the presented work, wavelength conversion of an undistorted RZ-DPSK signal induced a receiver power penalty of 3 dB, which prevented the usage of such a regenerator in a real system. However, in our demonstration, the power levels of the signal and pump were set at rather high values in order to equalize the large distortion applied in the experiment. In a real system, the amount of intensity distortion accumulated over several fiber spans is very likely much smaller than what was investigated in the presented work. Therefore, lower power levels would be required, which in turn will result in lower conversion power penalty. If a penalty-free wavelength conversion process would be implemented, the proposed regenerator could be used in practice to achieve improved signal quality and extended transmission range.

DQPSK

The use of DQPSK format enables generation of high-speed optical signals at a per channel bit rate that is twice the operating speed of the electronics involved. Wavelength conversion and transmission feasibility of DQPSK signals were investigated in Chapter 6.

The first demonstration of wavelength conversion of an 80 Gbit/s DQPSK signal in a simple FWM scheme was presented. By using a 1 km long HNLF, a conversion efficiency of -12.4 dB and a power penalty of 2.8 dB were achieved. No indication of error floor was observed, demonstrating the capability of FWM for wavelength conversion of multilevel phase modulated signals.

Using only 40 Gbit/s equipment, ultra-high speed RZ-DQPSK-ASK signals at 240 Gbit/s were generated using polarization multiplexing and combination of DQPSK with ASK and RZ pulse carving at a symbol rate of 40 Gbaud. No power penalty was measured after transmission of such multilevel modulated signals over 50 km fiber span. The spectrum width of a 120 Gbit/s RZ-DQPSK-ASK signal was the same as that of a 40 Gbit/s RZ-DPSK signal. It indicated that tripling the bit rate

using multilevel modulation would result in a reduction of the dispersion tolerance much less than the nine times reduction expected from binary modulation.

The work presented in this thesis has shown that DPSK is a very promising modulation format for the next generation long-haul high capacity optical communication systems. Direct detection of DPSK signals makes the format compatible with high-speed transmission systems. All-optical network functionalities that have already been studied for OOK format also become possible for phase modulated signals. All-optical signal processing, for example optical labeling, wavelength conversion and amplitude equalization, can be implemented for signals using DPSK format. We also demonstrated that DQPSK can be implemented at bit rates as high as 80 Gbit/s using only 40 Gbit/s electronics, and even higher bit rates were demonstrated when combining with amplitude modulation at 40 Gbaud. The results obtained in this work are believed to enhance the feasibility of phase modulation in future ultra-high speed spectrally efficient optical transmission systems.

Future work

With the advantages offered by DPSK over the conventional OOK format, upgrading of amplitude modulation based systems to phase modulation based systems becomes attractive when higher capacity is needed. In this connection, modulation format conversion from OOK to DPSK and from DPSK to OOK would be necessary at intermediate network nodes where the legacy sub-networks are still using OOK format. We have shown in this work, that DPSK can be converted to OOK with desired pulse widths. To become practical, format conversion from DPSK to OOK and vice versa need to be studied further. Meanwhile, compatibility of co-existing DPSK and OOK channels in a WDM grid such as inserting new 40 Gbit/s DPSK channels into the existing 10 Gbit/s WDM systems, needs to be investigated. Furthermore, all-optical 3R regeneration that can provide simultaneous phase and amplitude regeneration would be very attractive in long-haul DPSK transmission, and needs to be investigated.

List of Acronyms

AM	amplitude modulated
AMI	alternate mark inversion
ASE	amplified spontaneous emission
ASK	amplitude shift keying
ATM	asynchronous transfer mode
AWG	arrayed waveguide grating
BER	bit error rate
CW	continuous wave
DCF	dispersion compensation fiber
DFB	distributed feedback
DSF	dispersion shifted fiber
DPSK	differential phase shift keying
DQPSK	differential quadrature phase shift keying
DWDM	dense wavelength division multiplexing
EAM	electroabsorption modulator
ECL	external cavity laser
ED	error detector

EDFA	erbium doped fiber amplifier
ER	extinction ratio
ETDM	electrical time division multiplexing
FEC	forward error correction
FWM	four-wave mixing
HNLF	highly nonlinear fiber
HNL-PCF	highly nonlinear photonic crystal fiber
IDF	inverse dispersion fiber
IP	Internet protocol
ISI	inter-symbol interference
MZM	Mach-Zehnder modulator
MZI	Mach-Zehnder interferometer
NALM	nonlinear amplifying loop mirror
NOLM	nonlinear optical loop mirror
NRZ	nonreturn-to-zero
NZDSF	non-zero dispersion shifted fiber
OADM	optical add-drop multiplexer
OBPF	optical bandpass filter
OOK	on-off keying
OPC	optical phase conjugation
OTDM	optical time division multiplexing
OSNR	optical signal-to-noise ratio
PBG	photonic bandgap

PBS	polarization beam splitter
PMD	polarization-mode dispersion
POLSK	polarization shift keying
PRBS	pseudo random bit sequence
PSA	phase-sensitive amplifier
PSK	phase shift keying
RF	radio-frequency
RZ	return-to-zero
RZ-DPSK	return-to-zero differential phase shift keying
SCM	subcarrier multiplexing
SDH	synchronous digital hierarchy
SMF	single mode fiber
SOA	semiconductor optical amplifier
SOP	state of polarization
SPM	self phase modulation
UV	ultra-violet
WDM	wavelength division multiplexing
XOR	exclusive OR
XGM	cross gain modulation
XPM	cross phase modulation